TRANSFORMATION OF THE BIOCHEMICAL COMPOSITION OF *VACCINIUM CORYMBOSUM* FRUIT DURING STORAGE

Zhanna Rupasova,*[a] Vladimir Reshetnikov,[a] Tamara Vasilevskaya[a] and Nikolay Pavlovsky[a]

Keywords: *Vaccinium corymbosum*, highbush blueberry, berries, storage, biochemical composition

The biochemical composition of highbush blueberry fruit of 6 cultivars with different ripening periods, introduced in Belarus, is investigated on 14 indicators thrice a month at equal intervals. The nutrient and vitamin value of the fruit gradually decreased with the increasing amount of the dry matter, during storage, due to the depletion of free organic, ascorbic and phenol carboxylic acids, soluble sugars, pectic substances, tanning agents, anthocyanin pigments, catechins and flavonols. The transformation of the biochemical composition of the fruit, during storage, is strongly dependent on weather conditions of the season, rather than on their ripening period.

* Corresponding Authors
E-Mail: J.Rupasova@cbg.org.by
[a] Central Botanical Garden of the National Academy of Sciences of Belarus, 2v Surganova Str., 220012 Minsk, Republic of Belarus

Introduction

Currently, a special scientific and practical interest in cultivating highbush blueberry (*Vaccinium corymbosum*) is the matter related to its storage, , A short period limits possibilities of their selling and supplying to the market. The prolongation of the consumer properties of blueberry fruit by freezing and further storing at low sub-zero temperatures is ensuring, as some researchers state it, relative stability of their basic physical and chemical characteristics.

The results of the comparative study of the content of anthocyanins and levels of antioxidative activity of ethanolic extracts, made of frozen and dried blueberries after 3 months of storage with the similar extract from freshly harvested berries demonstrated no noticeable differences in the first case (frozen) and significant reduction of these characteristics in the second case (dried). [1]

The second study also demonstrated no significant changes in case of six-month storage of blueberries frozen at the temperatures of –18 ºC and –35 ºC with respect to both the quantitative content of phenolic compounds, including chlorogenic acid and anthocyanins, and the qualitative composition of such compounds. [2]

The third study incorporates the results of the comparative changes in the content of dry matters, titratable acids, vitamin C, soluble sugars and bioflavonoids of the fruits of several cultivars of highbush blueberry frozen at the temperature of –25 °C after 6- and 12-month storage.[3] The study demonstrated relative stability of the biochemical composition of the berries in general against expressed cultivar-specificity of the degree of the detected changes.

However, the inevitable trade loss of fruit after defrosting is significantly promoting the storage of blueberries in refrigeration units at low positive temperatures. Studies in this direction are of current interest, which will be demonstrated in the discussion of the results of this study.

This work establishes the essential regularities of the transformation of the biochemical composition of blueberry fruit during storage depending on plant genotypes and weather conditions of the season.

Material and Methods

Material

The research was carried out at the Central Botanical Garden of the National Academy of Sciences of Belarus in 2013 and 2014. The objects of the study were highbush blueberry fruits of 6 cultivars with different ripening periods: the first year – early ripening *Collins*, mid early ripening *Hardyblue* and mid ripening *Denise Blue*; the second year – early ripening *Bluetta*, mid ripening *Bluecrop* and late ripening *Elizabeth*. Berries were picked when in the state of economic maturity and immediately sent for storage. 400 ml disposable plastic food containers for berries and fruit with lids and holes were used as the storage containers. The berries had been stored for a month in the normal gas environment at the temperature of +3 or 4 ºC and relative humidity of 40-80 %.

Methods

Comprehensive analysis of the biochemical composition of blueberry fruit was performed three times throughout the entire storage period with a 10-day interval conditionally dividing the process into 3 stages. Correspondingly, the following contents were determined in the fresh averaged samples of blueberry fruit at the end of the 1st, 2nd and 3rd ten-day periods: dry matter – in accordance with the GOST (State Standard) 28561-90,[4] ascorbic acid (Vitamin C) – by the standard indophenol method,[5] titrate acids (total acidity) – by the volumetric method,[5] hydroxycinnamic acids (in

terms of chlorogenic acid) – by the spectrophotometric method,[6] soluble sugars – by the accelerated semi-micro method,[7] pectin substances – by the calcium pectate method,[8] the amount of anthocyanin pigments – by the method of T. Swain and W. E. Hillis[9] with a calibration curve made for the crystalline cyanidin derived from black chokeberry fruit and purified by the method of Y. G. Skorikova and E. A. Shaftan,[10] true anthocyanins and the amount of catechins (using vanillin reagent) – by the photocolorimetric method,[5,11] the amount of flavonols (in terms of rutin) – by the spectrophotometric method[5]; tannins – by the titrimetric method of Leventhal.[12] All analytical determinations were made with a three-time biological repeatability. The data were statistically processed using the Excel software programme.

Description of weather conditions

The weather conditions during the ripening of blueberry fruit varied considerably throughout the research period. Thus, the maturing of the early ripening and mid ripening breeds in the 2nd decade of July of 2013 occurred under the temperature settings close to the multiannual norm with insufficient moisture, while the ripening period for the late ripening cultivars at the end of the 3rd decade of July and the 1st decade of August was characterized by very hot and extremely dry weather. In 2014, the maturing of the early ripening breeds in the 1st week of July was characterized by the temperatures typical of this period, but with abundant precipitation which replaced the drought lasting over the last ten days of June. The maturing of the mid ripening cultivars in the 2nd decade of July was accompanied by moderate temperature with sufficient moisture. The ripening period of the late ripening cultivars in 2014 turned out to be very extreme in terms of weather conditions, namely extremely hot and dry 3rd decade of July and partly the 1st decade of August that on the contrary was characterized by the abundance of rains.

Results and Discussion

Prior to the establishment of the experiments, cultivars of fruit blueberry differed significantly in terms of the amounts of the compounds determined in the dry fruit which varied within the ranges in 2013: free organic acids: 3.18-5.70%, ascorbic acid: 332.1-428.5 mg in 100 g, hydroxycinnamic acids: 970.2-1458.3 mg in 100 g, soluble sugars: 56-63 % with the sugar-acid index equal to 9.8-19.8, pectic substances: 4.48-5.61 % including amount of hydropectin: 1.35-1.77 %, protopectin: 3.04-4.09 %, bioflavonoids: 7008.7-9760.5 mg in 100 g including anthocyanin pigments: 4682.0-6981.0 mg in 100 g with true anthocyanins in the amount: 2030.0-3330.0 mg in 100 g, leucoanthocyanins: 2652.0-3987.0 mg in 100 g, catechins: 559.0-663.0 mg in 100 g, flavonols: 1408.3-2220.5 mg in 100 g, tannins: 1.87-2.29 %, amount of the dry matter varying from 12.5 to 15.4 %. In 2014 the same ranges for fruit of model highbush blueberry cultivars were as follows: free organic acids: 3.38-4.47 %, ascorbic acid: 192.7-312.7 mg in 100 g, hydroxycinnamic acids: 563.7-1915.1 mg in 100 g, soluble sugars: 54-60 % with the sugar-acid index equal to 9.8-19.8, pectic substances: 11.6-16.5 %, bioflavonoids: 11055.2-16755.7 mg in 100 g including anthocyanin pigments: 8762.0-12956.7 mg in 100 g with true anthocyanins in the amount of 4930.0-9088.3 mg in 100 g, leucoanthocyanins: 3697.2-5256.7 mg in 100 g, catechins: 767.0-1419.2 mg in 100 g, flavonols: 1526.2-2379.8 mg in 100 g, tannins: 2.87-4.12 % with the amount of the dry matter varying from 13.3 to 18.9 %. The considerable variation in the ranges gives evidence of the pronounced genotypic differences of the nutrient and vitamin value of fruit of the studied blueberry taxa.

Based on the research held in 2013 on the degree of the transformation of the biochemical composition of blueberry fruit of the *Collins*, *Hardyblue* and *Denise Blue* cultivars after a month-long storage period, the depletion of free organic and ascorbic acids (by 15-41 % and 42-45 %, respectively), soluble sugars (by 7-17 %), pectic substances and tanning agents (by 18-20 % and 7-17 %, respectively), anthocyanin pigments and flavonols (by 20-35 % and 4-13 % respectively) with the increase in the amount of the dry matter and of the sugar-acid index (by 14-28 % and 5-40 % respectively) without any significant changes in the amount of catechins and ambivalent changes in the amount of hydroxycinnamic acids (Table 1).

Similar tendencies in the transformation of the biochemical composition of blueberry fruit were observed in the same-type experiment carried out in 2014 with *Bluetta*, *Bluecrop* and *Elizabeth* cultivars. These tendencies manifested themselves in the depletion of free organic, ascorbic and hydroxycinnamic acids (31-51 %, 29-62 % and 10-48 % respectively), soluble sugars (5-9 %), pectic substances and tanning agents (22-33 % and 10-47 % respectively), anthocyanin pigments, catechins and flavonols (15-39 %, 7-35 % and 8-26 % respectively) compared with the initial values with the increase of the amount of the dry matter and the sugar-acid index (10-19 % and 34-89 % respectively). The reported decrease in the acidity level in blueberry fruits in the process of two-month storage at 3 °C[13] corresponds to our results. The study on the impact of allyl isothiocyanate (AITC) on the activity of scavenging enzymes, the content of flavonols and the quality of *Duke* cultivar blueberry fruits in the process of storage at 10 °C also demonstrates the decrease in the content of phenolic acids, flavonols and anthocyans.[14] The studies devoted to changes in antioxidant activity of the fruits of a number of blueberry cultivars during storage at 1 and 8 °C also show the decrease of the named parameter by the end of the month storage, [15] which is an indirect proof of drop of the bioflavonoid level. The tendency of the growth of dry matter during storage in desiccator[16] is same as in our experiment.

The revealed loss of most organic compounds characterizing the decrease of the nutrient and vitamin value of blueberry fruit during storage was caused by their usage of these organic compounds as respiratory substrates, the relative amount of which was determined by their chemical nature, plant genotype and weather conditions of the season.

Table 1. Statistically valid relative differences as compared to the initial values of active substances contained in *Vaccinium corymbosum* fruit at different storage stages, (%)

Index	1 stage	2 stage	3 stage	1 stage	2 stage	3 stage	1 stage	2 stage	3 stage
2013	*Collins*			*Hardyblue*			*Denise Blue*		
Dry matter	-	-	**+14.1**	-	**+16.9**	**+27.9**	-	**+4.8**	**+19.2**
Free organic acids	-	-10.7	-15.4	-9.7	-20.8	-40.6	-	-14.5	-15.9
Ascorbic acid	-	-31.3	-41.8	-	-22.7	-44.6	-9.3	-19.1	-42.0
Hydroxycinnamic acid	-	-16.0	-9.1	**+28.2**	**+10.8**	-	**+35.9**	-	**+17.0**
Soluble sugars	-	-4.1	-6.6	-5.9	-14.8	-17.0	-5.8	-7.0	-7.0
Sugar-acid index	-	**+14.3**	**+5.1**	**+19.2**	-	**+39.4**	-	**+10.0**	-9.2
Pectic substances	-9.8	-13.4	-18.5	-8.2	-19.4	-19.4	-10.7	-11.9	-17.6
True anthocyanins	-	-11.4	-16.0	-17.1	-29.7	-41.4	**+3.0**	**+13.8**	**+24.1**
Leucoanthocyanins	-8.2	-9.5	-21.8	-15.9	-19.9	-29.5	-7.7	-25.1	-16.6
Amount of anthocyanin pigments	-5.9	-10.2	-19.6	-16.5	-24.6	-35.2	-3.3	-8.2	-
Catechins	-	-	-	-4.7	-7.0	-8.1	-	-	-
Flavonols	-3.7	-4.2	-4.2	-	-14.5	-13.0	**+2.8**	**+5.9**	**+15.4**
Amount of bioflavonoids	-5.1	-8.7	-16.0	-11.2	-21.3	-28.6	-1.9	-4.8	**+3.5**
Tannins	-	-10.9	-16.6	-	-3.6	-7.3	-3.2	-	**+13.4**
2014	*Bluetta*			*Bluecrop*			*Elizabeth*		
Dry matter	-	-	**+9.8**	-	-	-	**+9.5**	**+11.1**	**+18.5**
Free organic acids	-33.3	-43.8	-47.7	-26.3	-29.0	-30.5	-18.2	-44.8	-50.9
Ascorbic acid	-	-26.0	-29.2	-43.4	-44.9	-62.4	-15.1	-34.1	-45.8
Hydroxycinnamic acid	**+10.2**	**+17.9**	-10.2	**+11.6**	**+22.6**	**+14.3**	-47.8	-43.0	-48.2
Amount of soluble sugars	-	-5.6	-8.4	-	-3.7	-4.8	-	-4.6	-7.5
Sugar-acid index	**+48.1**	**+68.4**	**+74.4**	**+32.3**	**+38.5**	**+34.2**	**+20.9**	**+72.7**	**+89.2**
Amount of pectic substances	-15.8	-30.9	-32.7	-10.3	-17.2	-21.6	-	-13.7	-23.0
True anthocyanins	**+18.6**	**+17.1**	-34.5	-18.3	-18.3	-30.6	-22.8	-12.4	-39.7
Leucoanthocyanins	-	-	-	-13.8	-23.3	**+6.2**	-37.0	-11.4	-37.9
Amount of anthocyanin pigments	**+13.9**	**+12.9**	-25.7	-16.3	-20.5	-14.5	-28.6	-12.0	-39.0
Catechins	**+22.1**	**+17.7**	-	**+13.6**	-5.9	-17.0	-26.7	-21.2	-35.3
Flavonols	**+22.7**	**+15.0**	-7.7	**+5.6**	-6.4	**+6.4**	-31.7	-13.0	-25.5
Amount of bioflavonoids	**+15.4**	**+13.4**	-22.3	-11.2	-17.5	-11.8	-28.9	-12.9	-36.8
Tannins	-3.1	**+21.6**	**+5.9**	**+2.4**	-6.2	-9.8	-24.3	-22.3	-46.6

A dash (-) means that no statistically significant differences are observed at $p < 0.05$.

In order to identify the blueberry taxon with the lowest decrease in the amount of active substances in fruit, as well as to identify the storage stage at which the best preservation of the integral level of the nutrient and vitamin value of fruit is ensured, we used our own unique methods, based on comparing the tested objects, at various stages of storage with respect to their relative scales, amplitudes and correlations of statistically valid positive and negative deviations from the initial values of the studied parameters of the fruit biochemical composition.[17] The value of the overall amplitude of the detected deviations, regardless of their signs, made it possible to estimate the significance of the differences between the tested objects and the initial values of all the studied parameters at each stage of storage, which allowed ranging them according to the decrease of the degree of these differences. The correlation of the relative scales of the scopes of positive and negative differences as compared to the initial values of active substances contained in fruit served as a criterion for the estimation of the integral level of the nutrient and vitamin value of blueberry fruit in each cultivar at specific stages of storage.

The data presented in Table 2, characterizing the direction and the significance of the transformations in the biochemical composition of blueberry cultivars being tested, show the presence of significant genotypic and time-related differences in the direction and the extent of the above mentioned transformations testifying the marked specific character of different cultivars' responses in terms of exposure durations to low positive temperatures, based on the combination of all the parameters (dry matter, organic acids, carbohydrates and phenolic compounds) analyzed at different stages of storage compared to the initial values.

Table 2. The relative scale of the amplitude and the correlation of variously oriented differences with the initial values of active substances contained in fruit of the *Vaccinium corymbosum* cultivar at different storage stages

Cultivar	Storage stage	Relative scale of the shifts, %			
		+	-	amplitude	+/-
2013					
	1	1.0	53.0	54.0	0.02
Collins	2	14.3	158.2	172.5	0.09
	3	19.2	222.5	241.7	0.09
	1	47.4	105.1	152.5	0.45
Hardyblue	2	27.7	235.3	263.0	0.12
	3	67.3	324.6	391.9	0.21
	1	41.7	60.6	102.3	0.69
Denise Blue	2	34.5	114.7	149.2	0.30
	3	92.6	150.6	243.2	0.62
2014					
	1	151.0	52.2	203.2	2.89
Bluetta	2	184.0	62.5	246.5	2.94
	3	90.1	218.4	308.5	0.41
	1	65.5	139.6	205.1	0.47
Bluecrop	2	61.1	192.9	254.0	0.32
	3	61.1	203.0	264.1	0.30
	1	30.4	281.1	311.5	0.11
Elizabeth	2	83.8	245.4	329.2	0.34
	3	107.7	436.2	543.9	0.25

Thus, for the experiments held in 2013, in the setting of the gradual increase in the degree of the differences during storage compared to the initial values of the amount of active substances, the *Collins* and *Denise Blu*e cultivars were characterized by its smallest, but similar relative values – from 54.0 to 241.7 % and from 102.3 to 243.2 % respectively, while its largest value – from 152.5 to 391.9 % – became a characteristic of the *Hardyblue* cultivar indicating the most marked transformations of the biochemical composition of its fruit during storage. However, as shown above, alongside with the consumption of some organic compounds as respiratory substrates resulting in the decrease of their amount as compared to the initial values, their accumulation was also observed due to the inter-conversion of organic compounds, the cumulative relative effect of which at different stages of storage ranged from 1.0 to 19.2 % for the *Collins* cultivar, from 27.7 to 67.3 % for the *Hardyblue* cultivar and from 34.5 to 92.6 % for the *Denise Blue* cultivar; at the same time the two latter taxa showed the minimum values of this parameter at the second storage stage, whereas their maximum values, as well as for the *Collins* cultivar, were shown at the third stage of storage. To a certain degree, it corresponds to the data[18] on the dynamics of a number of biologically active compounds in the fruits of several cultivars, including highbush and lowbush blueberry, in the process of storage at different positive temperatures and have demonstrated no losses of ascorbic acid in 8 days of storage. There are no significant losses of phenolic compounds at a relative stability of antioxidative activity of blueberry fruits after 2-week storage at the temperature of +4 ºC.[19]

In the experiments in 2014, like in the other one held in the year before, the smallest, but similar relative degree of differences related to the amount of the tested substances as compared to their initial values – within 203.2-308.5 % and 205.1-264.1 % – became characteristics of the early and mid ripening *Bluetta* and *Bluecrop* blueberry cultivars, whereas the biggest degree – from 311.5 to 543.9 % – became a characteristic of the late-ripening *Elizabeth* cultivar indicating the most marked transformations of the biochemical composition of its fruit during storage. Besides, the relative increase of the amount of some substances contained in fruit at different stages of storage varied from 90 to 184 % for the *Bluetta* cultivar, 61.1 to 65.5 % for the *Bluecrop* cultivar and 30.4 to 107.7 % for the *Elizabeth* cultivar. The studies of A. M. Connor et al.[20] also demonstrate expressed cultivar-specificity of transformation of the biochemical composition of blueberry fruits in the process of storage at low positive temperatures. In this case, same as in our studies, growth of the content of anthocyanins and the total quantity of bioflavonoids during the first three weeks of storage is noted.

The most objective view on the degree of transformations of the biochemical composition of blueberry fruit during storage can be formed with the help of the many-fold scale of the correlation of the relative values of the scopes of positive and negative deviations from the initial value of the analyzed parameters combination. It turned out also that in the experiment in 2013 all the tested objects at all stages of storage had it at a level significantly lower than 1.0, which indicated prevalence of negative transformations in the quality of blueberry fruit over positive ones.

At the same time, at all storage stages the minimum value of this correlation became a characteristic of the *Collins* cultivar, while its maximum value was attributed to the *Denise Blue* cultivar, with the *Hardyblue* cultivar taking an intermediate position. This means that the most significant excess of the loss of nutrients over their accumulation during storage became a characteristic of the early ripening cultivar, while the lowest excess was attributed to the late ripening breed, with the high-level expression of this effect shown by the *Hardyblue* and *Denise Blue* cultivars at the end of the second stage of storage and its marked weakening at the end of the experiment, especially for the last object.

Based on the comparison of the scale of the given correlation within the taxonomic range, the quantitative assessment was given with respect to the decrease of the integral level of the nutrient and vitamin value of blueberry fruit and, consequently, the deterioration of their consumer properties after a month of storage. The *Collins* cultivar was rated the highest, whereas the *Hardyblue* and *Denise Blue* cultivars were rated by 2.3 and 6.9 times lower, respectively.

In the experiment in 2014, the scale of the correlation of the relative values of the scopes of positive and negative deviations from the initial values of the tested substances contained in the mid and especially late ripening cultivars of blueberry at all stages of storage was 2 to 9 times lower than 1.0, which indicated prevalence of negative transformations in the biochemical composition of blueberry fruit over positive ones; the same as was observed in the experiment in 2013. In contrast to these taxa, the early ripening *Bluetta* cultivar during first two stages of storage lasting 20 days showed an improvement of its qualitative characteristics as compared to the initial values, which was confirmed by nearly three-fold excess of the scope of positive changes in their biochemical composition as opposed to negative ones; and only at the final stage of storage a seven-fold decrease of the integral level of the nutrient and vitamin value of blueberry fruit of this cultivar as compared to its initial values was observed. It should be noted that in the experiment of the same type in 2013, but on other cultivars of blueberry, the opposite results were observed: the highest excess of the loss of the related compounds over their accumulation at all storage stages became a characteristic of the early ripening cultivar, while the lowest excess was attributed to the late ripening breed. In our opinion, this may indicate a greater dependence of the revealed effects in the transformation of the biochemical composition of blueberry fruit during storage at low positive temperatures on weather conditions of the season rather than on plant genotype and fruit ripening periods.

Based on the comparison of the scale of the given correlation within the blueberry taxonomic range, the quantitative assessment was given with respect to the decrease of the integral level of the nutrient and vitamin values of blueberry fruit and, consequently, the deterioration of their consumer properties after a month of storage.

The *Elizabeth* cultivar was rated the highest, whereas the *Bluetta* and *Bluecrop* cultivars were rated by 1.6 and 1.2 times lower, respectively. This indicates the increase of the preservation of the quality of blueberry fruit harvested in 2014 at low positive temperatures in the range from the early to the late ripening cultivars, while in the experiment held in 2013 the opposite situation was observed.

References

[1]Lohachoompol, V., Srzednicki, G., Craske, J., *J. Biomed. Biotechnol.*, **2004**, *5*, 248-252.

[2]Scibisz, I., Mitek, M., *Acta Sci. Pol., Technol. Aliment*, **2007**, *6(4)*, 75-82.

[3]Skupien, K., *Acta Sci. Pol., Hortorum Cultus*, **2006,** *5(1)*, 19-25.

[4]*Methods for determination of the dry matter: GOST (State Standard)* 8756. 2-82. **1982**, p.

[5]*Methods for biochemical studies of plants*. (Ed.) Ermakova, A. I. **1987**, p. 430. Leningrad. Russia [In Russian].

[6]Marsov, N. G. *Phytochemical studies and biological activity of cowberries, cranberries and blueberries*. **2006**, pp. 99-101. Perm, Russia [In Russian].

[7]Pleshkov, B. P. *Workshop on plant biochemistry*. **1985**, pp. 110-112. Moscow. Russia [In Russian].

[8]Rupasova, Z. A., V. N. Reshetnikov, T. I. Vasilevskaya, N. P. Varavina, N. B. Krinickaiy, A. M. Bubnova, N. B. Pavlovsky, A. G. Pavlovskay, T. V. Kurlovich, Y. M. Pinchukova. *Orcharding*. **2014**; *26*, 413-426. Samokhvalovichy, Belarus [In Russian].

[9]Swain, T., Hillis, W. J. *Sci. Food Agric*. **1959**; *10(1)*, 63-68.

[10]Skorikova Y. G., Shaftan, E. A. *Method for determination of anthocyanins in fruit and berries*. In: *Proc. 3rd All-union Semin. Biol. Active (Therapeutic) Subst. Fruit and Berries.* **1968**, pp. 451-461. Sverdlovsk, Russia [In Russian].

[11]Andreev, V. Y., Kalinkina, G. I., Kolomiyets, N. E., Isaykina, N. V. *Pharmacy*, **2013,** *3(19)* AM-21.

[12]*State Pharmacopoeia of the USSR*. **1987,** *1*, 286-287. Moscow. Russia [In Russian].

[13]Chiabrano, V., Giacalone, G., *Int. J. Food Nutr*., **2015,** *66(3)*, 248-253.

[14]Wang, S. Y., Chen, C-T., *Food Chem.,* **2010,** *122(4)*, 1153-1158.

[15]Remberg, S. F., Haffner, K., Blomhoff, R., *Acta Hort*., **2003,** *600*, 595-598.

[16]Basiouny, M., Chen, Y., *Proc. Fla. State Hort. Soc*., **1988,** *101*, 281 – 284.

[17]Rupasova, Z. A., Reshetnikov, V. N., Yakovlev, A. P. *Method for ranking plant taxa*: Belarus Patent No. 17648 dated 08.07.**2013**. Minsk, Belarus [In Russian].

[18]Kalt, W., Forney, C. F., Martin, A., Ptior, R. L. *J. Agric. Food Chem*., **1999.** *47*, 4638-4644.

[19]Yuan, W., Zhou, L., Deng, G., Wang, P., Creech, D., Li, S., *Pharm. Crops*, **2011**, *2*, 11-23.

[20]Connor, A. M., Luby, J. J., Hancock, J. F., Berkheimer, S, Hanson, E. J., *J. Agric. Food Chem*., **2002,** *50(4)*, 893-898.

Received: 08.02.2016.
Accepted: 09.05.2016.

SYNTHESIS AND CYTOTOXIC ACTIVITY OF NOVEL TETRAHYDROBENZO[*b*]THIOPHENE-DERIVED HETEROCYCLES

Wagnat W. Wardakhan[a]*, Faten I. Hamed[a], Eman M. Samir[a]

Keywords: Tetrahydrobenzo[*b*]thiophene, thiazole, pyrimidine, thieno[*d*]pyrimidine, cytotoxic activity.

Series of thiophene, thiazole, and pyrimidine derivatives based on the ethyl 2-amino-4,5,6,7-tetrahydrobenzo[*b*]thiophene-3-carboxylate starting material were synthesized, and cytotoxic activity of synthesized compounds was evaluated. Results showed that three compounds, *viz.* (2)-2-(4-methyl-3-phenylthiazole-2(3H)-ylidenea-mino)-4,5,6,7-tetrahydrobenzo[b]thiophene-3-carbonitrile, ethyl 2-(6-amino-4-imino-3-phenyl-2-thioxo-3,4-dihydropyrimidin-1(2H)-yl)-4,5,6,7-tetrahydrobenzo[b]thiophene-3-carboxylate, and 4-imino-3-phenyl-3,4,5,6,7,8-hexahydrobenzo[4,5]-thieno[2,3-d]pyrimidine-2-thiol, were the most active towards MCF-7 (breast adenocarcinoma), NCI-H460 (non-small cell lung cancer), and SF-268 (CNS cancer), but they were not active towards normal fibroblasts human cell line (WI-38). The toxicity of selected compounds against shrimp larvae was also studied.

Corresponding Author:
Fax: 002-35676873
E-mail: wagnatwahba @yahoo.com
[a] National Organization for Drug Control& Research P.O. Box 29, Cairo, Egypt.

Introduction

Organic compounds containing aromatic heterocyclic rings, like thiophene, are widely distributed in nature and play an important role in various biochemical processes. Therefore, they are often incorporated into new chemical entities by medicinal chemists.[1-3] Numerous thiophene derivatives of important therapeutic compounds containing benzene ring[10,11] were prepared for obtaining better biological activity than the parent compound. For example, a lot of compounds were found to have nematocidal,[4] insecticidal,[5] antibacterial,[6] antifungal,[7] antiviral,[8] and antioxidant activity.[9] Based on this, the aim in this work was to synthesize novel heterocyclic compounds from ethyl 2-amino-4,5,6,7-tetrahydrobenzo[*b*]thiophene-3-carboxylate (**1**) and to evaluate their antitumor activity.

Results and discussion

Synthesis of investigated compounds is summarized in Schemes 1-3. The reaction of the ethyl 2-amino-4,5,6,7-tetrahydrobenzo[b]thiophene-3-carboxylate (**1**) with ethyl-orthoformate in acetic acid gave the ethyl 2-((ethoxy-methylene)amino)-4,5,6,7-tetrahydrobenzo[b]thiophene-3-carboxylate (**3**). Compound **3** reacted with aniline to give the ethyl 2-((phenylamino)methylene)amino-4,5,6,7-tetra-hydrobenzo[*b*]thiophene-3-carboxylate derivative **5**. The elemental and spectral data of compound **5** were consistent with its proposed structure. Namely, ^{1}H-NMR spectrum of compound **5** showed the presence of a triplet at δ 1.12 ppm corresponding to the CH_3 group, a multiplet at δ 1.66-1.95 ppm corresponding to four CH_2 groups, a quartet at δ 4.22 ppm indicating the ethyl CH_2 group, a singlet at δ 6.65 ppm for CH group, a multiplet at δ 7.30-7.46 ppm corresponding to the C_6H_5 group, and a singlet at δ 8.32 ppm for NH group. On the other hand, the reaction of compound **3** with malononitrile (**6**) gave the iminomethyl malononitrile derivative **7**. The analytical and spectral data of compound **7** were in agreement with its structure.

The reaction of compound **1** with phenylisothiocyanate (**8**) and chloroacetone (**9**) gave the thiazole derivative **11**. Formation of the latter product took place through the intermediate formation of **10** followed by water elimination.

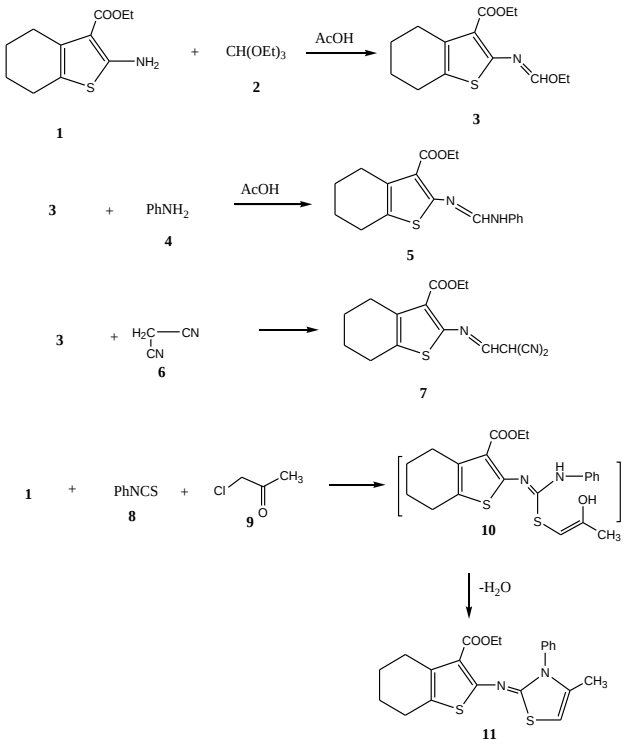

Scheme 1. Synthesis of compounds **3**, **5**, **7** and **11**

Next we studied the possibility of compound **1** to form thiourea derivative. Therefore, compound **1** was reacted with phenylisothiocyanate (**8**) in ethanol solution to give the *N*-phenylthioura derivative **12**. The latter reacted with ethyl chloroacetate (**13**) in ethanol to give the thiazole derivative **14**. The structure of compound **14** was confirmed on the basis of analytical and spectral data. Thus the ^{1}H-NMR showed a triplet at δ 1.16 ppm for CH_3 group, a multiplet at δ 1.48-1.73 ppm indicating four $4CH_2$, a quartet at δ 4.23 ppm for ethyl CH_2 group, a singlet at δ 6.14 ppm corresponding to H-2 thiazole, a multiplet at δ 7.25–7.38 ppm for C_6H_5 group, and a singlet at δ 10.31 ppm for OH. Similarly, the reaction of compound **12** with α-bromo-4-chloroacetophenone (**15**) gave the thiazole derivative **16**.

Compound **12** was also used to synthesize pyrimidine substituted derivatives with potential biological activities. Therefore, the reaction of compound **12** with malononitrile (**6**) or ethyl cyanoacetate (**17**) gave the 4,6-diamino-pyrimidine derivatives **18a** and **18b**, respectively. On the other hand the reaction of compound **12** with ethyl acetoacetate (**19**) gave the 4-methyl-6-oxopyrimidine derivative **20**. The reaction took place through ethanol and water elimination. The analytical and spectral data of compounds **18a,b** and **20** were consistent with their respective structures.

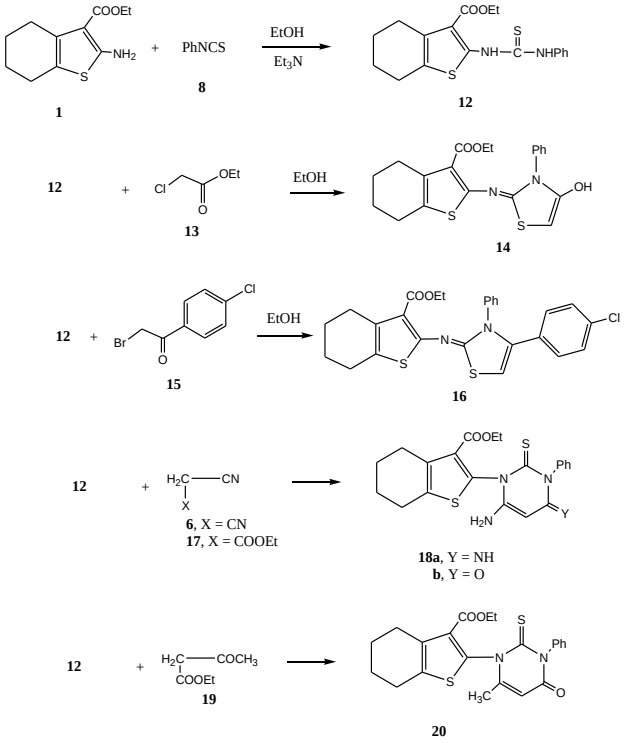

Scheme 2. Synthesis of compounds **12**, **14**, **16**, **18a,b** and **20**

The reaction of compound **12** with acetylacetone (**21**), however, gave 4,6-dimethyl-6-hydroxypyrimidine derivative **22**. The latter compound, due to the presence of the acidic pyrimidine H-5, was coupled with benzenediazonium chloride to form the phenylazo derivative **24**. Compound **12** underwent ready cyclization in 1,4-dioxane and piperidine to give the hexahydrobenzo[4,5]-thieno[2,3-*d*]pyrimidine derivative **25**. The ^{1}H-NMR spectrum of compound **25** showed a multiplet at δ 1.60-1.94 ppm corresponding to four CH_2 groups, a multiplet at δ 7.21-7.38 ppm for C_6H_5 group and a singlet at δ 10.62 ppm for SH group.

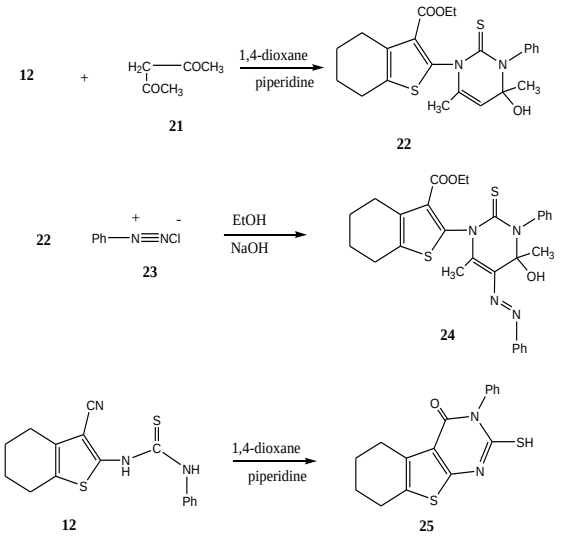

Scheme 3. Synthesis of compounds **22**, **24** and **25**

In vitro cytotoxicity evaluation of synthesized compounds.

The newly synthesized compounds were evaluated towards three cancer cell lines, namely [MCF-7 (breast adenocarcinoma), NCI-H460 (non-small cell lung cancer), SF-268 (CNS cancer)] and normal fibroblasts cells (WI38), and results obtained were presented in Table 1. The data obtained showed that some of the compounds proved to be promising candidate for antitumor applications.

The results were compared to the anti-proliferative effects of the reference control doxorubicin. All the compounds were dissolved in DMSO at 1.0 mg mL^{-1} concentration immediately before using and diluted just before addition to the cell culture. The data (Table 1) represents means ± SEM of three independent experiments performed in duplicate. The results indicated that most compounds showed substantial growth inhibitory effects against the human tumor cells at the concentrations tested.

Structure activity relationship

It is clear from Table 1 that compound **1** and **3** showed low potency against the three cancer cell lines investigated. The reaction of compound **3** with aniline gave compound **5** which showed high cytotoxicity against the three cancer cell lines. Compound **7** resulted from the reaction of compound **5** with malononitrile showed very low potency. The thiazole derivative **11** showed high potency and its cytotoxicity was higher than that of the thiazole derivatives **14** and **16**. Considering the pyrimidine derivatives **18a** and **18b** it is clear that compound **18a** with the C=NH moiety showed higher potency than **18b** with the C=O moiety. For the pyrimidine derivatives **22**-**25**, it is obvious that the hexahydrobenzo[4,5]-thieno[2,3-*d*]pyrimidine derivative **25** with the SH moiety showed the highest cytotoxicity among these compounds.

Table 1. Effect of synthesized compounds in GI_{50} (μM) on the growth of three human tumor cell lines and normal human cell line

Compound No..	GI_{50} (μM)[a]			
	MCF-7	NCI-H460	SF-268	WI-38
1	18.20 ± 2.23	14.29 ± 2.26	8.01 ± 2.39	>100
3	22.8 ± 7.21	20.8 ± 3.70	18.31 ± 1.89	> 100
5	8.29 ± 4.06	6.81 ± 2.29	15.29 ± 6.39	>100
7	72.02 ± 3.38	70.19 ± 8.24	68.21 ± 6.29	68.70± 10.2
11	0.01 ± 0.001	0.02 ± 0.006	0.06 ± 0.004	> 100
12	34.52 ± 2.24	28.67 ± 2.68	18.38 ± 8.65	>100
14	38.0 ± 3.92	30.81 ± 4.61	41.30 ± 2.92	>100
16	21.28 ± 6.18	20.19 ± 4.67	17.20 ± 4.63	>100
18a	0.01 ± 0.003	0.06 ± 0.008	0.03 ± 0.009	>100
18b	28.4 ± 6.18	26.05 ± 5.02	24.37 ± 2.49	>100
20	18.29 ± 3.51	14.11 ± 3.36	10.18 ± 3.53	>100
22	10.80 ± 2.39	12.02 ± 4.11	14.30 ± 2.12	>100
24	11.75 ± 1.16	14.58 ± 2.07	19.40 ± 24.22	>100
25	0.86± 0.01	0.53 ± 0.02	0.08 ± 0.006	>100
Doxorubicin	0.04 ±0.008	0.09 ± 0.008	0.09 ± 0.007	>100

[a]Drug concentration required to inhibit tumor cell proliferation by 50% after continuous exposure for 48 h; data are expressed as means ± SEM of three independent experiments performed in duplicates; *Doxorubicin was used as positive control.

Table 2. Toxicity of the most potent compounds against the cancer cell lines

Compound No.	Concentration, μg mL^{-1}	Mortality[a]	Toxicity	LC_{50}	Upper 95% lim.	Lower 95% lim.
5	10	6	Very toxic	16.06	-	-
	100	5				
	1000	10				
11	10	3	Very toxic	16.30	-	-
	100	5				
	1000	10				
18a	10	0	Non toxic	977.18	-	-
	100	0				
	1000	3				
22	10	0	Harmful	512.30	114.29	80.32
	100	7				
	1000	10				
24	10	0	Non toxic	904.29	-	-
	100	1				
	1000	4				
25	10	0	Non toxic	922.30	-	-
	100	0				
	1000	3				

[a]Ten organisms (*A. salina*) tested for each concentration.

Toxicity

Bioactive compounds are often toxic to shrimp larvae. Therefore, in order to monitor these chemicals, *in vivo* lethality to shrimp larvae (*Artemia salina*), Brine-Shrimp Lethality Assay[12] was used. Results were analyzed with LC_{50} program to determine LC_{50}values and 95 % confidence intervals.[13] Results are given in Table 2 for the compounds which exhibited optimal cytotoxic effect against cancer cell lines; the six compounds are **5**, **11, 18a, 22**, **24** and **25.** The shrimp lethality assay is considered as a useful tool for preliminary assessment of toxicity, and it has been used for the detection of fungal toxins, plant extract toxicity, heavy metals, cyanobacteria toxins, pesticides, and cytotoxicity testing of dental materials,[14] natural and synthetic organic compounds.[12] It has also been shown that *A. Salina* toxicity test results have a correlation with rodent and human acute oral toxicity data. Generally, a good correlation was obtained between *A. Salina* toxicity test and the rodent data. Likewise, the predictive screening potential of the aquatic invertebrate tests for acute oral toxicity in man, including *A. Salina* toxicity test, was slightly better than the rat test for test compounds.[15]

In order to prevent the toxicity results from possible false effects originated from solubility of compounds and DMSO's possible toxicity effect, compounds were prepared by dissolving in DMSO in the suggested DMSO volume ranges. It is clear from Table 2 that compounds **18a, 24**, and **25** showed no toxicity against the tested organisms. On the other hand, compound **5** and **11** were very toxic, and in addition, compounds **22** is harmful.

Experimentals

All melting points were determined using an Electro thermal digital melting point apparatus and are uncorrected. IR spectra (KBr disks) were recorded on a FTIR plus 460 or Pye Unicam SP-1000 spectrophotometer. ^{1}H-NMR and ^{13}C-NMR spectra were recorded with Varian Gemini-200 (200 MHz) (Cairo University) and Jeol AS 500 MHz (National Research center) instruments in DMSO-d6 as solvent using TMS as internal standard. Chemical shifts are expressed as δ ppm. The mass spectra were recorded with Hewlett Packard 5988 A GC/MS system and GCMS-QP 1000 Ex Shimadzu instruments. Analytical data were obtained from the Micro-analytical Data Unit at Cairo University and were performed on Vario EL III Elemental CHNS analyzer.

Ethyl 2-((ethoxymethylene)amino)-4,5,6,7-tetrahydrobenzo[b]-thiophene-3-carboxylate (3).

To a solution of **1** (2.25 g, 0.01 mol) in acetic acid (20 mL), ethylorthoformate (1.06 g, 0.01 mol) was added. The reaction mixture was heated under reflux for 2 h, then cooled and neutralized by pouring onto ice/water mixture. The solid product formed was collected by filtration and crystallized from acetic acid.

Compound **3:** Yellow crystals, yield: 80 % (2.20 g); m.p: 180-184 °C. IR (KBr): ν/cm^{-1} = 2990-2938 (CH_2, CH_3), 1689 (CO), 1622 (C=N). ^{1}H-NMR (DMSO-d_6): δ = 1.20, 1.16 (2t, 6H, $2CH_3$), 1.73-2.54 (m, 8H, $4CH_2$), 4.12, 4.22 (2q, 4H, $2CH_2$), 6.56 (s, 1H, CH). MS (relative intensity) m/z: 281 (M^+, 20 %). Analysis for $C_{14}H_{19}NO_3S$ Calcd: 59.76; H, 6.81; N; 4.98; S, 11.40. Found: C, 60.01; H, 6.98; N, 5.33; S, 11.64 %.

Ethyl 2-(((phenylamino)methylene)amino)-4,5,6,7-tetrahydro-benzo[b]thiophene-3-carboxylate (5) and ethyl 2-(2,2-dicyano-ethylidene)amino)-4,5,6,7-tetrahydrobenzo[b]thiophene-3-car-boxylate (7)

General procedure: To a mixture of equimolar amount of compound **3** (2.81 g, 0.01 mol) in acetic acid (20 mL), either aniline (0.93 g, 0.01 mol) or malononitrile (0.66 g, 0.01 mol) was added. The reaction mixture was heated under reflux for 2 hours, and then cooled by pouring onto ice/water mixture. The solid product formed collected by filtration and crystallized from acetic acid.

Compound **5**: Yellow crystals, yield: 65 % (2.10 g); m.p. 220-224 °C. IR (KBr): ν/ cm^{-1} = 3480-3320 (NH), 3050 (CH-aromatic), 2990, 2960 (CH_3, CH_2), 2217 (CN), 1689 (CO), 1622 (C=C). ^{1}H-NMR (DMSO-d_6): δ = 1.12 (t, 3H, CH_3), 1.66-1.95 (m, 8H, $4CH_2$), 4.22 (q, 2H, CH_2), 6.65 (s, 1H, CH), 7.30-7.46 (m, 5H, C_6H_5), 8.32 (s, 1H, NH). MS (relative intensity) m/z: 328 (M^+, 22%). Analysis for $C_{18}H_{20}N_2O_2S$ Calcd: C, 65.83; H, 6.14; N; 8.53; S, 9.75. Found: C, 65.66; H, 5.92; N, 8.72; S, 9.80 %.

Compound **7:** Brown crystals, yield: 77 % (2.30 g); m.p. 198-202 °C. IR (KBr): ν/cm^{-1} = 2988, 2971 (CH_3, CH_2), 1692 (CO). ^{1}H-NMR (DMSO-d_6): δ = 1.16 (t, 3H, CH_3), 1.65-2.68 (m, 8H, $4CH_2$), 4.25 (q, 2H, CH_2), 6.11, 6.35 (2d, 2H, 2CH). MS (relative intensity) m/z: 301(M^+, 28%). Analysis for $C_{15}H_{15}N_3O_2S$ Calcd: C, 59.78; H, 5.02; N; 13.94; S, 10.64. Found: C, 59.93; H, 4.92; N, 14.11; S, 10.80 %.

Synthesis of (2)-2-(4-methyl-3-phenylthiazole-2(3H)-ylidenea-mino)-4,5,6,7-tetrahydrobenzo[b]thiophene-3-carbonitrile (11).

To an equimolar amount of **1** (2.25 g, 0.01 mol) in absolute ethanol (25 mL) containing a catalytic amount of triethylamine (0.50 mL), α-chloroacetone **9** (0.92 g, 0.01 mol) and phenylisothiocyanate **8** (1.35 g, 0.01 mol) were added. The reaction mixture was heated under reflux for 3 hours and cooled by pouring onto acidified ice/water mixture. The solid product formed in each case was collected by filtration, washed with water, and crystallized from absolute ethanol.

Compound **11:** Yellow crystals, yield: 68 % (2.70 g); m.p. 180-184 °C. IR (KBr): ν/ cm^{-1} = 3066 (CH aromatic), 2974, 2983 (CH_3, CH_2), 1688 (CO), 1648 (exocyclic C=N), 1580 (C=C). ^{1}H-NMR (DMSO-d_6): δ = 1.13 (t, 3H, CH_3), 2.29 (s, 3H, CH_3), 1.54-2.30 (m, 8H, $4CH_2$), 4.21 (q, 2H, CH_2), 6.32 (s, 1H, thiazole), 7.27-7.38 (m, 5H, C_6H_5). MS (relative intensity) m/z: 398 (M^+, 34 %). Analysis for $C_{21}H_{22}N_2O_2S_2$ Calcd: C, 63.29, H, 5.56; N; 7.03; S, 16.09. Found: C, 63.08; H, 5.48; N, 6.88; S, 16.27 %.

Ethyl 2-(3-phenylthioureido)-4,5,6,7-tetrahydrobenzo[b]thio-phene-3-carboxylate (12).

To an equimolar amount of compound **1** (2.25 g, 0.01 mol) in absolute ethanol (25 mL) containing a catalytic amount of triethylamine (0.50 mL) phenylisothiocyanate (1.35 g, 0.01 mol) was added. The reaction mixture was heated under reflux for 2 hours and cooled by pouring onto acidified ice/water mixture. The solid product formed was collected by filtration, washed with water, and crystallized from absolute ethanol.

Compound **12:** Orange crystals, yield: 60 % (2.30 g); m.p. 130-132 °C. IR (KBr): ν/ cm^{-1} = 3487, 3349 (2 NH), 3045 (CH-aromatic), 1690 (CO), 1580 (C=C), 1253 (C=S). ^{1}H-NMR (DMSO-d_6) : δ = 1.13 (t, 3H, CH_3), 1.54-2.65 (m, 8H, $4CH_2$), 4.22 (q, 2H, CH_2), 7.28 –7.39 (m, 5H, C_6H_5), 8.23, 8.41(2s, 2H, 2NH). MS (relative intensity) m/z: 360 (M^+, 22). Analysis for $C_{18}H_{20}N_2O_2S_2$ Calcd: C, 59.97; H, 5.59; N, 7.77; S, 17.79. Found: C, 60.12; H, 5.39; N, 7.93; S, 18.80 %.

Ethyl 2-((4-hydroxy-3-phenylthiazol-2(3H)-ylidene)amino)-4,5,6,7-tetrahydrobenzo[b]thiophene-3-carboxylate (14) and ethyl 2-(4-(4-chlorophenyl)-3-phenylthiazol-2(3H)-ylidene)ami-no)-4,5,6,7-tetrahydrobenzo[b]thiophene-3-carboxylate (16)

General procedure: To a solution of **12** (3.60 g, 0.01 mol) in absolute ethanol (25 mL) containing a catalytic amount of triethyleamine (0.50 mL), either ethyl chloroacetate (1.22 g, 0.01 mol) or α-bromo-4-chloroacetophenone (2.33 g, 0.01 mol) was added. The reaction mixture was heated under reflux for 2 hours. The formed solid products, in each case, upon pouring onto ice/water mixture containing few drops of hydrochloric acid were collected by filtration and crystallized from absolute ethanol.

 DOI: 10.17628/ecb.2016.5.82-87

Compound **14**: brown crystals, yield: 80 % (3.20 g); m.p. 190-193 ºC. IR (KBr): ν/ cm^{-1} = 3045 (CH aromatic), 2980-2873 (CH_3, CH_2), 1706 (C=O), 1618 (C=N). ^{1}H-NMR (DMSO-d_6) : δ = 1.16 (t, 3H, CH_3), 1.48-1.73 (m, 8H, $4CH_2$), 4.23 (q, 2H, CH_2), 6.14 (s, 1H, thiazole H-2), 7.25–7.38 (m, 5H, C_6H_5), 10.31 (s, 1H, OH). MS (relative intensity) m/z: 400 (M^+, 38%). Analysis for $C_{20}H_{20}N_2O_3S_2$ Calcd: C, 59.98; H, 5.03; N; 6.99; S, 16.01. Found: C, 60.21; H, 4.92; N, 7.23; S, 15.85 %.

Compound **16:** Orange crystals, yield: 69 % (3.40 g); m.p. 67-69 ºC. IR (KBr): ν/cm^{-1} = 3050 (CH aromatic), 2977-2870 (CH_3, CH_2), 1677 (CO), 1629 (exocyclic C=N), 1436 (C=C). ^{1}H-NMR (DMSO-d_6): δ=1.l6 (t, 3H, CH_3), 1.49-2.80 (m, 8H, $4CH_2$), 4.24 (q, 2H, CH_2), 6.16 (s, 1H, thiazole H-2), 7.23–7.93 (m, 9H, C_6H_4, C_6H_5). MS (relative intensity) m/z: 495 (M^+, 62%). Analysis for $C_{26}H_{23}ClN_2O_2S_2$ Calcd: C, 63. 08; H, 4.68; N, 5.66; S, 12.95. Found: C, 62.83; H, 4.92; N, 5.80; S, 13.08 %.

Ethyl 2-(6-amino-4-imino-3-phenyl-2-thioxo-3,4-dihydropyrimidin-1(2H)-yl)-4,5,6,7-tetrahydrobenzo[b]thiophene-3-carboxylate (18a) and ethyl 2-(6-amino-4-oxo-3-phenyl-2-thioxo-3,4-dihydropyrimidin-1(2H)-yl)-4,5,6,7-tetrahydrobenzo[b]-thiophene-3-carboxylate (18b)

General procedure: To a solution of compound **12** (3.60 g, 0.01 mol), in absolute ethanol (25 mL) containing triethylamine (0.50 mL), either malononitrile (0.66 g, 0.01 mol) or ethyl cyanoacetate (1.13 g, 0.01 mol) was added. The reaction mixture was heated under reflux for 3 hours then poured into a beaker containing acidified ice/water mixture. The formed solid products were collected by filtration and crystallized from absolute ethanol.

Compound **18a:** Pale yellow crystals, yield: 77 % (3.20 g); m.p. >300 ºC. IR (KBr): ν/ cm^{-1} = 3469-3318 (NH_2, NH), 3070 (CH aromatic), 2994, 2840 (CH_3, CH_2), 1702 (CO), 1620 (exocyclic C=N), 1238 (C=S). ^{1}H-NMR (DMSO-d_6): δ = 1.14 (t, 3H, CH_3), 1.50-2.69 (m, 8H, $4CH_2$), 4.21 (q, 2H, CH_2), 4.53 (s, 2H, NH_2), 6.90 (s, 1H, pyrimidine H-5), 7.26-7.44 (m, 5H, C_6H_5), 8.22 (s,1H, D_2O exchangeable, NH). MS (relative intensity) m/z: 426 (M^+, 66 %). Analysis for $C_{21}H_{22}N_4O_2S_2$ Calcd: C, 59.13; H, 5.20; N, 13.13; S, 15.03. Found: C, 59.30; H, 4.39; N, 13.29; S, 14.92 %.

Compound **18b:** Pale yellow crystals, yield: 80 % (3.40 g); m.p. 233-236 ºC. IR (KBr): ν/ cm^{-1} = 3490, 3348 (NH_2), 3070 (CH aromatic), 2994, 2840 (CH_3, CH_2), 1702, 1688 (2CO), 1242 (C=S).^{1}H-NMR (DMSO-d_6): δ = 1.12 (t, 3H, CH_3), 1.44-2.71 (m, 8H, $4CH_2$), 4.23 (q, 2H, CH_2), 4.59 (s, 2H, NH_2), 6.93 (s, 1H, pyrimidine H-5), 7.29-7.40 (m, 5H, C_6H_5). MS (relative intensity) m/z: 427(M^+, 40%). Analysis for $C_{21}H_{21}N_3O_3S_2$ Calcd: C, 58.99; H, 4.95; N, 9.83; S, 15.00. Found: C, 59.14; H, 4.83; N, 9.64; S, 14.84%.

Ethyl 2-(6-methyl-4-oxo-3-phenyl-2-thioxo-3,4-dihydropyrimidin-1(2H)-yl)-4,5,6,7-tetrahydrobenzo[b]thiophene-3-carboxylate (20).

To a solution of compound **12** (3.60 g. 0.01 mol) in absolute ethanol (25 mL) containing a catalytic amount of piperidine (0.05 mL), ethyl acetoacetate (1.30 g, 0.01 mol) was added. The reaction mixture was heated under reflux for 3 hours then poured onto acidified ice/water mixture. The formed solid product was collected by filtration and crystallized from absolute ethanol.

Compound **20:** Pale yellow crystals, yield: 77 % (3.20 g); m.p. 288-292 ºC, IR (KBr): ν/ cm^{-1} = 3060 (CH-aromatic), 2980, 2878 (CH_3, CH_2), 1708, 1693 (2CO), 1539 (C=C), 1237 (C=S). ^{1}H-NMR (DMSO-d_6): δ = 1.13 (t, 3H, CH_3), 1.66-1.80 (m, 8H, $4CH_2$), 2.23 (s, 3H, CH_3), 4.20 (q, 2H, CH_2), 6.39 (s, 1H, pyrimidine H-5), 7.27-7.42 (m, 5H, C_6H_5). MS (relative intensity) m/z: 426 (M^+, 62 %). Analysis for $C_{22}H_{22}N_2O_3S_2$ Calcd: C, 61.95, H, 5.20; N, 6.57; S, 15.03. Found: C, 61.90; H, 5.43; N, 6.70; S, 15.28 %.

Synthesis of 4,5,6,7-tetrohydro-2-(2,3dihydro-4-hydroxy-4,6-dimethyl-3-phenyl-2-thioxopyrimidine-1(2H-yl) benzo[b]thiophene-3-carbonitrile (22).

To a solution of compound **12** (3.60 g. 0.01 mol) in absolute ethanol (25 mL) containing a catalytic amount of piperidine (0.05 mL), acetylacetone (1.00 g, 0.01mol) was added. The reaction mixture was heated under reflux for 3 hours then poured onto acidified ice/water mixture. The solid products were collected by filtration and crystallized from absolute ethanol.

Compound **22:** Pale yellow crystals, yield: 65 % (2.80 g); m.p. 166-168 ºC, IR (KBr): ν/cm^{-1} = 3055 (CH-aromatic), 2967, 2873 (CH_3, CH_2), 1704, 1690 (2CO), 1539 (C=C), 1232 (C=S). ^{1}H-NMR (DMSO-d_6): δ=1.12 (t, 3H, CH_3), 1.61-1.84 (m, 8H, $4CH_2$), 2.26, 2.44 (2s, 6H, $2CH_3$), 4.22 (q, 2H, CH_2), 6.36 (s, 1H, pyrimidine H-5), 7.29-7.40 (m, 5H, C_6H_5), 10.09 (s, 1H, OH). m/z: 442 (M^+, 73 %). Analysis for $C_{23}H_{26}N_2O_3S_2$ Calcd: C, 62.42; H, 5.92; N, 6.33; S, 14.49. Found: C, 62.32; H, 5.88; N, 6.42; S, 14.38 %.

Ethyl 2-(4-hydroxy-4,6-dimethyl-3-phenyl-5-(phenyldiazenyl)-2-thioxo-3,4-dihydropyrimidin-1(2H)-yl)-4,5,6,7-tetrahydrobenzo[b]thiophene-3-carboxylate (24)

To a cold solution (0-5 ºC) of **22** (4.42 g, 0.01 mol) containing sodium hydroxide (1.00 g), an equimolar amount of benzenediazonium chloride (0.01 mol) [prepared by adding sodium nitrite solution (0.70 g, 0.01 mol) in water (10 mL) to a cold solution (0-5 ºC) of aniline (0.93 g, 0.01 mol) in concentrated hydrochloric acid (30 mL)] was gradually added with continuous stirring. The solid product formed upon cooling in an ice-path was collected by filtration, washed with water, and crystallized from absolute ethanol.

Compound **24:** Pale yellow crystals, yield: 88 % (4.80 g); m.p. 210-212 ºC. IR (KBr): ν/ cm^{-1} = 3052 (CH-aromatic), 2997, 2870 (CH_3, CH_2), 1704, 1690 (2CO), 1539 (C=C), 1232 (C=S). ^{1}H-NMR (DMSO-d_6): δ = 1.12 (t, 3H, CH_3), 1.64-1.99 (m, 8H, $4CH_2$), 2.24, 2.46 (2s, 6H, $2CH_3$), 4.23 (q, 2H, CH_2), 7.22-7.43 (m, 10H, $2C_6H_5$), 10.22 (s, 1H, OH). MS (relative intensity) m/z: 546 (M^+, 55%). Analysis for $C_{29}H_{30}N_4O_3S_2$ Calcd: C, 63.71; H, 5.53; N, 10.25; S, 11.73. Found: C, 63.84; H, 5.70; N, 10.49; S, 11.93 %.

 DOI: 10.17628/ecb.2016.5.82-87

Synthesis of 4-imino-3-phenyl-3,4,5,6,7,8-hexahydrobenzo[4,5]-thieno[2,3-d]pyrimidine-2-thiol (25).

To a solution of compound **12** (3.60 g, 0.01) in 1,4-dioxane (25 mL) a catalytic amount of piperidine (0.5 mL) was added and the reaction mixture was heated under reflux for 3 hours. The formed solid product after pouring the solution into acidified ice/water mixture was collected by filtration and crystallized from 1,4-dioxane.

Compound **25:** Yellow crystals, yield: 69 % (2. 10 g); m.p. 177-180 ^{o}C. IR (KBr): ν/ cm^{-1} = 3056 (CH-aromatic), 2992, 2883 (CH_3, CH_2), 1701 (CO), 1542 (C=C), 1239 (C=S). ^{1}H-NMR (DMSO-d_6): δ = 1.60-1.94 (m, 8H, 4CH_2), 7.21-7.38 (m, 5H, C_6H_5), 10.62 (s, 1H, SH). MS (relative intensity) m/z: 314 (M^+, 40%). Analysis for $C_{16}H_{14}N_2OS_2$ Calcd: C, 61.12, H, 4.49; N, 8.91; S, 20.40. Found: C, 61.29; H, 4.38; N, 9.17; S, 20. 28 %.

Conclusions

In this work, we used ethyl 2-amino-4,5,6,7-tetrahydrobenzo[*b*]thiophene-3-carboxylate for the synthesis of various N-alkylated heterocyclic derivatives. The cytotoxicity of the synthesized products showed that compound **11**, **18a** and **25** were the most potent compounds towards the three cancer cell lines investigated. In addition, compound **18a** and **25** showed no toxicity against shrimp larvae.

References

[1]Dalvie, D. K. , Kalgutkar, A. S. , Khojasteh-Bakht, C. S. , Scott Obach, R. , O'Donnell, P.O., *Chem. Res. Toxicol*., **2002**, *15*, 269.

[2]Kagan, J., Arora, S. K. , Prakash, I. , Ustunol, A. , *Heterocylic*, **1983**, *20* (*7*), 1341.

[3]Gribble, G.W., Saulnier, M. G. , Sibi, M. P. , Obaze-Nutaitis, J. A. , *J. Org. Chem.*, **1984**, *49*, 4518.

[4]Bakker, *J.* , Gommers, F. *J.* , Nieuwenhuis, *I.* , Wynberg, H. , *J. Biol. Chem.* , **1979**, *254*, 1841.

[5]Iyengar, S. , Arnason, J. T. , Philogene, B. J. R. , Murand, P. , Werstink, N. H. , Timmins, G. , *Biochem. Phys.* , **1987**, *29 (1)*, 1.

[6]Matsuura, H. , Saxena, G. , Farmer, S.W. , Hancock, R. E. W. , Towers, G. H. N. , *Planta Med.* , **1996**, *62 (3)*, 256.

[7]Chan, G. F. Q. , Towers, G.H.N. , Mitchell, J. C. , *Phytochemistry*, **1975**, *14*, 2295.

[8]Hudson, J. B. , Graham, E. A. , Miki, N. , Towers, G. H. N. , Hudson, L. L. , Rossi, R. , Carpita, A. , Neri, D. *Chemosphere*, **1989**, *19*, 1329.

[9]Malmstroem, *J.* , Jonsson, M. , Cotgreave, I. A. , Hammarstro¨m, L. , Sjo¨ din, M. , Engmann, L. , *J. Am. Chem. Soc.* , **2001**, *123*, 3434.

[10]Nobles, W. L ., DeWitt Blanton, C. , Jr. , *J.* Pharm. Sci. , **1964**, *53*, 115.

[11]Shams, H. Z. ; Mohareb, R. M. ; Helal, M. H. Mahmoud, A., *Molecules*, **2011**, *16*, 52.

[12]Maltais R. , Fournier M. A. , Poirier D. , *Bioorg. Med. Chem.* , **2011**, *19*, 4652.

[13]Kanchithalaivan S. , Kumar R. R. , Perumal S. *Steroids*, **2013**, *78*, 409.

[14]Djigoué G. B., Kenmogne L. C. , Roy J. , Poirier D. , *Bioorg. Med. Chem. Lett.* , **2013**, *23*, 6360.

[15]Garry P. J. , Owen G. M. , Lashley D. W. , *Clin. Biochem.* **1974** , *7*, 119.

Received: 08.04.2016.
Accepted: 10.05.2016.

PREPARATION AND CHARACTERIZATION OF SOME NEW OXAZEPINE COMPOUNDS

Natiq G. Ahmed[a]* and Hussein Y. Al-Hashimi[a]

Keywords: Mannich bases, Schiff bases, oxazepines; benzo[1,3]oxazepines.

The ketonic compound (**1**) is synthesized from equal moles of morpholine, 4-nitrobenzaldehyde, and 3-nitro acetophenone. Schiff base compounds (**2**)-(**4**), prepared by reacting (**1**) with different aromatic amines (4-aminoantipyrine, *p*-phenylenediamine, 2-aminopyridine), contain a set of one or more of azomethine (-C=N-) groups that have been used in the preparation of many heterocyclic compounds, which when reacted with maleic anhydride give 1,3-oxazepine compounds (a ring with seven atoms) (**5**)-(**7**), and seven membered ring benzo[1,3]oxazepine compounds (**8**)-(**10**) are obtained by reaction with phthalic anhydride. The synthesized compounds are identified using physical (melting points, colour change, thin layer chromatography) and spectral methods such as IR, UV, and NMR spectra). The biological effectiveness of some of the prepared compounds is measured.

* Corresponding Authors
E-Mail: natiq.ahmad@yahoo.com
Chemistry Department, College of Education, Mosul University, Mosul, Iraq

Introduction

Mannich bases (β-amino ketones) are known to possess potent biological activities,[1] and are known for their use as additives in detergents, resins, polymers, surface active agents etc.[2] Schiff's bases, (RHC=N-R1, where R and R1 are alkyl, aryl, cycloalkyl or heterocyclic groups,[3]) are condensation products of primary amines with carbonyl compounds like Mannich bases exhibit a broad range of biological activities including antifungal, antibacterial, antimalarial, antiproliferative, anti-inflammatory, antiviral, and antipyretic properties.[4]

Oxazepine, un-saturated non-homologous seven membered heterocycle containing oxygen in position 1 and nitrogen in position 3, is prepared by the pericyclic cycloaddition of Schiff bases with maleic, phthalic, nitrophthalic and succinic anhydrides. Since oxazepine derivatives exhibit a vast variety of biological activities,[5] therefore some new oxazepine derivatives have been synthesized and studied for their biological activity.

Experimental

All reagents and chemicals are from BDH and Sigma-Aldrich, and have been used without further purification. Melting points are measured using hot stage Gallen Kamp melting point apparatus and are uncorrected (Maximum temperature 240 °C). The FT-IR spectra, in the range (4000-400) cm^{-1}, are recorded using KBr disk on Shimadzu FT-IR-8300 spectrophotometer. UV/VIS spectra are recorded on a Uv-Cary-100 spectrophotometer. ^1H NMR spectra are recorded on a BRUKER-400 MHz operating with TMS as an internal standard in $CDCl_3$ or DMSO-d_6 as a solvent. TLC is carried out by using alumina plates percolated with silica gel, supplied by Merck. Spots were detected with iodine vapour.

Synthesis of 3-morpholino-1-(3-nitrophenyl)-3-(4-nitrophenyl)propan-1-one (1)

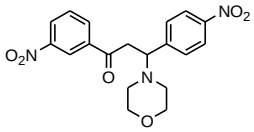

In a typical procedure,[6-8] an ethanolic solution (30 mL) of 4-nitrobenzaldehyde (1.51 g, 0.01 mol), 3-nitroacetophenone (1.65 g, 0.01 mol) and morpholine (0.88 mL, 0.01 mol) were mixed and continuously stirred for 4 h under ice cold condition. The solid formed is filtered and recrystallized using absolute ethanol. The purity of the compound is checked with TLC.

The obtained compound is off white in colour (77 %), m.p. 64-66 °C. Molecular formula $C_{19}H_{19}N_3O_6$. IR (KBr): 1689 cm^{-1} (C=O). UV-VIS (DMSO): 250 nm ($\pi \rightarrow \pi^*$), 325 nm ($n \rightarrow \pi^*$). ^1H NMR (400 MHz): δ = 7.8-8.16 (m, 8H, Ar-H), 3.32-3.35 (s, 4H, morpholine CH_2O), 2.48 (s, 4H, morpholino CH_2-N), 3.48 (s, 1H, CH), 2.67-2.72 (d, 2H, CH_2).

Synthesis of Schiff bases (2)- (4)

Schiff bases are prepared by adding few drops of glacial acetic acid with stirring to a solution of compound (**1**) (0.96 g, 0.0025 mol) in absolute ethanol (20 mL) followed by 0.0025 mol of 4-aminoantipyrine (**2**) or 2-aminopyridine (**4**) dissolved in 20 mL of absolute ethanol. For the preparation of compound (**3**), 0.005 mol of the compound (**1**) is mixed with (0.0025 mol) of *p*-phenylenediamine. The mixture is refluxed for 8-12 h with follow-up by TLC.

 DOI: 10.17628/ecb.2016.5.88-91

Table 2. Some physical properties of compounds (**2**)-(**10**).

Compound No.	Structure	Reaction Time (h)	Molecular formula and weight	m.p. in °C and colour	Yield %	R_f
2	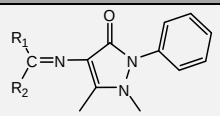	10	$C_{30}H_{30}N_6O_6$ 570	191-193 Light orange	80	0.83
3	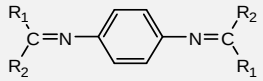	8	$C_{44}H_{42}N_8O_{10}$ 842	184-186 Yellow	77	0.76
4	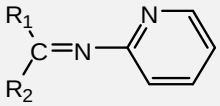	12	$C_{24}H_{23}N_5O_5$ 461	94-96 Reddish orange	94	0.85
5	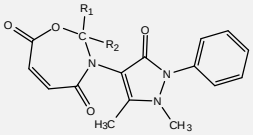	10	$C_{34}H_{32}N_6O_9$ 668	185-187 Reddish brown	73	0.61
6	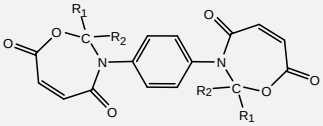	10	$C_{52}H_{46}N_8O_{16}$ 1038	167-169 Light brown	65	0.95
7	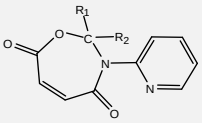	10	$C_{28}H_{25}N_5O_8$ 559	134-136 Yellow	93	0.88
8	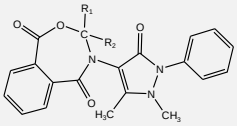	10	$C_{38}H_{34}N_6O_9$ 718	144-146 Reddish brown	82	0.66
9	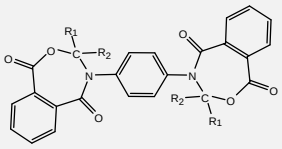	10	$C_{60}H_{50}N_8O_{16}$ 1138	221-223 Desert	68	0.70
10	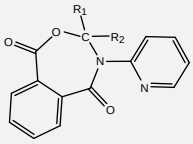	10	$C_{32}H_{27}N_5O_8$ 609	176-178 Yellow	54	0.82

R_1 = 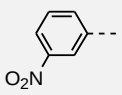 R_2 = 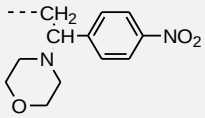

Table 2. UV and IR spectral characteristics of compounds (**1**)-(**4**).

Comp. No.	ν (cm-1) IR (KBr)								λ_{max}, nm
	Ar C-H	R C-H	C=O	C=N	C-N-	C-O-C	$-NO_2$	Others	
1	3099	2962, 2924, 2852, 2819	1689	----	1247	1008, 1105	1342	----	325, 250
2	3090 3066	2999, 2968,2920, 2850	----	1645	1249	1020, 1107	1338	C=O 1689 conj. 1612 C=C conj.	302, 247
3	3101 3043	2983, 2881, 2847	----	1595	1192	1012, 1107	1338	----	338, 261
4	3043	2912, 2881, 2847	----	1626	1180	1008, 1105	1340	C=N 1597 endo	359, 276

At the end of the reaction, solution is cooled to room temperature. The solvent is then evaporated to obtain the precipitate, which is recrystallized from absolute ethanol.

Synthesis of 1,3-oxazepine derivatives (5)-(7)

A mixture of Schiff base (**2**) or (**4**) (0.0004 mol) and 0.0006 mol of maleic anhydride in 20 mL of dry benzene is refluxed, and followed-up by TLC. At the end of the reaction, solution is cooled to room temperature and the solvent evaporated to obtain a precipitate which is washed with distilled water, filtered and recrystallized from absolute ethanol.[12,13]

The compound (**6**) is prepared by the same method except 0.0004 mol of the compound (**3**) and 0.0012 mol of maleic anhydride are used.

Synthesis of benzo[1,3]oxazepine derivatives (8)-(10)

A mixture of Schiff base (**2**) or (**4**) (0.0004 mol) and 0.0006 mol of phthalic anhydride in 20 mL of dry benzene is refluxed, and followed -up by TLC. At the end of the reaction, solution is cooled to room temperature and the solvent evaporated to obtain a precipitate, which is washed with distilled water, filtered and recrystallized from absolute ethanol.[12,14] The compound (**9**) is similarly prepared except 0.0004 mol of the compound (**3**) and 0.0012 mol of phthalic anhydride are used.

Physical properties and reaction time of compounds (**2**)-(**10**) are listed in Table 2.

Results and Discussion

A new ketone (**1**), a Mannich base, is synthesized from the reaction of 4-nitrobenzaldehyde, 3-nitroacetophenone and morpholine in ethanolic solution. The product is characterized using UV-VIS, IR and NMR spectra. Three new Schiff bases are synthesized from the reaction of compound (**1**) with 4-aminoantipyrine, 2-aminopyridine or *p*-phenylene diamine in absolute ethanol and in the presence of catalytic amount of acetic acid (Scheme 1).

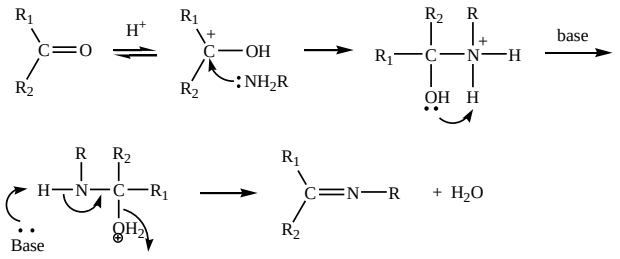

Scheme1. Mechanism of synthesis of Schiff base (**2**)-(**4**).

The main features of UV and IR spectra of the compounds **(1)-(4)** are given Table 2. The ^{1}H NMR spectrum of (**2**) showed the following peaks.

Compound (**2**): ^{1}H NMR (400 MHz): δ = 7.37-8.60 (m, 13H, Ar-H), 3.32 (s, 4H, morpholine CH_2O), 2.67 (s, 4H, morpholine CH_2N), 3.35 (t, 1H, CH), 3.24 (s, 3H, CH_3-N), 2.48 (s, 3H, CH_3-C=C), 2.72 (d, 2H, CH_2).

Oxazepines (**5**)-(**10**) are synthesized from the reaction of Schiff bases (**2**)-(**4**) with maleic or phthalic anhydride in dry benzene (Scheme 2).

The FT-IR spectrum,[13,14,18-20,22-24] of oxazepine compounds (**5**)-(**10**) showed the disappearance of peak of azomethine (C=N) group outside the ring. The new peaks which appears at 1689-1722 cm^{-1} can be attributed to the C=O group of ester and the peak at 1627-1693 is attributed to the C=O (amide) group. The UV/VIS Spectrum (in DMSO) shows absorption peak in the regions of 209-301 nm due to π → π* and 294-354 nm due to n → π* transitions.

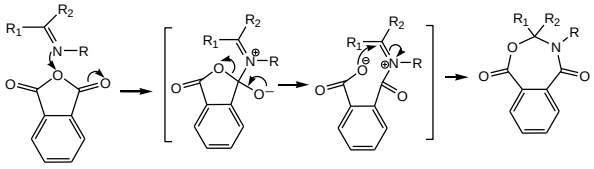

Scheme 2. Mechanism of synthesis of compounds (**5**) – (**10**).

Biological Studies

Biological activity has been studied[25,26,27] for some of the synthesized compounds by studying their impact on the growth of *Staphylococcus aureus*, *Escherichia coli* and *Pseudomonas aeruginosa*. The biological activity of compounds is determined by measuring the diameter of the empty region around the well (inhibition zone). The organisms are activated in a nutrient growth medium at 37 °C for 24 h prior to the experiments. The results of preliminary screening tests (Table 3) indicated that compounds (**1**, **3**, and **10**) showed moderate activity and compounds (**2**, **5**, and **6**) showed slight activity against *Staphylococcus aureus*. Compounds (**1**, **2**, **3**, **5**, **6**, and **10**) are slightly active against *Escherichia coli*. Compound (**3**) is moderately active and compounds (**1**, **2**, **5**, **6**, and **10**) are slightly active against *Pseudomonas aeruginosa.*

Table 3. Antibacterial activities of some prepared compounds.

Comp. No.	S. Aureus Gr +Ve	E. Coli Gr -Ve	P. Aeruginosa Gr -Ve
1	++	+	+
2	+	+	+
3	++	+	++
5	+	+	+
6	+	+	+
10	++	+	+

References

[1]Joshi, S., Khosla, N., Tiwari, P., *Bioorg. Med. Chem.*, **2004**, *12*, 571.

[2]Bala, S., Sharma, N., Kajal, A., Kamboj, S., Saini, V., *Inter. J. Med. Chem.*, **2014**, ID 191072.

[3]Arulmurugan, S., Kavitha, P. H., Venkatraman, R. P., *Rasayan J. Chem*., **2010**, *3*, 385.

[4]Przybylski, P., Huczyński, A., Pyta, K., Brzezinski. B., Bartl, F., *Curr. Org. Chem*., **2009**, *13*, 124.

[5]Dhanya, S., Ranjitha, C., Rama, M., Pai, K., *Int. J. Inno. Res. Sci. Eng. Technol.*, **2014**, *3*, 15357.

[6]Shanmugapriya, M., Jameel, A. A., Padusha, M. S., *Int. J. Chem. Tech. Res*., **2012,** *4*, 12.

[7]Jayachandramani, N., Priya, S., Kumaran, J. S., Sathya, D., Emelda, A. R., Mahalakshmi, S., *Int. J. Chem. Tech. Res.*, **2011**, *3*, 248.

[8]Shanmugapriya, M., Sulthana, A. R., Jameel, A. A., Padusha, M. S., *Int. J. Curr. Pharm. Clin. Res*., **2014**, *4*, 47.

[9]Hussain, Z., Yousif, E., Ahmed, A., Altaie, A., *Org. Med. Chem. Lett.*, **2014**, *4*, 1.

[10]Lakum, H. P., Shah ,D. R., Chikhalia, K. H., *Int. Lett. Chem. Phys. Astron*., **2014**, *38*, 56.

[11]Al-Mosawi, S. K., *Rese. J. Pharm. Bio. Chem. Sci*., **2014,** *5*, 411.

[12]Jassim, I. K., Jassim, W. K., Shubber, S. K., Reaad S., *Kerbala J. Pharm. Sci.*, **2014**, 12.

[13]Yass, I. A., *Kerbala J. Pharm. Sci*., **2010**, 49.

[14]Alrammahi, F. A., Alrammahi, A. S., *Int. J. Adv. Multidisc. Res*., **2014**, *1*, 38.

[15]Bele, D. S., Singhvi, I., *Int. J. Res. Pharm. Chem.*, **2011**, *1*, 1058.

[16]Mahmoud, M. J., Jassim, I. K., Mahmoud, M. A., *Baghd. Sci. J*., **2013**, *10*, 803.

[17]Wadher, S. J., Puranik , M. P., Karande, N. A., Yeole, P. G., *Int. J. Pharm. Tech Res*., **2009**, *1*, 22.

[18]Majeed, I. Y., Al-Saady, D., Saoud, S. A., *Int. J. Sci. Technol*., **2013**, *8*, 6.

[19]Sallal, Z. A., Ghanem, H. T., *J. Kufa Chem. Sci.*, **2011,**6**,**11.

[20]Hameed , A., *J. Al-Nahrain Univ.*, **2012**, *15*, 47.

[21]Al-Hashimi, H. Y. R., M.Sc. Thesis, *University of Mosul*, **2012**, 68.

[22]Aljamali, N. M., *J. Sci. & Inno. Res*., **2013**, *2*, 53.

[23]Yadav, V. S., Verma, P., Gupta, S., *Pelagia Res. Libr*., **2015,** *6*, 86.

[24]Naser, A. W., Abdullah, A. F., *J. Chem. Pharm. Res.*, **2014**,*6*, 872.

[25]Murrey, K. S., Murray, R., *Medical Microbiology*, 15th Ed., Elsevier, **2008**,.

[26]Tortora, G. J., Funke, B. R., Case, C. L., *Microbiology*, 10th Ed., Benjamin/Cummings, **2009**.

[27]Boon, N. A., Colledge, N. R., Walker, B. R., *Davidson's Principle and Practice of Medicine*, 20th Ed., Churchill Livingstone, **2006**, 686.

Received: 14.01.2016.
Accepted: 12.05.2016.

SYNTHESIS, CHARACTERIZATION AND BIOLOGICAL EVALUATION OF TRIAZINE BASED SCHIFF BASE METAL COMPLEXES

Kiran Singh,[a] Sunita Raparia[a]* and Shashi Raparia[b]

Keywords: 1,2,4-triazine, Schiff base, metal complexes, fluorescence, antimicrobial activity

A new series of Co(II), Ni(II), Cu(II) and Zn(II) complexes with a Schiff base derived from 4-amino-3-mercapto-5-oxo-1,2,4-triazine and 2,4-dichlorobenzaldehyde have been synthesized and characterized by spectroscopic studies. The coordination possibility of the Schiff base towards the metal ions have been determined by analytical, spectral (IR, ^{1}H NMR, electronic spectroscopy, fluorescence, ESR) and thermal techniques. IR and thermal data support the presence of coordinated water in the metal complexes. The low molar conductance values in DMF indicate the non-electrolytic nature of the metal complexes. All the synthesized metal complexes show enhancement in fluorescence intensity in comparison to the ligand. The cyclic voltammetric studies of the Co(II), Ni(II) and Cu(II) complexes suggested the single electron transfer quasi-reversible nature of the complexes. Antimicrobial studies of the ligand and its metal complexes have been carried out *in vitro* against gram positive (*S. aureus, B. subtilis*), gram negative bacteria (*E. coli, P. aeruginosa*) and yeasts (*S. cerevisiae, C. albicans*).

Corresponding Authors
Tel:+91 8397098959
E-Mail: sunitaraparia@gmail.com
[a] Department of Chemistry, Kurukshetra University, Kurukshetra, Haryana 136 119, India
[b] Department of Zoology, Kurukshetra University, Kurukshetra, Haryana 136 119, India

Introduction

The increasing number of infectious diseases and development of resistance by pathogens to most of the known antibiotics is becoming a serious health problem. To conquer this rapid development of drug-resistance, the design and synthesis of new compounds with effective and potent antimicrobial activities is of substantial need for medicinal chemists. Numerous 1,2,4-triazines are biologically active[1-4] and could be used as preventive and therapeutic agents against various diseases. The development of new drugs based on 1,2,4-triazines such as anticancer drug; tirapazamine and potent anticonvulsant; lamotrigine further reinforces the interest in synthesis of these compounds. Also, it has been reported that the triazine ring skelton possess significant antibacterial, antioxidant, antifungal, anti-tuberculosis and anti-inflammatory activities.[5-9] In addition, they have been used in dyes, agriculture[10] and present an important core in many natural[11-12] and synthetic[13-14] biologically active compounds. Triazine derivatives with additional N or S donor atoms exhibit strong chelating ability and provide potential binding sites for complexation with various metal ions.[15-16] Apart from the wide range of applications, the varied structural aspects of the coordination compounds derived from triazine derivatives cause considerable interest in their synthesis. The complexation of Schiff bases with transition metal ions further enhances their antimicrobial properties.[17-18] Recently, a novel antifungal agent named CTBT (7-chlorotetrazolo[5,1-c]benzo[1,2,4]triazine had been identified which induced oxidative stress in filamentous fungi[19] resulting in cell death. Encouraged by the above findings and as a part of our continuous effort, here we report the synthesis of some Schiff base metal complexes bearing the 1,2,4-triazine moiety with a view to explore their potency as better antimicrobial agents.

Experimental

Standard gravimetric methods were used to estimate the metal contents; cobalt was estimated as cobalt pyridine thiocyanate, nickel as nickel dimethyl glyoximate, copper was estimated as cuprous thiocyanate and zinc as zinc ammonium phosphate.[20] The IR spectra of the Schiff base and its Co(II), Ni(II), Cu(II) and Zn(II) complexes were recorded on a MB-3000 ABB Spectrophotometer in the 4000-250 cm^{-1} region. The electronic spectra of the complexes were recorded in DMF on a T 90 (PG Instruments ltd) UV/Vis spectrophotometer in the region of 1100-200 nm. The ^{1}H NMR spectra were recorded in DMSO-d_6 on a Bruker 300 MH_Z ACF 300 spectrometer at room temperature using TMS as an internal reference. The fluorescence spectra of the ligand and its metal complexes were recorded in DMF on SHIMADZU RF-5301 PC spectrophotometer. Thermal analysis of metal complexes in the range 50-800 °C was carried out on a Perkin Elmer (Pyris Diamond) instrument at a heating rate of 10°C Min^{-1}. The ESR spectra were performed on X-Band at a frequency of 9.1 GHz on a Varian E-112 ESR spectrometer under the magnetic field 3000 Gauss at SAIF, IIT Bombay. Cyclic voltammeter measurements were carried out in DMF on an Ivium Stat Electrochemical Analyzer using tetrabutylammonium perchlorate as supporting electrolyte. Magnetic moment measurements were carried out on a Vibrating Sample Magnetometer (Model 155) at Institute Instrumentation Centre, IIT Roorkee. The molar conductivity measurements of all the complexes were measured in DMF using 10^{-3} M solutions at room temperature on a Systronics-306 Conductivity Bridge.

Table 1. Analytical data of the ligand and its metal complexes

S. No.	Compound	Yield%	Elemental analysis calcd. (found) %			
			C	H	N	M
1	Schiff base ($C_{10}H_6N_4OSCl_2$)	84 %	39.88 (39.91)	2.01 (2.02)	18.60 (18.54)	-
2	Co(L)(OAc).3H_2O [$C_{12}H_{14}N_4O_6SCl_2Co$]	81 %	30.52 (30.47)	2.99 (3.02))	11.87 (11.83)	12.48 (12.42)
3	$Co(L)_2$.2H_2O [$C_{20}H_{14}N_8O_4S_2Cl_4Co$]	83 %	34.55 (34.57)	2.03 (2.03)	16.12 (16.18)	8.48 (8.46)
4	Ni(L)(OAc).3H_2O [$C_{12}H_{14}N_4O_6SCl_2Ni$]	82 %	30.54 (30.59)	2.99 (2.94)	11.87 (11.82)	12.44 (12.49)
5	$Ni(L)_2$.2H_2O [$C_{20}H_{14}N_8O_4S_2$ Cl_4Ni]	84 %	34.56 (34.49)	2.03 (2.08))	16.12 (16.11)	8.44 (8.41)
6	Cu(L)(OAc).H_2O [$C_{12}H_{10}N_4O_4SCl_2Cu$]	85 %	32.70 (32.65)	2.29 (2.32)	12.71 (12.68)	14.42(14.41))
7	$Cu(L)_2$ [$C_{20}H_{10}N_8O_2S_2Cl_4Cu$]	84 %	36.19 (36.23)	1.52 (1.54)	16.88 (16.84)	9.57 (9.58)
8	Zn(L)(OAc).3H_2O [$C_{12}H_{14}N_4O_6SCl_2Zn$]	77 %	30.11 (30.17)	2.95 (2.91)	11.71 (11.74)	13.66 (13.61)
9	$Zn(L)_2$.2H_2O [$C_{20}H_{14}N_8O_4S_2$ Cl_4Zn]	79 %	34.23 (34.21)	2.01 (2.06)	15.97 (15.94)	9.32 (9.34)

4-Amino-3-mercapto-5-oxo-1,2,4-triazine[21] was prepared by reported literature method.

4-(2,4-dichlorobenzylideneamino)-3-mercapto-5-oxo-1,2,4-triazine

To a solution of 4-amino-3-mercapto-5-oxo-1,2,4-triazine (0.5 g, 3.47 mmol) in absolute alcohol was added a solution of 2,4-dichlorobenzaldehyde (0.607 g, 3.47 mmol) in absolute alcohol and refluxed for four hours. The volume of the solution was reduced on a rotary evaporator. The product formed was filtered off, washed with ice cold methanol and recrystallized from the same solvent. Yield 84%; m.p.: 232-235°C

Synthesis of metal complexes (1:1)

The solutions of 0.20 g (0.66 mmol) of the ligand dissolved in ethanol were added with stirring to hot ethanolic solutions of Co(II) acetate (0.17 g, 0.66 mmol), Ni(II) acetate(0.17 g, 0.66 mmol), Cu(II) acetate (0.13 g, 0.66 mmol) and Zn(II) acetate (0.15 g, 0.66 mmol) respectively. The corresponding solid complexes were filtered, washed several times with warm water, followed by ethanol and acetone and finally dried.

Synthesis of metal complexes (1:2)

The hot ethanolic solutions of Co(II) acetate (0.17 g, 0.66 mmol), Ni(II) acetate (0.17 g, 0.66 mmol), Cu(II) acetate (0.13 g, 0.66 mmol) and Zn(II) acetate (0.15 g, 0.66 mmol) were added to the hot ethanolic solutions of the ligand (0.40 g, 1.32 mmol) with continuous stirring. The precipitates formed immediately were filtered off, washed with warm water, ethanol followed by acetone and dried.

Biological assay

The antimicrobial activity of the synthesized compounds was evaluated *invitro* by the agar well diffusion method against the bacteria (*Staphylococcus aureus* MTCC 96; *Bacillus subtilis* MTCC 121, *Escherichia coli* MTCC 1652; *Pseudomonas aeruginosa* MTCC 741) and yeasts (*Candida albicans* MTCC 227; *Saccharomyces cerevisiae* MTCC 170). The bacteria were subcultured on Nutrient agar whereas yeast on Malt yeast agar. Ciprofloxacin and amphotericin B was used as the standard antibacterial and antifungal drug respectively. All the microbial cultures were procured from Microbial Type Culture Collection (MTCC); IMTECH, Chandigarh. The activity was measured in terms of zone of inhibition appearing around the well against bacteria and fungus. The procedure was performed in three replicate plates for each organism and the mean values of the diameter of inhibition zones ± standard deviations were calculated.

The *in vitro* minimal inhibitory concentrations **(**MICs) of the various compounds were determined by modified agar well diffusion method[15].

Results and discussion

The elemental analysis data of the metal complexes is given in Table 1. The Schiff base is soluble in common organic solvents whereas the metal complexes are only soluble in DMF and DMSO. All complexes are colored non-hygroscopic solids and stable at room temperature. The molar conductance values found (12-16 ohm^{-1} cm^2 mol^{-1}) indicate non-electrolytic behavior of all the complexes.

IR spectra

The IR spectra of the complexes are consistent with the structural data given in this paper (Table 2). The band at 1605 cm^{-1} in the spectrum of the free Schiff base is assigned to the azomethine (–CH=N) group. This band is shifted to lower frequencies (1582-1589 cm^{-1}) in the spectra of metal complexes indicating the coordination of the –CH=N nitrogen to the metal ion.[22] A characteristic strong band at 2650 cm^{-1} due to -SH in the spectrum of ligand disappeared on complex formation[23] indicating deprotonation and coordination through sulphur. The spectra of the metal complexes exhibit a broad band around 3171-3410 cm^{-1} due to ν (OH) which is assigned to water molecules associated with the complexes.[24] The coordination of ligand to the metal centers through the azomethine nitrogen atom and sulfur atom of the triazine ring is further substantiated by ν (M-N)[25,26] and ν (M-S)[26] stretching bands in the range 460-470 cm^{-1} and 315-345 cm^{-1} respectively, in the spectra of metal complexes confirming binding of the ligand to center metal ions.

Table 2. Important IR spectral bands (cm^{-1}) of Schiff base and its metal complexes

Compound	ν(N=CH)	ν(C-S)	ν(S-H)	ν(OOCCH$_3$)	ν(H$_2$O/OH)	ν(M-S)	ν(M-N)
Schiff base	1605	-	2650	-	-	-	-
Co(L)(OAc).3H$_2$O	1582	764	-	1736	3255	345	470
Co(L)$_2$.2H$_2$O	1589	756	-	-	3325	318	468
Ni(L)(OAc).3H$_2$O	1582	756	-	1744	3255	341	470
Ni(L)$_2$.2H$_2$O	1582	756	-	-	3374	342	470
Cu(L)(OAc).H$_2$O	1586	756	-	1774	3410	318	468
Cu(L)$_2$	1589	756	-	-	-	315	470
Zn(L)(OAc).3H$_2$O	1582	756	-	1744	3171	342	470
Zn(L)$_2$.2H$_2$O	1587	756	-	-	3286	342	468

^{1}H NMR Spectra

The ^{1}H NMR data of the Schiff base and its Zn(II) complexes have been summarized in Table 3. A singlet at δ 8.77 in the spectrum of ligand is assigned to the proton attached to imino (-CH=N-) group. The signal of azomethine proton shows a downfield shift in the spectra of 1:1 and 1:2 Zn(II) complexes indicating the coordination of nitrogen with the metal ion. The spectrum of the free ligand exhibits a signal at 13.7 ppm for the thiol proton. The absence of the signal for –SH proton in the spectra of Zn(II) complexes indicates the coordination of Schiff base through sulfur atom to the metal ion by deprotonation of the thiol group[15]. The aromatic protons of the Schiff base appeared in the region 7.38 - 8.19 ppm. These signals remained almost unaltered in the spectra of metal complexes.

Table 3. ^{1}H NMR spectral data of Schiff base and its Zn(II) complexes

Compounds	^{1}H NMR (ppm)
Schiff base	8.19 (d, 1H, Ar-H), 7.38 (s, 1H, Ar-H), 7.57(s, 1H, triazine -H), 7.26 (d, 1H, Ar-H), 8.77 (s,1H, -N=CH-), 13.7 (s, 1H, -SH)
Zn(L)(OAc).3H$_2$O	8.16 (d, 1H, Ar-H), 7.59 (s, 1H, triazine-H), 7.39 (s, 1H, Ar-H), 7.25 (d, 1H, Ar-H), 8.82 (s, 1H, -N=CH-)
Zn(L)$_2$ .2H$_2$O	8.18 (d, 2H, Ar-H), 7.57 (s, 2H, triazine -H), 7.37 (s, 2H, Ar-H), 7.16 (d, 2H, Ar-H), 8.86 (s, 2H, -N=CH-)

Electronic spectra and magnetic moment studies

The electronic spectral and magnetic moment data are given in Table 4. Two absorption bands in the region, 10893 cm^{-1} – 11,086 cm^{-1} (ν_1) and 20492 - 21008 cm^{-1} (ν_3) have been observed in the electronic spectra of the 1:1 and 1:2 Co(II) complexes indicative of $^4T_{1g}$ (F) → $^4T_{2g}$ (F) and $^4T_{1g}$ (F) → $^4T_{1g}$ (P) transitions[27] respectively. These transition are suggestive of octahedral geometry around the Co(II) ion. The magnetic moment values of 4.4 and 4.6 BM for the 1:1 and 1:2 Co(II) complexes further support octahedral geometry[23]. The electronic spectra of the Ni(II) complexes exhibits three absorption bands in the region 10,148 - 10,173 cm^{-1} (ν_1), 17,212 – 17,241 cm^{-1} (ν_2) and 23,981 – 24,272 cm^{-1} (ν_3) due to $^3A_{2g}$ (F) → $^3T_{2g}$ (F), $^3A_{2g}$ (F) → $^3T_{1g}$ (F) and $^3A_{2g}$(F) → $^3T_{1g}$ (P) transitions, respectively. These transitions support octahedral geometry for the Ni(II) ion[26]. The magnetic moment values (3.18 and 3.23 BM) further confirm the above geometry[28]. The ligand field parameter[29] Dq, B, β, β % have been calculated for the Co(II) and Ni(II) complexes (Table 4). The values of these parameters indicate partial covalent character of the metal-ligand bond.

In the electronic spectra of 1:1 and 1:2 Cu(II) complexes, a single absorption band at 18904 and 18248 cm^{-1} respectively, has been assigned to $^2B_{1g}$ → $^2A_{1g}$ transition, characteristic of square planar geometry around the Cu(II) ion[30]. The magnetic moment values for the Cu(II) complexes (1.81 and 1.83) are in agreement with those reported for square planar complexes.

Fluorescence Spectral Studies

The fluorescence properties of the ligand and its metal complexes have been studied at room temperature in 10^{-3} DMF solutions with excitation wavelength 290 nm. The Schiff base shows a weak band with fluorescence intensity of 80 (345 nm). The complexes exhibit strong bands with fluorescence intensity of 263 (334 nm) for Co(II), 143 (344 nm) for Ni(II), 264 (344) nm for Cu(II) and 677 (348) nm for Zn(II) complexes (Fig. 1).

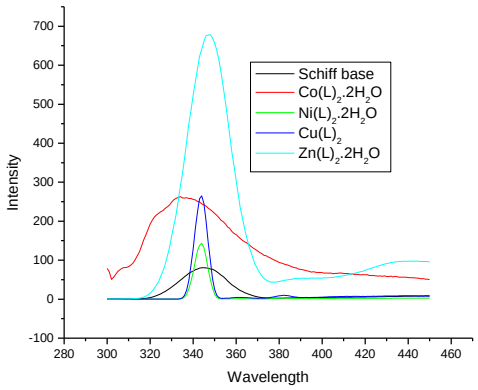

Figure 1. Fluorescence spectra of Schiff base and its metal complexes.

The increase in emission maxima is in the order of Schiff base < Ni(II) < Co(II) < Cu(II) < Zn(II). The higher fluorescence intensity of the complexes as compared to the ligands may be attributed to increased rigidity of the ligand on coordination, inhibition of the PET process, etc., thereby, reducing the loss of energy by thermal vibrational decay.[31,32]

 DOI: 10.17628/ecb.2016.5.92-98

Table 4. Electronic spectral data and ligand field parameters of metal complexes

Compound	Transitions (cm^{-1})			*Dq* cm^{-1}	*B* cm^{-1}	ν_2/ν_1	β	β%	μ_{eff} (BM)
	ν_1	ν_2	ν_3						
$Co(L)(OAc).3H_2O$	11086	23374†	20492	1228.7	707	2.10	0.73	27.17	4.40
$Co(L)_2.2H_2O$	10893	23024†	21008	1223.1	757	2.11	0.78	22.05	4.60
$Ni(L)(OAc).3H_2O$	10173	17212	24272	1017.3	731	1.69	0.70	29.78	3.18
$Ni(L)_2.2H_2O$	10148	17187	24226	1014.8	731	1.69	0.70	29.75	3.23

†Calculated value

Table 5. Thermogravimetric data of metal complexes

Compound	Temperature, °C	Decomposed moiety	Mass %		Residue %	
			Calcd.	Found	Calcd.	Found
$Co(L)_2.2H_2O$	110-215	H_2O	5.18	5.27	10.77	10.86
	215-420	Organic moiety	45.73	45.56		
	421-515	Triazine	38.25	38.14		
$Ni(L)(OAc).3H_2O$	115-250	H_2O	11.44	11.62	15.8	15.74
	250-400	Organic moiety	46.19	46.11		
	400-510	Triazine	26.48	26.55		
$Cu(L)(OAc).H_2O$	110-170	H_2O	4.08	4.10	18.03	18.09
	170-410	Organic moiety	49.46	49.35		
	410-650	Triazine	28.36	28.29		
$Zn(L)_2.2H_2O$	105-220	H_2O	5.13	5.15	11.6	11.44
	220-410	Organic moiety	45.31	45.87		
	410-495	Triazine	37.91	37.23		

The Zn(II) complexes exhibit highest fluorescence emission which may be due to stable d^{10} configuration. Enhanced fluorescence properties exhibited by the metal complexes may offer wide applicability as fluorescent probes, sensor devices and in various fields of medicine.

Thermal analysis

Thermogravimetric analysis of $Co(L)_2.2H_2O$, $Ni(L)OAc.3H_2O$, $Cu(L)(OAc).H_2O$ and $Zn(L)_2.2H_2O$ was carried out in atmospheric air at a heating rate of 10 °C min^{-1} up to 800 °C. The data are provided in Table 5. The TG curve of $Co(L)_2.2H_2O$ indicates first weight loss of 5.27 % (calcd. 5.18 %) in the temperature range 110-215 °C attributed to loss of three coordinated water molecules. The second step represents a mass loss of 45.56 % (calcd. 45.73 %) from 215 – 420 °C corresponding to the loss of organic moiety. The third step shows decomposition of triazine ring with mass loss of 38.14 % (calcd 38.25 %) from 421 °C to 515 °C leaving CoO as residue. For complex, $Ni(L)OAc.3H_2O$, first weight loss of 11.62 % (calcd. 11.44 %) occurs between 115 ˚C and 250 ˚C, attributed to the loss of three coordinated water molecules. The subsequent steps with weight loss of 46.11% (calcd. 46.19 %) within the temperature range 250 - 400˚C and weight loss of 26.55 % (calcd. 26.48 %) from 400 – 510 ˚C correspond to the decomposition of organic moiety and triazine ring respectively. The TG curve of $Cu(L)(OAc).H_2O$ shows three decomposition steps within the temperature range 110-170 ˚C, 170-410 ˚C and 410-650 ˚C corresponding to loss of organic moiety and triazine ring respectively whereas the complex $Zn(L)OAc.2H_2O$ shows three decomposition steps in the temperature range 105-220˚C, 220-410 ˚C and 410-495 ˚C respectively (Table 5, Fig. 2).

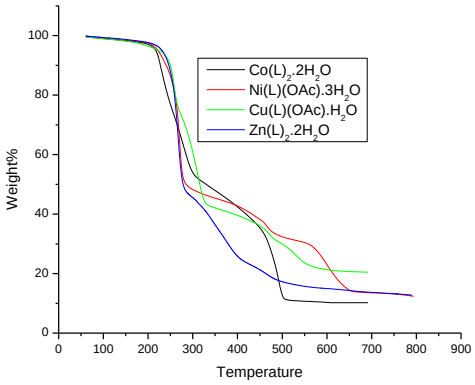

Figure 2. TG curves of metal complexes.

ESR spectra

The ESR spectra of the 1:1 and 1:2 Cu(II) complexes have been recorded. The observed g values for the complex $Cu(L)OAc.H_2O$ are $g_{\parallel} = 2.18$, $g_{\perp} = 2.07$, $g_{av} = 2.11$ and for $Cu(L)_2$, $g_{\parallel} = 2.19$, $g_{\perp} = 2.05$, $g_{av} = 2.10$. The g values can be used to derive the ground state. The results obtained from the ESR spectra of 1:1 and 1:2 Cu(II) complexes follow the trend, $g_{\parallel} > g_{\perp} > 2.0023$, indicating the unpaired electron to be in the $d_{x^2-y^2}$ orbital and corresponding to square planar geometry around the Cu(II) ion.[33] The small difference in the $g_{\parallel}$ and $g_{\perp}$ values indicates that the complexes exhibit typical axial behavior. The values of exchange interaction coupling constant (G) are 2.62 and 3.3, respectively for the 1:1 and 1:2 complexes, suggesting that there is considerable exchange coupling in the solid complexes.[34] The value of $g_{\parallel} < 2.3$ is in agreement with the covalent character of the metal ligand bond.

 DOI: 10.17628/ecb.2016.5.92-98

Table 6. *In vitro* antimicrobial activity of synthesized compounds through agar well diffusion method.

S. No.	Compound	Diameter of growth of Inhibition zone (mm)[a]					
		B. subtilis	*S. aureus*	*E. coli*	*P. aeruginosa*	*C. albicans*	*S. cerevisiae*
1a	Schiff base	26±2.16^{ab}	24±2.03^{b}	17±1.59^{c}	30±2.32^{a}	24±1.72 ^{b}	26±1.99^{ab}
2a	Co(L)(OAc).3H_2O	17±1.64^{b}	16±1.6^{b}	15±1.35^{c}	21±1.75^{a}	15±1.90^{c}	20±1.67^{a}
3a	Co$(L)_2$.2H_2O	15±1.28^{d}	14±1.3^{de}	13±1.08^{e}	17±1.44^{c}	25±1.26^{a}	22±1.19^{b}
4a	Ni(L)(OAc).3H_2O	18±1.65^{c}	16±1.42^{cd}	15±1.38^{d}	19±1.92^{bc}	20±1.86^{b}	22±2.06 ^{a}
5a	Ni$(L)_2$.2H_2O	19±1.88^{a}	15±1.72^{b}	10±0.42^{d}	16±1.03^{b}	12±0.81^{c}	19±0.98^{a}
6a	Cu(L)(OAc).H_2O	20±1.36^{a}	18±1.54^{b}	14±1.12^{d}	16±0.94^{c}	10±0.57^{e}	20±1.64^{a}
7a	Cu$(L)_2$	24±1.99^{ab}	23±1.74^{b}	25±1.66^{a}	23±2.49^{b}	-	24±2.04^{ab}
8a	Zn(L)(OAc).3H_2O	26±2.18^{b}	25±1.73^{c}	25±1.61^{c}	26±1.87 ^{b}	-	30±2.56^{a}
9a	Zn$(L)_2$.2H_2O	21±2.12^{b}	18±0.94^{c}	17±0.88^{c}	21±2.23^{b}	12±0.68^{d}	32±2.34^{a}
10a	Ciprofloxacin	24±1.68 ^{b}	26.6±3.24^{a}	25±2.02^{ab}	22±1.72^{c}	-	-
11a	Amphotericin B	-	-	-	-	16.6±1.17^{b}	19.3±1.14^{a}

-: No activity. All values are Mean ± S.E of mean. Means with different letters in the same row are significantly (P<0.05) different. (Data were analyzed by Duncan's Multiple Range test). a Values, including diameter of the well (8mm), are means of three replicates

Electrochemistry

The cyclic voltammograms of the all the metal complexes were recorded in DMF at a scan rate of 0.1 V s^{-1} in the potential range -1.5 to 0.5 V. Tetrabutylammonium perchlorate was used as a supporting electrolyte. The cyclic voltammogram of the Co(II) complex exhibits a cathodic reduction peak at -1.3 V and associated anodic oxidation peak at -0.9 V corresponding to formation of Co(II)/Co(I) couple.[33] The peak separation (ΔE_p = 0.4 V) indicates a quasi reversible one electron process. The Ni (II) complex shows a cathodic peak at -1.14 V characteristic of the Ni(II) → Ni(I) couple and associated anodic peak at -0.6 V indicating Ni(I) → Ni(II) couple (Fig. 3a). The peak separation value (ΔE_p = 0.54 V) between the cathodic and anodic potential is high indicating one electron, quasi-reversible process[23].

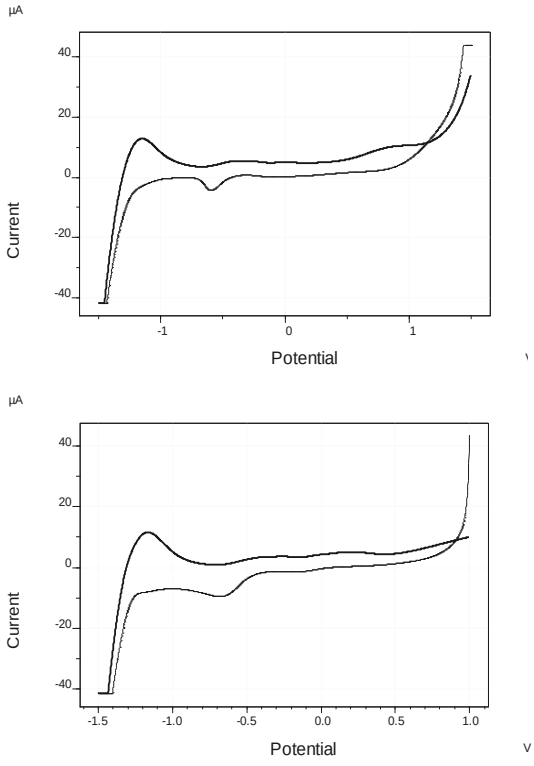

Figure 3. Cyclic voltammogram of (a) Ni$(L)_2$.2H_2O (b) Cu(L)OAc.H_2O.

The Cu(II) complex displays a reduction peak at E_{pc} = -1.16 V with a corresponding oxidation peak at E_{pa} = -0.65 V (ΔE_p = 0.51 V) indicating quasi-reversible one electron Cu(II)/Cu(I) couple (Fig. 3b).

The Zn(II) complexes do not show any oxidation or reduction peak. The value of half wave potentials, $E_{1/2}$ was found to be -1.1 V, -0.87 V and -0.91 V for the Co(II), Ni(II) and Cu(II) complexes respectively attributed to one electron transform.

Antimicrobial discussion

The enhanced lipophilic character favours the permeation of the central metal ion through the lipid layer of the microorganisms thus inhibiting the growth of the microorganisms and destroying them more aggressively.

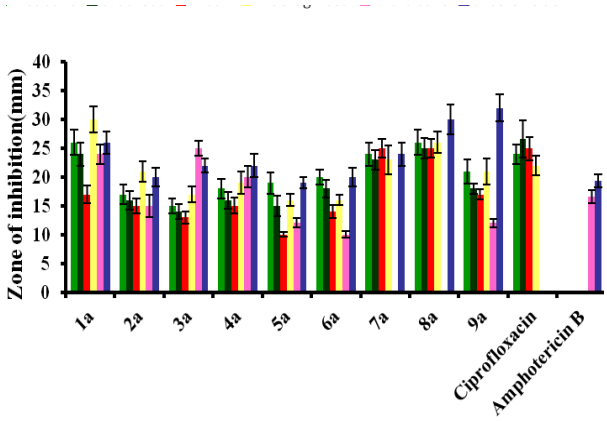

Figure 4a. Antimicrobial activity of compounds/standard drugs showing zone of inhibition.

The antimicrobial studies inferred that the complexes act as more powerful and potent antimicrobial agents as compared to the Schiff base. This may be due to change in structure due to coordination thereby reducing the polarity of metal ion due to partial sharing of its positive charge with the donor groups within the chelate ring system which, in turn, increases the lipophilic nature of the central metal atom.[17]

 DOI: 10.17628/ecb.2016.5.92-98

Table 7. Minimum inhibitory concentration (MIC) (in µg mL^{-1}) of compounds

S. No.	Compound	*B. subtilis*	*S. aureus*	*E. coli*	*P. aeruginosa*	*C. albicans*	*S. cerevisiae*
1a	Schiff base	12.5	25	50	6.25	25	12.5
2a	$Co(L)(OAc).3H_2O$	50	50	nt	25	nt	25
3a	$Co(L)_2.2H_2O$	nt	nt	nt	50	12.5	25
4a	$Ni(L)(OAc).3H_2O$	50	50	nt	25	25	25
5a	$Ni(L)_2.2H_2O$	25	nt	nt	50	nt	25
6a	$Cu(L)(OAc).H_2O$	25	50	nt	50	nt	25
7a	$Cu(L)_2$	25	25	12.5	25	-	12.5
8a	$Zn(L)(OAc).3H_2O$	12.5	12.5	12.5	12.5	-	6.25
9a	$Zn(L)_2.2H_2O$	25	50	50	25	nt	6.25
10a	Ciprofloxacin	6.25	6.25	6.25	12.5	-	-
11a	Amphotericin B	-	-	-	-	12.5	12.5

- : No activity

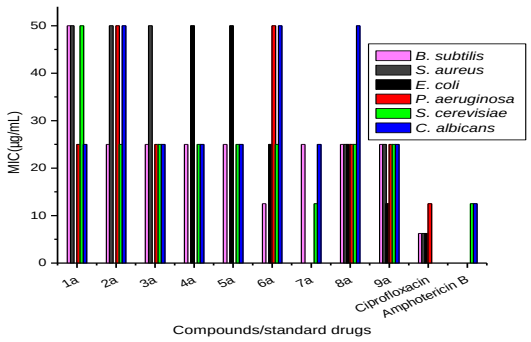

Figure 4b. Comparison of MIC of compounds with standard drugs.

The results of the antibacterial studies reveal that all the Co(II), Ni(II), Cu(II) and Zn(II) complexes (**2a-9a**) possess strong antibacterial activities against *Bacillus subtilis* with low MIC values in the range of 6.25 - 25 µg mL^{-1}. The Zn(II) complexes exhibit good antibacterial activities against *Staphylococcus aureus, Escherichia coli* and *Pseudomonas aeruginosa* whereas other compounds shown moderate activities against these bacteria. All the complexes also show potential antifungal activities against the tested fungi that are better than the reference drug amphotericin B. The The antimicrobial activities of the investigated compounds are shown in Table 6, Fig. 4a. and the minimum inhibitory concentration (MIC) values are summarized in Table 7 (Fig. 4b).

Statistical analysis

Significant differences among treatment groups were tested by Analysis of variance (ANOVA) Duncan's multiple range tests for the experiment (Table 6). Statistical significance was settled at a probability value of $P<0.05$. All statistics was performed using SPSS Version 11.5 for Windows.

Structural information by computational methods

Chem 3D Ultra was used to perform the geometrical optimization calculations. The optimized geometries and the plot of highest occupied molecular orbital (HOMO), lowest unoccupied molecular orbital (LUMO) of the ligand and some of the metal complexes are shown in Figs. 5-7.

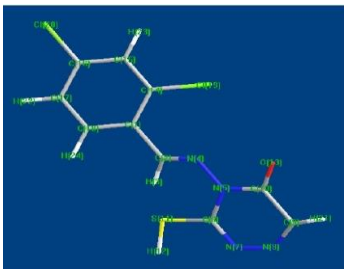

Figure 5a. Optimized geometry of Schiff base

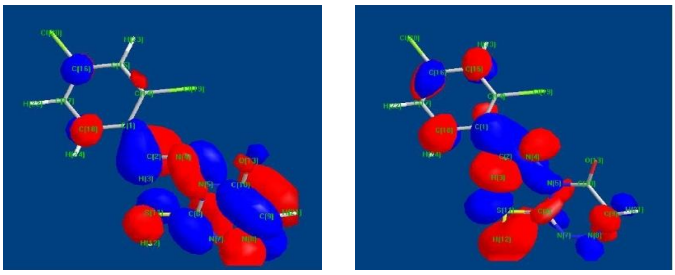

Figure 5b. Plot of HOMO, LUMO, HOMO-1 and LUMO+1 calculated molecular orbital levels for Schiff base.

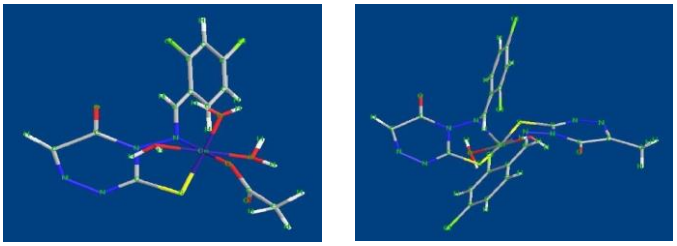

a) **b)**

Figure 6. (a) The optimized geometry of $Co(L)(OAc).3H_2O$, **(b)** The optimized geometry of $Zn(L)_2.2H_2O$.

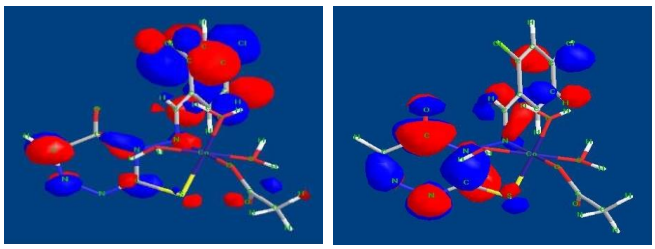

a) b)

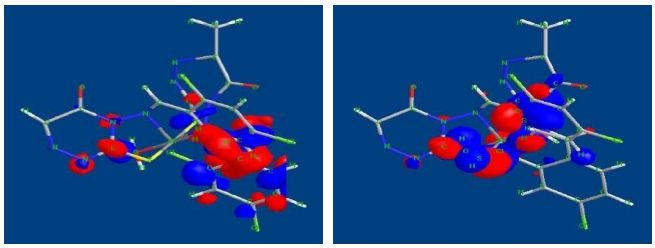

c) d)

Figure 7. (**a**) HOMO level for Co(L)(OAc).3H_2O complex , **(b)** LUMO level for Co(L)(OAc).3H_2O complex, (c) HOMO level for $Zn(L)_2$.2H_2O complex **(d)** LUMO level for $Zn(L)_2$.2H_2O complex.

Conclusions

The Co(II), Ni(II), Cu(II) and Zn(II) complexes derived from the Schiff base, 4-(2,4-dichlorobenzylideneamino)-3-mercapto-5-oxo-1,2,4-triazine were synthesized and characterized on the basis of analytical and spectral data. The results of the investigation suggest octahedral geometry for the Co(II), Ni(II) and Zn(II) complexes and square planar geometry around the Cu(II) ion. The Schiff base and their metal complexes were found highly active against the bacterial and fungal species and therefore can be used as new antimicrobial drugs after testing their toxicity.

Acknowledgements

Authors are also grateful to SAIF, Panjab University Chandigarh for providing far IR data, SAIF, IIT Bombay for ESR analysis, NIT kurukshetra for CHN analysis and IIC, IIT Roorkee for magnetic moment data.

Conflicts of interest

The author(s) declare that there is no conflict of interest regarding the publication of this manuscript.

References

[1]Abdel-Rahman, R. M., *Phosphorus Sulfur Silicon Relat. Elem*., **2000**, *166*, 315.

[2]Sangshetti, J. N., Shinde, D. B., *Biorg. Med. Chem. Lett.*, **2010**, *20*, 742.

[3]Salimon, J., Salih, N., *Int. J. Pharm. Tech. Res.*, **2010**, *2*, 1041.

[4]Singh, K., Kumar, Y., Puri, P., Sharma, C., Aneja, K. R., *Med. Chem. Res.*, **2012**, *21(8)*, 1708.

[5]Mullick, P., Khan, S. A., Begum, T., Verma, S., Kaushik, D., Alam, O., *Acta Pol. Pharm. Drug Res.*, **2009**, *66*, 379.

[6]El-Gendy, Z., Morsy, J. M., Allimony, H. A., Ali, W. R., Abdel-Rahman, R. M., *Pharmazie*, **2001**, *56*, 376.

[7]El-Sayed Ali, T., *Eur. J. Med. Chem.*, **2009**, *44*, 4385.

[8]Abdel-Rahman, R. M., *Pharmazie*, **2001**, *56*, 18.

[9]Hynes, J., Kanner, S. B., Yang, X., Tokarski, J. S., Schieven, G. L., Dyckman, A. J., Lonial, H., Zhang, R., Sack, J. S., Lin, S., *J. Med. Chem.*, **2008**, *51*, 4.

[10]Courme, C., Gresh, N., Vidal, M., Lenoir, C., Garbey, C., Florent, J. C., Bertounesque, E., *Eur. J. Med. Chem.*, **2010**, *45*, 244.

[11]Roje, S., *Photochemistry*, **2007**, *68*, 1904.

[12]Newman, D. J., Cragg, G. M., *J. Nat. Prod.*, **2004**, *67*, 1216.

[13]Stavenger, R. A., *Annu. Rep. Med. Chem.*, **2008**, *43*, 87.

[14]Jain, K. S., Chitre, T. S., Miniyar, P. B., Kathiravan, M. K., Bendre, V. S., Veer, V. S., Shahane, S. R., Shishoo, C. J., *Curr. Sci.*, **2006**, *90*, 793.

[15]Singh, K., Kumar, Y., Puri, P., Sharma, C., Aneja, K. R., *Med. Chem. Res.*, **2012**, *21(8)* 1708.

[16]Singh, K., Barwa, M. S., Tyagi, P., *Eur. J. Med. Chem*., **2006**, *41*, 147.

[17]Anitha, C., Sheela, C. D., Tharmaraj, P., Raja, S. J., *Spectrochim Acta A Mol Biomol Spectr*., **2012**, *98*, 35.

[18]Raman, N., Raja, S. J., Sakthivel, A., *J. Coord. Chem.*, **2009**, *62*, 691.

[19]Culakova, H., Dzugasova, V., Gbelska, Y., Subik, J., *FEMS Microbiol. Lett*., **2012**, *328*, 138.

[20]Vogel, A. I., *A text book of quantitative chemical analysis*, 5th edition, Addison Wesley Longman, London, **1999**.

[21]Ramachandra, B., Narayana, B., *Indian J. Chem.*, **1999**, *38 A*, 1297.

[22]Yadawe, M. S., Patil, S. A., *Transit. Met. Chem.*, **1997**, *22*, 220.

[23]Patil, S. A., Unki, S. N., Kulkarni, A. D., Naik, V. H., Badami, P. S., *Spectrochim. Acta A Mol. Biomol. Spectrosc.*, **2011**, *79*, 1128.

[24]Rupini, B., Mamatha, K., Mogili, R., Ravinder, M., Srihari, S., *J. Indian Chem.*, **2007**, *84(6)*, 629.

[25]Nakamoto, K., *Infrared and Raman spectra of inorganic coordination compounds*, 3rd edition, John Wiley, New York, **1978**.

[26]Bagihalli, G. B., Avaji, P. G., Patil, S. A., Badami, P. S., *Eur. J. Med. Chem.*, **2008**, *43*, 2639.

[27]Khalil, S. M. E., *Chem. Pap.*, **2000**, *54 (1)*, 12.

[28]Balhausen, C. J., *Introduction to Ligand Fields*, McGraw Hill, New York, **1962**.

[29]Drago, R. S., *Physical Methods in Inorganic Chemistry*, Reinhold Publishing Corporation, New York, **1968**.

[30]Kalanithi, M., Kodimunthiri, D., Rajarajan, M., Tharmaraj, P., *Spectrochim. Acta A*, **2011**, *82*, 290.

[31]Boghaei, D. M., Asl, F.B., *J. Coord. Chem.*, **2007**, *60(15)*, 1629.

[32]Maxim, C., Pasatoiu, T. D., Ch. Kravtsov, V., Shova, S., Muryn, C. A., Winpenny, R. E. P., Tuna, F., Andruh, M., *Inorg. chim. Acta*, **2008**, *361*, 3903.

[33]Singh, K., Raparia, S., Surain, P., *Med. Chem. Res.*, **2015**, *24*, 2336.

[34]Hathaway, B. T., *Struct. Bonding*, **1973**, *14*, 60.

Received: 21.02.2016.
Accepted: 12.05.2016.

EFFECT OF CAFETERIA DIET ON LIPID METABOLISM AND LIPASE ACTIVITIES IN WISTAR RATS

Bensalah Meryem,[a] Bouanane Samira,[a]* Baba Ahmed Fatima Zohra,[a] Merzouk Hafida,[a] Sid Ahmed Merzouk [b] and Narce Michel[c]

Keywords: cafeteria diet, obesity, lipids, lipoproteins, lipase activities

Nowadays, diseases associated with lipid accumulation in the human body such as obesity are becoming very important health issues. The aim of this study is to evaluate the impact of cafeteria diet feeding by Wistar rats, used as an experimental model of nutritional obesity, during 8 weeks, on lipid metabolism. Thus, we determined the levels of total cholesterol (TC) and triglycerides (TG) in plasma, lipoproteins and organs (liver, adipose tissue, muscle), and the activities of lipoprotein lipase (LPL) in organs, and hormone-sensitive lipase (HSL). The results show that cafeteria diet causes increased accumulation of lipids in adipose tissue leads to obesity with ectopic accumulation of lipids in other organs as liver, and induce lipoproteins metabolic disorders. Our results also show a disruption in the pathway of lipid storage enzyme (LPL) and lipid mobilization enzyme (HSL). Cafeteria diet is not only a primary risk for obesity, but also acts indirectly by adversely affecting other primary risk factors to serious chronic disease.

* Corresponding Author
E-Mail: sambouanane@hotmail.fr
[a] Laboratory of Physiology and Biochemistry of Nutrition, Department of Biology, Faculty of Natural and Life Sciences, Earth and Universe, University of Tlemcen 13000, Algeria.
[b] Department of Technical Sciences, Faculty of Engineering, University of Tlemcen 13000, Algeria
[c] INSERM UMR 866, "Lipids Nutrition Cancer", University, of Burgundy, Faculty of Sciences, 6 Boulevard Gabriel, Dijon 21000, France

Introduction

The prevalence of obesity has increased significantly in developed countries, and also, although less rapidly, in developing ones.[1,2] Both genetic and environmental factors have been identified as potential causes of obesity,[3,4] but the relative significance of each or the interplay between the two may vary. The rise in the prevalence of obesity might result from the increasingly sedentary lifestyle of western civilization associated with a reduction in daily physical activity and/or from changes in eating behavior, both quantitatively and qualitatively. Whatever the complexity of risk factors, excess body weight and obesity always result from an imbalance between energy intake and energy expenditure with a positive energy balance due to either excessive calorie intake, decreased calorie expenditure or both. Other scientists have looked at the composition of the diet and reported that excessive consumption of dietary fat may be a more important determinant of obesity than excessive consumption of either carbohydrate or protein.[5,6]

Obesity is progressing in epidemic proportions, and demonstrates no signs of reduced incidence. As weight loss is not only difficult to achieve but more difficult to sustain in long term,[7,8] there must be mechanisms in body to defend the expanded fat mass. Following weight reduction, increases in energy intake, decreases in energy expenditure, and modifications of energy partitioning, storage and oxidation all contribute towards regaining of weight.[9,10] Therefore, it becomes increasingly important to understand how body weight and adipose tissue are regulated including the role of macronutrient partitioning.

Lipid partitioning is important for insulin action, energy balance and the regulation of body weight and composition. The normal physiology of lipid and lipoprotein fuel partitioning is controlled by the transport and uptake of adipose tissue-derived free fatty acids and lipoprotein-derived triglyceride fatty acids. As previously stated, lipoprotein lipid partitioning is largely dependent on the enzymatic action of lipoprotein lipase (LPL) [EC 3.1.1.34], and free fatty acids mobilization is largely dependent on the enzymatic action of hormone-sensitive lipase (HSL) [EC 3.1.1.79].

The aim of this study is to evaluate the impact of high fat and high caloric diet feeding by Wistar rats, used as an experimental model of nutritional obesity, during 8 weeks, on the metabolism of lipids and lipoproteins. Thus, we determined the levels of total cholesterol (TC) and triglycerides (TG) in plasma, lipoproteins and organs (liver, adipose tissue, muscle), and the activities of lipoprotein lipase (LPL) in organs, and those of hormone-sensitive lipase (HSL).

Experimentals

Adult Wistar rats were housed in wood-chip-bedded plastic cages at constant temperature (25 °C) and humidity (60 ± 5 %) with a 12-hour light-dark cycle. They had free access to water and were assigned to two dietary groups, with one group (control, *n*=6) fed a control commercial diet (O.N.A.B), whereas the second group (experimental group, *n*=6) was fed a fat-rich hypercaloric diet "cafeteria diet" during 8 weeks. The control diet was composed of 19 % of energy as protein, 8.50 % of energy as lipids and 56 % of energy as carbohydrate by dry weight. The components of the cafeteria diet were pate, cheese, bacon, chips, cookies and chocolate (in a proportion of 2:2:2:1:1:1, by weight) and control diet (mix/control diet), was given to each rat daily as published previously.[11,12]

The composition of the cafeteria diet, by dry weight, was 21.50 % of energy as protein, 33.50 % of energy as lipids and 33.50 % of energy as carbohydrates. The study was

conducted in accordance with the national guidelines for the care and use of laboratory animals. All the experimental protocols were approved by the Regional Ethical Committee.

At 12 weeks of age, rats were anaesthetized with intraperitoneal injection of 10 % chloral (0.3 ml per 100 g of body weight). The abdominal cavity was opened and blood was drawn from the abdominal aorta into EDTA and sec tubes. Blood samples were centrifuged to obtain the plasma for determination of glucose and lipids parameters, and serum for determination of total proteins and lipoproteins composition.

Liver, gastrocnemius muscle and fat tissue were removed, washed with ice-cold saline, and quickly blotted and weighed. An aliquot of each tissue was used immediately to measure the activities of lipoprotein lipase; an aliquot of adipose tissue was used to measure the activity of hormone-sensitive lipase. The rest was stored at –20 °C for determination of lipids tissues content.

Glucose, triglycerides and total cholesterol, were determined using colorimetric enzymatic assays, in plasma and in different lipoprotein fractions after separation by precipitation according to the method of Burstein *et al.*[13] Protein contents of lipoprotein fractions were determined by the method of Lowry *et al.*,[14] and total proteins serum contents were determined by the method of Biuret,[15] with BSA as the standard.

Liver, muscle and fat tissue triglycerides and total cholesterol levels were measured using colorimetric enzymatic essays after homogenization an aliquot of each tissue in phosphate/EDTA buffer, pH = 7.2, containing sodium dodecyl sulfate (SDS 1 %) (1/1, V/V), in an Ultraturax homogenizer, and centrifugation at 3000 g for 10 min.

Lipase activity (LPL, EC 3.1.1.34; LHS, EC 3.1.1.79) was measured by pH-stat by titrimetric measurement of fatty acids released after hydrolysis of triglycerides of synthetic substrate with NaOH 0.05 M at pH 8 and at 25 °C. Enzyme activity was expressed in international units (IU). One unit corresponds to the release of a micro-equivalent of fatty acid per minute.

Results are expressed as means ± standard deviation (SD). The significance of differences between experimental and control rats was assessed using Student's *t* test. The calculations were performed using STATISTICA, version 4.1 (Statsoft, Tulsa, OK). Differences were considered statistically significant at $p < 0.05$.

Results

Body weight, relative weight, triglycerides and total cholesterol contents of organs

The cafeteria diet was associated with increased body weight and weight gain compared to control diet (Figure 1). Relative liver and muscle weight did not differ between animals fed the cafeteria diet and control diet (Table 1); however, cafeteria-diet-fed rats had a higher relative adipose tissue weight compared with control rats.

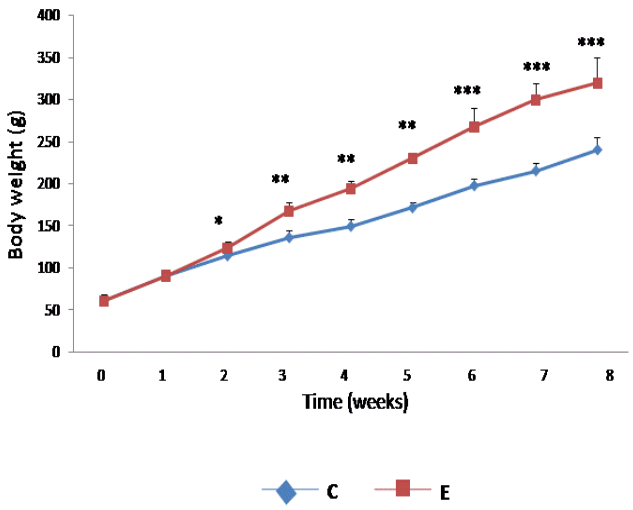

Figure 1. Changes in body weight in control and experimental rats during the 8 weeks of diet. Values are means ± SD. Significant differences between control and experimental rats, at each week, are indicated as follows: *p <0.05; **p< 0.01; ***p<0.001.

The cafeteria diet significantly increased triglycerides and total cholesterol adipose tissue contents (Table 1). Liver triglycerides and total cholesterol contents were significantly higher in experimental rats compared to the control rats, muscle triglycerides and total cholesterol contents did not change significantly between the two groups of rats (**Table 1**).

Table 1. Body weight, organ relative weights and lipids composition in control and experimental rats.

Parameter	Animals	
	Control	**Treated**
Body weight (g)	241.00±15.23	320.00±29.99***
	Adipose tissue	
Relative weight (g)	2.6±0,69	6.17±1.05***
Total cholesterol (mg g^{-1} of tissue)	9.46±0,67	11.29±1.02*
Triglycerides (mg g^{-1} of tissue)	33.70±0.96	52.16±2.89***
	Liver	
Relative weight (g)	9.7±0.82	12.00±2.42
Total cholesterol (mg g^{-1} of tissue)	11,47±0.52	13.06±0.82*
Triglycerides (mg g^{-1} of tissue)	23.29±0.77	36.34±4.71***
	Muscle	
Relative weight (g)	2.48±0.20	2.55±0.17
Total cholesterol (mg g^{-1} of tissue)	5.90±0.82	6.09±1.30
Triglycerides (mg g^{-1} of tissue)	17.75±0.49	17.89±0.71

Values are means ± SD. Significant differences between control and experimental rats are indicated as follows: *p <0.05; **p<0.01; ***p<0.001.

 DOI: 10.17628/ecb.2016.5.99-103

Table 2. Serum and lipoproteins compositions in control and experimental rats

Parameter	Animals	
	Control	Treated
Serum		
Glucose (mg dL^{-1})	120.13±6.10	152.05±5.83***
Total cholesterol (mg dL^{-1})	124.19±5.14	179.51±3.65***
Triglycerides (mg dL^{-1}l)	82.44±2.88	124.07±3.01***
Total proteins (mg dL^{-1})	777.28±13.16	766.43±12.91
VLDL		
Total cholesterol (mg dL^{-1})	24.33±1.54	60.10±3.15***
Triglycerides (mg dL^{-1})	40.82±1.06	75.50±1.19***
Total proteins (mg dL^{-1})	88.09±1.26	93.50±1.51*
LDL		
Total cholesterol (mg dL^{-1})	34.70±2.10	66.82±4.01***
Triglycerides (mg dL^{-1})	28.22±2.35	32.19±2.20
Total proteins (mg dL^{-1})	248.10±2.86	256.01±3.01*
HDL		
Total cholesterol(mg dL^{-1})	65.11±3.12	52.03±1.81**
Triglycerides (mg dL^{-1})	16.22±0.33	13.01±1.41**
Total proteins (mg dL^{-1})	430.72±1.60	419.01±2.03*

Values are means ± SD. Significant differences between control and experimental rats are indicated as follows: *p <0.05; **p< 0.01; ***p<0.001.

Table 3. Lipoprotein lipase and hormone-sensitive lipase activities in control and experimental rats.

Parameter	Animals	
	Control	**Treated**
LPL (mol g^{-1} min^{-1})		
Adipose tissue	0.049±0.0015	0.0632±0.0011**
Liver	0.0543±0.002	0.0827±0.0013**
Muscle	0.0321±0.003	0.0386±0.002*
HSL (mol g^{-1} min^{-1})		
Adipose tissue	0.0294±0.0014	0.0555±0.0018***

Values are means ± SD. Significant differences between control and experimental rats are indicated as follows: *p <0.05; **p< 0.01; ***p<0.001.

Plasma and lipoproteins biochemical parameters

The cafeteria diet induced a significant increase in plasma glucose in experimental rats compared to control rats (Table 2).

A significant increase in the total cholesterol level was found in the plasma, LDL and VLDL of experimental rats compared to the control rats; however, HDL total cholesterol was low in experimental rats compared with control rats values (Table 2).

Plasma and VLDL triglycerides contents were significantly higher in experimental rats than in control rats (Table 2). There were no significant differences between experimental and control rats concerning LDL triglycerides contents. On the other side, HDL triglycerides contents were significantly decreases in experimental rats compared with control rats (Table 2).

Higher VLDL and LDL apoprotein levels were observed in experimental rats compared with controls (Table 2). However cafeteria-diet-fed rats had a lower HDL apoproteins levels compared with standard-diet-fed rats (Table 2). There were no significant differences between experimental and control rats concerning totals proteins serum contents (Table 2).

Lipoprotein lipase (LPL) and hormone-sensitive lipase (HSL) activity

Adipose and hepatic LPL activities was significantly higher in cafeteria-diet-fed rats compared with control rats (Table 3), also a higher muscular LPL activity was observed in experimental rats compared with controls rats (Table 3). The cafeteria diet induced a significant increase in HSL activity compared to control diet (Table 3).

Discussion

The present study has evaluated the role of cafeteria diet in induction of lipids and lipoproteins metabolic abnormalities.

The rats that received the cafeteria diet had an increase in body weight, as described previously in the literature with animals fed cafeteria diet.[16,17] The enhancement of body weight in cafeteria-diet-fed rats was strongly associated with the increase in weight of adipose depots, confirming the obesigenic properties of the cafeteria diet, these results are in agreement with previous studies.[17,18,19]

In the other hand, our results show that liver and muscle relative weight did not change between cafeteria-diet-fed rats and control-fed-rats. Similar observations have been made in previous studies.[17] However, analysis of the lipids contents of organs suggests the existence of alterations in experimental rats compared to controls rats; triglycerides and total cholesterol contents of liver and adipose tissue were higher in rats feeding cafeteria diet compared with controls. Rats fed cafeteria diet exhibited a markedly increased adiposity. The increased adiposity was characterized both by an increase in fat pad weight as well as intrahepatic lipid deposition.[20]

Adipose tissue is the site of safe storage of fat and is indispensable for normal metabolic function. A lack of adipose tissue leads to insulin resistance[21] and is responsible for accumulation of fat in the "wrong places".[22,23] The built up of fat in organs other than adipose tissue is believed to alter the normal function of these organs and leads to insulin resistance.

The analysis of blood lipids yields information about the predominant metabolic pathway (carbohydrate utilizing or fat utilizing) active in the body. Blood lipids values are also risk markers for obesity, diabetes, and coronary heart disease. Our results show alterations in plasma lipid and lipoproteins levels. These dyslipidemia manifested as high plasma and VLDL triglycerides levels, low total cholesterol-HDL and high total cholesterol-LDL in experimental rats compared with control, these results are in agreement with previous studies.[24,25,26] Disturbances in lipoproteins metabolism in visceral obesity may be attributable to insulin resistance,[27] insulin resistance increase hepatic synthesis of lipid substrates and the secretion of VLDL apo B-100,[28] it also down regulates LDL receptors.[32] These effects

potentially increase the plasma concentrations of remnant lipoproteins containing apo B-100 and increase competition for hepatic uptake between chylomicron and VLDL remnants.[29]

Arshag *et al.*[26] suggested that the low plasma HDL cholesterol concentrations in obese people could be the result of an increased fractional clearance of HDL secondary to reduced cholesterol content, and reduced production of the main cardioprotective apoprotein, notably apo A-I. Although, low HDL cholesterol levels in obese people are commonly a concomitant of hypertriglyceridemia, it can occur independently of elevated serum triglyceride levels.

Lipoprotein lipase plays a major role in the metabolism and transport of lipids; it is the rate-limiting enzyme for the hydrolysis of the triglyceride core of circulating triglyceride-riche lipoproteins, chylomicrons and very low density lipoproteins.

The present study revealed a significant increase in adipose LPL activity, in agreement with previous studies reporting that, LPL activity has been reported to increase as a function of fat cell size [30,31,32,33], also, LPL is an important marker for adipocyte differentiation [34], and LPL expression increases in parallel with cellular triglyceride accumulation as preadipocytes differentiate[35]. Although, adipose tissue can synthesize free fatty acids *de novo*, free fatty acids for lipid storage are preferentially provided by LPL-mediated hydrolysis of plasma triglyceride-rich lipoproteins [36]. LPL is thus considered a gatekeeper enzyme to play an important role in the initiation and/or development of obesity.

Glucose also increases adipose tissue LPL activity. The glucose stimulatory effect appears to be mostly through the glucosylation of LPL, which is essential for LPL catalytic activity and secretion. Glucose also stimulates LPL synthetic rate and potentiates the stimulatory effect of insulin.[37,38] Our results show an increase in serum glucose level in cafeteria-diet-fed rats.

In our study, a higher activity of hepatic LPL was observed in experimental rats in agreement with Kim *et al.*[39] who reported that, when LPL is over expressed in the liver in mince, a 2-fold increase in liver triglyceride content and insulin resistance was observed. In those mince, increase in hepatic LPL activity impaired the ability of insulin to suppress endogenous glucose production in the liver, and the defect in insulin action and signaling in the liver is associated with increases in intracellular fatty acid-derived metabolites.

Skeletal muscle is a major site for LPL synthesis; it is also the major tissue responsible for whole-body insulin-stimulated glucose uptake/disposal. Arguably the most productive line of research related to the tissue-specific effects of LPL on lipid fuel partitioning, body weight regulation, and insulin action have come from genetic modifications of the LPL gene in skeletal muscle.

The present study revealed a higher muscular LPL activity in the cafeteria-diet-fed rats. Several studies have reported that mice transgenic for LPL overexpression in skeletal muscle are insulin resistant.[39,40] and have increased muscle triglycerides.[39,41,42] Decreases in insulin-stimulated glucose uptake in skeletal muscle and insulin activation of insulin receptor substrat-1 (IRS-1)-associated phosphatidylinositol (PI)3-Kinase activity are also associated with increases in intracellular fatty acid derived metabolites.[39] Pervious study showed that LPL deletion in skeletal muscle seems to reduce lipid storage and increase insulin signaling in skeletal muscle without change in body composition.[43]

Accumulating evidences have defined important functions for HSL in normal physiology affecting adipocyte lipolysis, it has been suggested that HSL is the rate limiting enzyme in intracellular lipolysis,[44] however, direct links between abnormal expression of HSL and human disorders, such as obesity, insulin resistance and hyperlipidemia, await clarifications. In our study a higher HSL activity was observed in experimental rats, these results are in agreement with previous studies reporting a positive relationship between fat cell size and HSL expression in rats with high fat feeding, where fat feeding was associated with an increase in adipocyte cell size and an increase in both basal and stimulated HSL activity.[45] The high HSL activity may be due to insulin resistance, in which insulin has little effect on lipolysis. Insulin stimulation of adipocytes prevents HSL activation, leading to a decrease in the release of free fatty acids and glycerol.[46]

Conclusion

In summary, the data presented in this paper show that rats fed cafeteria diet were characterized by lipid accumulation in adipose tissue leads to visceral obesity associated with insulin resistance and ectopic accumulation of lipids in other organs as liver. In addition cafeteria diet induces lipid and lipoproteins metabolic disorders, associated with abnormal expression of pathway enzymes lipid storage (LPL) and lipid mobilization enzyme (HSL). High fat- and caloric-diet is not only a primary risk factor for obesity, but also acts indirectly by adversely affecting other primary risk factors, such as lipid profile and glycemic control, to serious chronic disease.

References

[1]World health organisation, Obesity: preventing and managing the global epidemic, *WHO technical report series 894*, Geneva, **2000.**

[2]Del Río-Navarro, B. E., Velázquez-Monroy, O., Sánchez-Castillo, C. P., *Obes Res*., **2004**, *12*, 215- 223.

[3]Gillis, L. J., Kennedy, L. C., Gillis, A. M., *Int. J. Obes*., **2002**, 26, 458- 463.

[4]Knerr, I., Topf, H. G., Hablawetz, B., *Gesundheitswesen*, **2005**, *67*, 183- 188.

[5]Reilly, J. J., *Proc. Nutr. Soc*., **2008**, *67*, 317- 325.

[6]Francis, D. K., Vanden Broeck, J., Younger, N., *Public Health Nutr*., **2009**, *12(8)*, 1106- 1114.

[7]Miller, W. C., Koceja, D. M., Hamilton, E. J., *Int. J. Obes. Relat. Metab. Disord.*, **1997**, *21*, 941- 947.

[8]Dansinger, M. L., Tatsioni, A., Wong, J. B., Chung, M., Balk, E. M., *Ann Intern Med.*, **2007**, *147*, 41- 50.

[9]Aja, S., Moran, T. H., *Adv Psychosom Med.*, **2006**, *27*, 1- 23.

[10]Eckel, R. H., *N Engl J Med*., **2008,** *358*, 1941- 1950.

[11]Darimont, C., Turini, M., Epitaux, M., Zbinden, I., Richelle, M., Montell, E., Ferrer-Martinez, A., Mace, K., *Nutr. Metab*., **2004**, *1*, 4 13

[12]Milargo, F. I., Campion, J., Martinez, J. A., *Obesity*., **2006**, *14*, 1118- 1123.

[13]Burstein, M., Fine, A., Atger, V., *Biochem.*, **1989**, *71*, 741- 746.

[14]Lowry, O. H., Rosenbrough, N. J., Farr, A. L., Randali, R. I., *J Biol Chem*., **1951**, *193*, 265- 275.

[15]Gornall, A. G., Bardawill, C. J., David, M. M., *J Biol Chem*., **1949**, *177*, 751-66.

[16]Pellizzon, M., Buison, A., Ordiz, F., Santa Ana, L., Jen, K. C., *Obes. Res*., **2002**, *10*, 945- 955.

[17]Bouanane, S., Benkalfat, N. B., Baba ahmed, F. Z., Merzouk, H., Soulimane Mokhtari, N., Merzouk, S. A., Gresti, J., Tessier, C., Narce, M., *Clin. Sci*., **2009**, *116(8)*, 669-680.

[18]Soulimane-Mokhtari, N., Guermouche, B., Yessoufou, A., Saker, M., Moutairou, K., Hichami, A., Merzouk, H., Khan, N. A., *Clin. Sci*., **2005**, *109*, 287- 295.

[19]Petit, V., Arnould, L., Martin, P., Monnot, M. C., Pineau, T., Besnard, P., Niot I., *J. Lipid Res*., **2007**, *48* , 278-287.

[20]Bayol, S. A., Simbi, B. H., Stickland, N. C., *J. Physiol*., **2005**, *567(3)*, 951–961

[21]Moitra, J., Mason, M. M., Olive, M., Krylov, D., Gavrilova, O., Marcus-Samuels, B., *Genes Dev*., **1998**, *12*, 3168-3181.

[22]Friedman, J., *Nature*, **2002**, *415*, 268, 269.

[23]Hegarty, B. D., Furler SMYeJ., Cooney, G. J., Kraegen, E. W., *Acta Physiol. Scand*., **2003**, *178*, 373- 383.

[24]Denke, M. A., *Curr. Opin. Lipidol*., **2001**, *12*, 625- 628.

[25]Verges, B., *Diabetes Metab*., **2001**., *27*, 223- 227.

[26]Arshag D Mooradian., Michael J Haas., Kent R Wehmeier., Norman CW Wong., *Obesity*, **2008**, *16*, 1152- 1160.

[27]Despres, J. P., Moorjani, S., Lupien, P. J., Tremblay, A., Nadeau, A., Bouchard, C., *Atherosclerosis*, **1990**, *10*, 497-511.

[28]Watts, G. F., Cummings, M. H., Keel, J. M., Umpleby, A. M., O'Brien, S. F., Sonksen, P. H., *Endocrinol. Metab*., **1996**, *3*, 253- 63.

[29]Dick, C., Chan Gerald, F., Watts, P., Hugh Barrett, John C. L. Mamo., Trevor, G., *Clin. Chem.*, **2002**, *48(2)*, 278, 283

[30]Greenwood, M. R., Maggio, C. A., Koopmans, H. S., Sclafani, A., *Int. J. Obes.*, **1982**, *6*, 51- 525.

[31]Sadur, C. N., Yost, T. J., Eckel, R. H., *J. Clin. Endocrinol. Metab*., **1984**, *59*, 1176-1182.

[32]Eckel, R. H., Yost, T. J.,. *J. Clin. Invest.*, **1987**, *80*, 992- 997.

[33]Bessesen, D. H., Robertson, A. D., Eckel, R. H., *Am. J. Physiol*., **1991**, *26*, 246- 251.

[34]Bjorntorp, P., Karlsson, M., Pertoft, H., Pettersson, P., Sjostrom, L., Smith, U., *J. Lipid Res*., **1978**, *19*, 316- 324.

[35]Semenkovich, C. F., Wims, M., Noe, L., Etienne, J., Chan, L., *J. Biol. Chem.*, **1989**, *264*, 9030- 9038.

[36]Hollenberg, C. H., *J. Clin. Invest*., **1966**, *45*, 205-216.

[37]Kern, P. A., Mandic, A., Eckel, R. H., *Diabetes.*, **1987**, *36*, 1238-1245.

[38]Ong, J. M., Kern, P. A., *J. Biol. Chem*., **1989**, *264*, 3177-3182.

[39]Kim, J. K., Fillmore, J. J., Chen, Y., Yu, C., Moore, I. K., Pypaert, M., Lutz, E. P., Kako, Y., Velez Carrasco, W., Goldberg, I. J., Breslow, J L., Shulman, G. I., *Proc. Natl. Acad. Sci. USA*, **2001**, *98*, 7522-7527.

[40]Ferreira, L. D., Pulawa, L. K., Jensen, D. R., Eckel, R. H., *Diabetes*, **2001**, *50*, 1064- 1068.

[41]Jensen, D. R., Schlaepfer, I. R., Morin, C. L., Pennington, D. S., Marcell, T., Ammon, S. M., Gutierrez-Hartmann, A., Eckel, R. H., *Am. J. Physiol*., **1997**, *273*, R683- R689.

[42]Voshol, P. J., Jong, M. C., Dahlmans, V. E., Kratky, D., Levak-Frank, S., Zechner, R., Romijn, J. A., Havekes, L. M., *Diabetes*, **2001**, *50*, 2585- 2590.

[43]Wang, H., Knaub, L. A., Jensen, D. R., Young, J. D., Hong, E. G., Ko, H. J., Coates, A. M., Goldberg, I. J., de la Houssaye, B. A., Janssen, R. C., McCurdy, C. E., Rahman, S. M., Soo, C. C., Shulman, G. I., Kim, J. K., Friedman, J. E., Eckel, R. H., *Diabetes.*, **2009**, *58*, 116- 124.

[44]Sztalryd, C., Komaromy, M. C., Kraemer, F. B., *J. Clin. Invest*., **1995**, *95***,** 2652-2661.

[45]Berger, J. J., Barnard, R. J., *J. Appl. Physiol*., **1999**, *87***,** 227- 232.

[46]Langin, D., Holm C., LaFontan M., *Proc. Nutr. Soc.*, **1996**, *55***,** 93-109.

Received: 08. 03. 2016
Accepted: 18. 05. 2016.

MICROVESSELS OF LIVER AND BRAIN AT CHRONIC STRESS

N. S. Kukurtchyan,[a] G. R. Karapetyan,[a] G. A. Kevorkian,[b] N. S. Alchujyan[b], Zh. E. Harutyunyan[c], N. H. Movsesyan[d] and Zh. R. Alaverdyan[e]

Keywords: Chronic stress, liver, brain, blood vessel, sprouting and intussusception angiogenesis

The system of microcirculation is the first link that is involved in pathological process at different extremely situations. Stress is followed with disturbance of microcirculation, development of organs' hypoxia and oxidative stress. The aim of this study is to show the type of angiogenesis in liver and brain under the influence of chronic variable physical stressors. In this study the influence of different stressors such as forced swimming inhalation, restraint stress, cold stress, orthostatic shock and food deprivation on the microcirculatory stream of liver and brain was observed. Investigation of sections of liver and brain yielded proof of changes of microvessels on chronic stress (CS). Thus CS influences a reorganization of blood vessels of liver and brain and it causes angiogenesis of lever sinusoids and brain capillaries.

* Corresponding Authors: Karapetyan, G. R.
Fax: +374 -10-28 19 51
E-Mail: sapootraa_a@yahoo.com
[a] H. Buniatian Institute of Biochemistry, of National Academy of Sciences of Republic Armenia, Paruir Sevag str. 5/1, 0014, Yerevan, Republic of Armenia.

INTRODUCTION

Stress is a non-specific general mobilized answer of organism to any kind of irritant that disturbs its homeostasis. Stressor means all irritants that really threaten homeostasis such as pain, hypoxia, hunger, infection and many other extreme factors.

Blood vessels are intricate networks of hollow tubes that transport blood throughout the entire body. The system of microcirculation is the first link that is involved in pathological process at different extreme situations.[1] Stress is followed with disturbance of microcirculation, development of hypoxia of organs and oxidative stress.[17] Hypoxia is thought to be a primary trigger of angiogenesis. Vicarious angiogenesis sprouts[21] as an answer to hypoxia through hypoxia-inducible factor and following induction as a result of appropriate gene expression of the main growth factor - vessel endothelium growth factor (VEGF).

Angiogenesis is a process of growth of new capillaries from the existing ones through capillary sprouting or intussusception.[4,18] Non-sprouting angiogenesis by means of intussusception (growth within itself) is an important mode of capillary formation and it is termed intussusceptive microvascular growth.[2,6,16] Comprehension of the structural and functional characteristics of hepatic microcirculation can help to improve the design, planning and practice of image-guided treatment for hepatic tumors and for portal vein embolization (PVE).[23] Brain vessels are the most important structures in the brain to deliver energy and substrates to neurons.[7] Brain vessels are composed of a complex interaction between endothelial cells, pericytes and astrocytes, controlling the entry of substrates into the brain. Damage of brain vessels and vascular impairment are general pathologies observed in different neurodegenerative disorders including e.g., Alzheimer's disease.[1]

The aim of this study is to show the type of angiogenesis in liver and brain under the influence of variable physical stresses.

EXPERIMENTAL

General

Powdered paraformaldehyde, OsO_4, sodium cacodylate trihydrate, 96 % ethyl alcohol, acetone, Epon 812, Epon Hardener MNA, Epon Hardener DDSA, Epon accelerator DNP-30, uranyl acetate, sodium citrate, lead nitrate and all other reagents used were of analytical grade and purchased from Sigma Chemical Co. (USA).

All procedures involving animals were approved by the Institutional Review Board\ Institutional Animal Care and Use Committee (H. Buniatian Institute of Biochemistry, Yerevan, NAS RA) and Ethics Committee of the National Academy of Sciences, the Republic of Armenia, and they were conformed to the European Communities Council's directives (86\609\EC).

After overnight fasting, rats were subjected to chronic variable physical stress (CVS). Animals underwent CVS regimen for 14 days consisted some times of twice a daily exposures to alternating stressors.[9] Animals were divided into three groups: one group served as control and the other two as CVS-exposed groups - after CVS (stress group) 6 animals and four days later (post stress group) 6 animals.

Treatment of material

At the end of the experiment, small pieces of the liver and brain have immediately put in cold 4 ºC mix of paraformaldehyde in a sodium cacodylate buffer and glutaraldehyde for 12 h with post fixation in 1% OsO_4 solution for 2 h, dehydration in ascending series of spirits, saturation in a mixture of acetone and Epon resins of different proportions and pouring in gelatinous capsules into Epon.

Observation under light microscope

Semithin epoxy sections thickness to up1 μm were made using ultracut LKB (Swedish) and Reichert (Austria). The semithin epoxy sections were stained with Azur 2 and observed under the light microscope with resolution by volume x40 x10 ocular lens.

Results

In this study the influence of different stressor such as forced swimming, inhalation, restraint stress, cold stress, orthostatic shock and food deprivation on the microcirculatory stream of liver and brain was observed. Samples of tissues of control, first and second group of experimental animals were analyzed.

As have shown the results of our study visually the condition of animals in two groups was different. In the first group just after the termination of the experiment the fell? of rats was white and in normal state, liver was a little red and the brain of all animals was with hemorrhage. In the second group of animals after four days of termination of the experiment the fell? looked crumpled and not very white. The liver was bright red and the brain looked normal outwardly. Investigation of semi thin epoxide sections of liver and brain, stained by Azur 2 by our method,[11] revealed morphological changes in microvessels induced by chronic stress. It must be mentioned that the use of semi thin sections of up to 1 μm thickness allowed us getting deeper picture of bloodstream without investigating liver and brain cells' parenchyma.

A number of structural changes of liver vessels of 1 group are seen as compared to the liver of control rat (Figure 1).

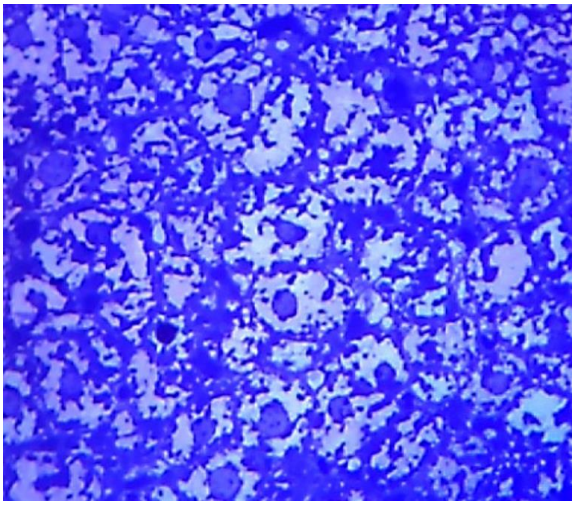

Figure 1. The blood vessels of the liver of control rats. X400

In the lobules the central vein has been changed in size and in quantity. The lobules are different. There are present as very small-sized lobules without central vein and quite big lobules with 3 or 4 small central veins. The last ones were obtained by means of bridge formation in the big vein. The vessels surrounding the lobules have also changed. They have widened for most of their length and bridges from one side of vessel to the other side are also seen (Figures 2a and 2b).

a)

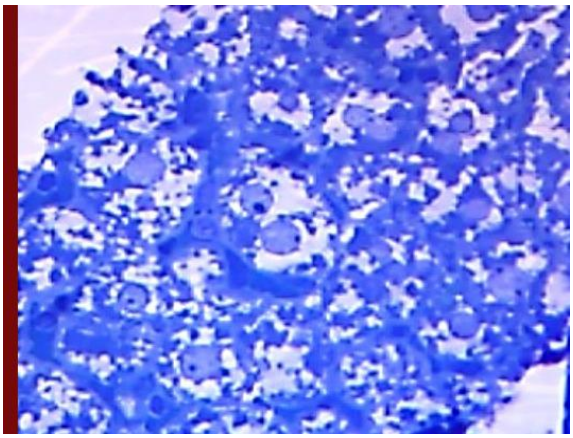

b)

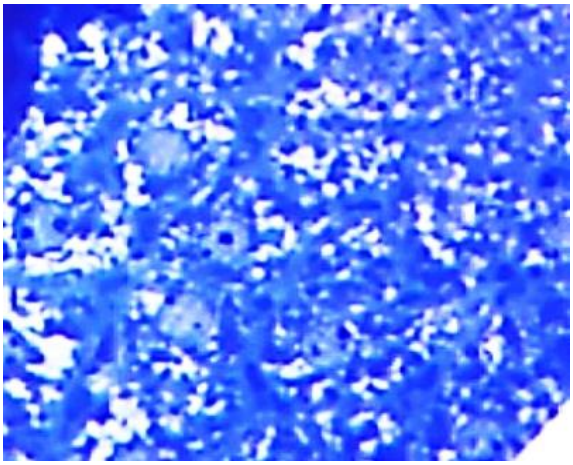

Figure 2a and 2b. Stress group. Rat liver. The increasing of the quantity of central venous. Intususception growths of blood vessels by translumenal bridge formation. X400

Sinusoids are widened with plenty of bridges. Their quantity has increased. In the 2 group animals, after four days of termination of the experiment, plenty of branches of sinusoids as well also formation of the bridges and their separations have been observed (Figures 3a and 3b).

During the investigation of microvessels of the brain in the first group of the animals, the vessels with wide lumen are observed as the ones with narrow lumen. Different inosculations between vessels have become evident In the first and the second group of the animals considerable number of capillaries with the formation of the bridges are observed (Figure 4). There is a large number of newly-formed capillaries.

DISCUSSION

It It has been shown that, at the alarm stage of stress reaction i.e., free swimming in a cage (an hour after FSC), the structure of the liver underwent dystrophic changes of hepatocytes and blood flow in the liver lobules had increased. These changes was present at the resistance stage (48 hours after FSC), as well. At the exhaustion stage (FSC within 10 days) it caused greater dystrophy of hepatocytes, the occurrence of necrosis in them and microcirculatory disturbances in the lobules.[5]

 DOI: 10.17628/ECB.2016.5.104-107

a)

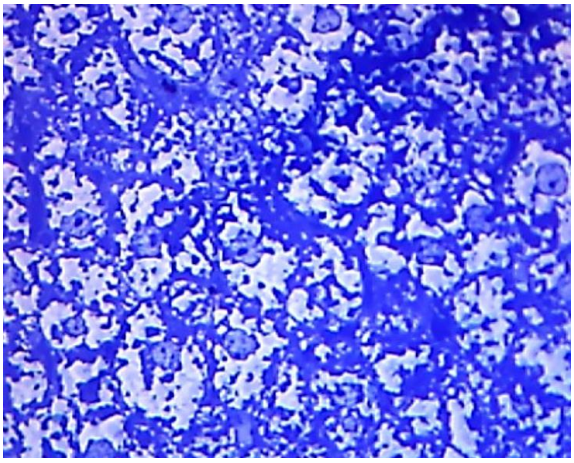

b)

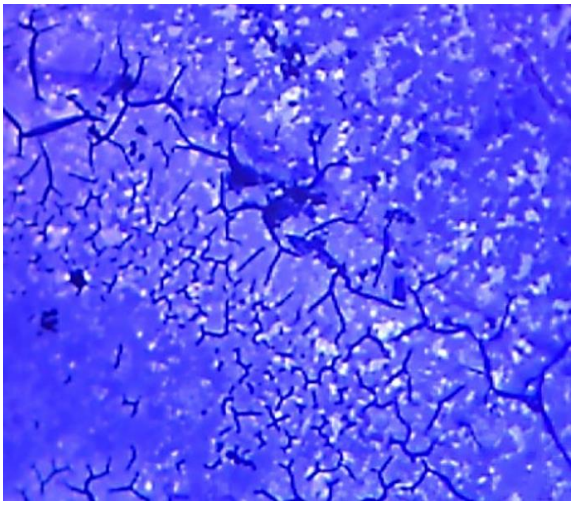

Figure 3a and 3b. Post stress group. Rat liver. It is characterized by sprouting angiogenesis. The transition from sprouting angiogenesis to intussusception angiogenesis. X400.

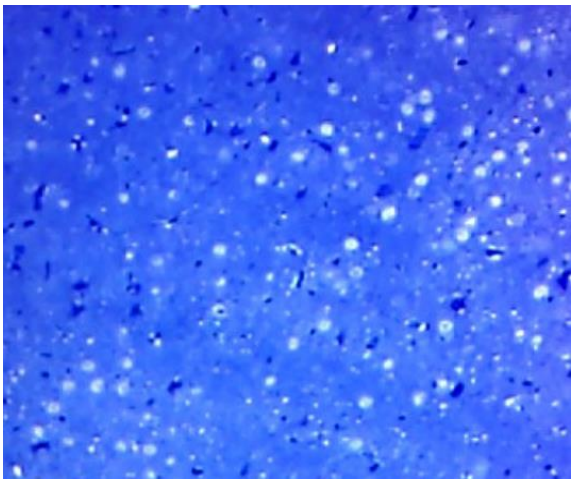

Figure 4. Post stress group. Rat brain. The intususception growths of blood vessels. X400

That agreed with our data concerning pathological remodelling of liver microcirculation structures when we dealt with multifactorial influence at CVS. Bigger vessels have shown changes like intussusceptive microvascular growth along with sinusoids. Typically the blood vessels showed the presence of the second type of angiogenesis i.e. sprouting angiogenesis, the major type of vasculature development in both liver regeneration and cancer development,[3,8,15,19] and intussusception angiogenesis like translumenal bridge formation as shown earlier by us.[10] The formation of new vessels and the establishment of an abnormal angioarchitecture of the liver are clearly related to the progressive fibrogenesis which finally leads to cirrohosis and liver cancer.[22]

In the brain of experimental animals pathogenic remodeling microvessel at CVS was also diagnosed. Brain microcirculation plays an important role in the pathogenesis of various brain diseases.[20] The brain is extremely sensitive to hypoxia, and brain edema is more dangerous than edema in other tissues. Brain vessels are part of the blood-brain barrier, which prevents the penetration of some of the substances in the blood into the brain tissue Increased vascular density at CVS has also been observed after stroke.

The density and architecture of capillary beds that are formed within a tissue depends on many factors, including local metabolic demand and blood flow.[12,13,14]

The formation of new vessels in brain at CVS intussusceptions of angiogenesis occurs just like in the liver by means of translumenal bridge formation.

CONCLUSION

CS influences the reorganization of blood vessels of liver and brain and it causes angiogenesis of liver sinusoids and brain capillaries.

ACKNOWLEDGEMENT

Current work was performed by support of H. Buniatian Institute of Biochemistry Natl. Acad. Sci. of RA.

REFERENCES

[1]Bratus', V. V., Talaeva, T. V., *Medbe.ru*, **2014**

[2]Burry, P., Dgonov, V., *Mol. Aspects Med*., **2002,** *23(65),* 1-27.

[3]Coulon, S., Heindryckx, F., Geerts, A., *Histol. Histopathol.*, **2009**, *24*, 1323 – 41.

[4]Djonov, V. G., Kurtz, H. and Burri, P. H., *Dev. Dinam*., **2002**, *224*, 391-402.

[5]Gusakova, E. A., Gorodetskaya, I. V., *Bull. Vitebsk State Med. Univ.*, **2014,** *1*, 13.

[6]Haymo, K. P., Burri, P. H., Djonov, G., *Physiology*, **2003**, *18(2),* 65-70.

[7]Hutter-Schmid, B., Kniewallner, K. M., Humpel, C., *Front Cell Dev. Biol.*, **2015**, *3*, 52.

[8]Leake, *I., Nature Rev. Gastroenterol. Hepatol.*, **2015**, *12*, 63.

[9]Barseghyan, K. A., Alchujyan, N. Kh., Aghababova, A. A., Movsesyan, N. H., Avagyan, H. Kh., Melkonyan, L. H., Hayrapetyan, H. L., Guevorkyan, A. G., Kevorkian, G. A., *Eur. Chem. Bull*., **2013**, *2(6),*373 -382.

[10]Karapetyan, G. R, Kukurtchyan, N. S., *Eur. Chem. Bull*., **2015,** *4(5)*, 275 – 278.

[11]Kukurtchyan, N. S., Karapetyan, G. R., *Patent 2844A, Rep. Armenia*, **2014.**

[12]Kobek, M., Skowronek, R., Jankowski, Z., Patasz, A., *March. Med. Sad. Kryminol.***, 2015**, *65(2)*, 112-124.

[13]Cavaglia, M., Ddombrowski, S. M., Drazba, J., Vasanji, A., Bokesch, P. M., Janigro, D., *Brain Res.*, **2001**, *910(1-2)*, 81 - 93.

[14]Ritz, M. F., Fluri, F., Engelter, S. T., Schaeren-Wiemers, N. and Lyrer, P. A., *Curr. Neurovasc. Res.*, **2016,** *13(4)*, 279-287.

[15]Fernandez, M., Semela, D., Bruix, J., Colle, I., Pinzani, M., Bosch, J., *J. Hepatol*., **2009,** *50(3)*, 604–620.

[16]Schiodt, F. V., Rochling, F. A., Casey, D. I., Lee, W. M., *New England J. Med*., **1997**, *337(16)*, 1112-1117.

[17]Solin, A. B., Lyashev, Yu. D., *Bull. Exp. Biol. Med.*, **2014,** *5*, 584-586.

[18]Simons, M., *Circulation***, 2005**, *lll*, 1556-66.

[19]Thabut, D., Shan, V. J., *Hepatol*, **2010**, *53*, 976-80.

[20]Kolinko, Y., Krakorova, K., Cendelín, J., Tonar, Z., Kralickova, M., *Rev. Neurosci.*, **2014,** *26(1)*, 75-93.

[21]Radak, Zs., Zhao, Z. F., Koltai, E., Ohno, H. and Atalay, M., *Antioxid. Redox Signal*., **2013**, *18(10)*, 1208—1246.

[22]Zhang, Z. L., Zhang, F., Lu, Y. and Zheng S. Z., *Hepatology Res.*, **2015**, *45*, 162 -78.

[23]Kan, Z. X. and Madoff, *D. C., Semin. Intervent. Radiol.*, **2008,** *25(2)*, 77–85.

Received: 28.03.2016.
Accepted: 20.05.2016.

COPOLYMERIZATION OF 2-(4-VINYLPHENYL)CYCLO-PROPYLMETHYL CINNAMATE WITH GLYCIDYL METHACRYLATE

K. G. Guliyev,[a] A. M. Aliyeva,[a] S. B. Mamedli,[a] D. R. Nurullayeva,*, [a] A. M. Guliyev[a]

Keywords: microstructure; monomers; copolymerisation; 2-(4-vinylphenyl)cyclopropylmethyl cinnamate; photosensitivity.

The radical copolymerization of 2-(4-vinylphenyl)cyclopropylmethyl cinnamate with glycidyl methacrylate has been studied and new cyclopropane- and epoxy-group containing photosensitive copolymers have been prepared. The relative activity of monomers and the parameters of *Q* and *e* by Alfrey and Price method have been determined. The copolymerization constants of 2-(4-vinylphenyl)cyclopropylmethyl cinnamate (r_1) and glycidyl methacrylate (r_2) were determined by the Fineman-Ross method and proved to be r_1 = 1.05 and r_2 = 0.4, respectively; the parameters Q_1 and e_1 were found to be 1.82, -0.79, respectively. The composition and structure of this copolymer have been established. The photochemical investigations of the synthesized copolymer have been carried out. It has been established that during the photochemical transformation a re-structuring takes place due to cyclopropane and epoxide ring opening and reaction of double bond in cinnamate fragment as well.

* Corresponding Authors
Fax: (+99418) 642-04-00
E-Mail: guliyev.kazim.pm@mail.ru; ipoma@science.az
[a] Institute of Polymer Materials, Azerbaijan National Academy of Sciences, 124, S.Vurgun str., Az5004, Sumgait, Azerbaijan

INTRODUCTION

Rapid increasing of information requires new type new type of materials to record, storage and reproduce data. The polymers and copolymers containing various reactive groups possess valuable properties and possibility of cross-linking under action of radiation which allows to prepare various materials used in microelectronics.[1-3] This is one of the main reasons for interesting of the researchers for the preparation of new types of the photosensitive polymers.[4-8]

Polymerization of functionally substituted cyclopropyl styrenes[9-11] is a known way to prepare this kind of materials, and the polymers prepared from unsaturated ethers of cinnamic acid undergo cross-linking processes upon UV irradiation with forming negative photoresists with high light sensitivity.[12, 13] Copolymerization of the cyclopropanes containing vinyl groups with other reactive monomers results polymers containing cyclopropane groups located in side part of macrochain is also well known.[14, 15]

This work has been devoted to investigate the copolymerization of 2-(p-vinylphenyl)cyclopropylmethyl cinnamate (PhCPC) with glycidyl methacrylate (GDMA) and study of properties of the copolymers prepared on their basis with the aim of creation of new photosensitive copolymers. The choice of this monomer has been stipulated with large number and chemical nature of double bonds and presence of cyclopropane ring in combination with carbonyl group in the monomer which has influence on such important photolithographic parameters of resists as photosensitivity, adhesion.[16,17]

PhCPC is a new reactive monomer, its synthesis and homopolymerization have been presented recently.[18] The choice of this compound to copolymerize it with GDMA has been stipulated by the presence of light absorbing carbonyl, cyclopropane and epoxide groups or double bond in the molecule. In the copolymerization of the studied GDMA-PhCPC system is an important task is choosing the conditions when the polymerization is proceeded only by participation of vinyl group and the reactive fragments would be remained in the side chain without changes.

EXPERIMENTAL

The synthesis of PhCPC was carried out by methodology described in our work.[18] The copolymerization of PhCPC with GDMA was carried out in benzene solution in the presence of 0.5 % azobisisobutyronitrile (AIBN) (from total mass of monomers) at 70 C. The total concentration of the initial monomers was 1.0 mol·L^{-1}, and a ratio of the initial monomers was changed as it is given in Table 1. The copolymers of various composition have been isolated after 10-20 min by addition excess of MeOH to the reaction mixture. The resulting copolymers were re-precipitated twice from theirs benzene solution with methanol and sulphuric acid and dried in vacuum (15-20 Hgmm) at 30 °C until constant weight.

The copolymers formed were white solids which are well soluble in aromatic and chlorinated hydrocarbons. Elemental analysis for $C_{28}H_{30}O_5$: Calculated: C, 75.33 %, H, 6.72. Found: C, 75.20, H, 6.35.

The content of constituents in the co-polymers could be determined from their bromine number (relates to the number of double bonds). The characteristic viscosity value was determined in benzene solution with using an Ubbelode viscosimeter which was proved to be η =0.7-0.72 dL·g^{-1}.

The IR-spectra of the copolymers were registered on spectrometer UR-20, PMR-spectra – on spectrometer BS-487B Tesla (80 MHz) in solution of deuterated chloroform.

The photosensitivity of co-polymers was determined at various concentrations (4-13 % solutions) with making a layer on the glass substrate in a dust-free medium with centrifuging at 2500·min^{-1}. The photoresists were kept for less than 20 min for increasing of adhesion to the substrate before cutting on contour on contour of the procurement preventing the film detachment.

Thickness of the prepared film-resists was measured by microinterferometer „LINNIKA", which was proved to be 0.20-0.25 μm after drying for 10 and 20 min at room temperature and 30-35 °C/10 Hgmm, respectively.

The exposure of the procurements was carried out on a device with light point source through photomask with a DPT-220 mercury lamp (current intensity was 2.2 A, distance from source of radiation was 15 cm, mobile shutter rate of exponometer was – 720 mm·h^{-1}, exposure time was 5-20 s).

The development was carried out in a jet installation. As a developer dioxane and isopropyl alcohol was used at ratio 1:2 at temperature of 18-25 °C.

The photosensitivity is evaluated on the basis of the completeness of photochemical polymerization (cross-linking). The photosensitivity – the inverse of the dose of UV-light absorbed means an UV dose necessary for transformation of photoresist to crosslinked (insoluble) state.

$$S = \frac{1}{H} = \frac{1}{E \times t}$$

where

H –exposure (or dose of irradiation with UV light), J·cm

E – intensity, Wt·cm^{-2}

t – irradiation duration, s

RESULTS AND DISCUSSION

During radical co-polymerization of polyfunctional PhCPC with GDMA formation of reactive polyfunctional co-polymer showed in Formula 1 could be expected.

Comparing of the IR-spectra of the copolymers formed with the spectra of the initial monomer (PhCPC) showed that the deformation and valence vibrations of the vinyl group in the initial monomer at 990 and 1640 cm^{-1} are disappeared.

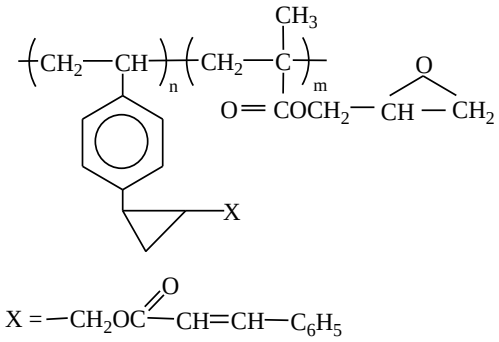

Formula 1. The structural formula of the expected polyfunctional co-polymer

The absorption bands characteristic for benzene and cyclopropane rings (1410-1460 and 1500-1600 cm^{-1}) and the absorption bands at 1720, 1030 and 1110 cm^{-1}, referring to the carbonyl vibrations of the cyclopropyl ester fragment are remained unaffected. The absorption band belong to valence vibration of the vinyl group located in cinnamic acid ester fragment at 1635 cm^{-1} is appeared in the co-polymers spectra.

Availability of the characteristic absorption bands of epoxide groups in structure of the copolymers is confirmed by the absorption band at 830, 920 and 1260 cm^{-1}, 1388 cm^{-1} referring to the deformation vibrations of C–CH$_3$ group in the cinnamate fragment.

In addition, in the range of frequencies 800-680 cm^{-1} and at 780, 750, 730 and 680 cm^{-1} absorption bands characterizing monosubstituted benzenes in esters of cinnamic acid could be observed. The IR-spectrum of PhCPC copolymer with glycidyl methacrylate is presented in Fig 1a (non-irradiated film).

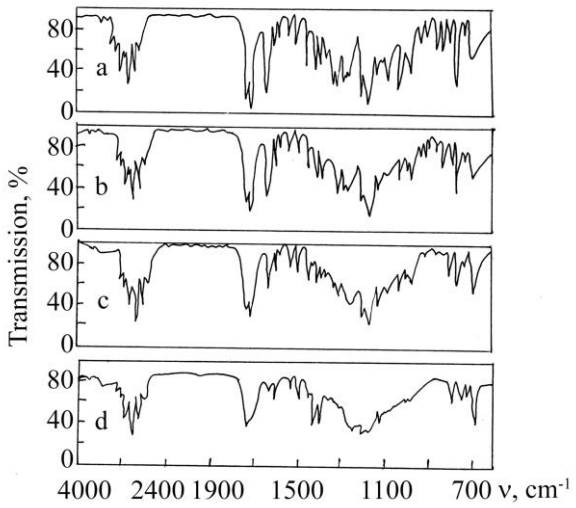

Figure 1. IR-spectra of copolymer film of PhCPC with GDMA: unirradiated (a) and irradiated for 1-st (b), 3-rd (c) and 4-th (d) min., m_1 : m_2 = 78.7 : 21.3 mol%.

 DOI: 10.17628/ecb.2016.5.108-112

In the PMR-spectrum of copolymer the resonance signals referring to protons of benzene nucleus (δ = 6.60-7.30 ppm) and cyclopropane ring (δ = 0.65-1.66 ppm) are clearly appeared, and the signals referring to protons of vinyl group (δ = 5.10-6.65 ppm) – are absent. The protons of epoxide ring are characterized with signals at 2.30-2.60 ppm(–CH_2–) and at 2.96 ppm (–CH–). The signals of CH=CH-groups of cinnamic fragment are δ = 6.4-7.4 ppm. As r_1 and r_2 is less than 1, in this system there is a tendency to alternation of links.

According to the data of spectroscopy the copolymerization of PhCPC with GDMA proceeds only due to opening of double bonds of the vinyl groups with maintenance of the other reactive functional fragments of the both monomers. Thus, on the basis of the analysis of IR- and PMR-spectra of the copolymers prepared by copolymerization of PhCPC with GDMA, the structure of copolymers is assumed as it is given in Formula 1.

The copolymerization was carried out at various ratios of the initial monomers. It has been revealed that the composition of forming copolymers depends on the composition of the initial monomer mixture.

For estimation of polymerization activity of PhCPC there have been calculated the values of relative activity constants of monomers by Fineman-Ross method[19] and the parameters *Q-e* by Alfrey and Praice method.[20] The microstructure parameters of the copolymers were calculated by using the copolymerization constants on formulas.[20] The obtained data are presented in Table 1.

The values of the relative activity constants (Table 1) evidence about greater reactivity of PhCPC in comparison with GDMA, which may be the consequence of the influence of cyclopropane ring substituent (–CH_2OOC–CH=CH–C_6H_5) on the electron density of double bond in the vinyl group.[21] The conjugation of the ester group causing redistribution of electron density both in the monomer and in the radical formed from it, thus the energy necessary for appearance of transition state is decreased leading to the increase of reactivity of monomer.

The calculated values of parameters Q_1 and e_1 during copolymerization with GDMA indicate increased conjugation in monomer (PhCPC) connected with influence of substituent – cinnamate fragment -stipulating relatively high reactivity of monomer and more low reactivity of the radicals. In calculation of factor e_1 it was chosen the negative mark based on the fact that the electron density of double bond of vinyl group in PhCPC should be less than in GDMA, since the influence of substituent of PhCPC leads to redistribute of density of double bond in the vinyl group changing polarity of the radical. This has been connected to the large reactivity of PhCPC in comparison with GDMA confirmed by copolymerization constant (r_1 = 1.07, r_2 = 0.42, respectively).

On the basis of the calculated copolymerization constants there have been obtained the data about microstructure of copolymers (Table 1). A length of blocks L_{M_1} is increased with increase of fraction of PhCPC in the composition of copolymers. It is seen from the Table 1 that R and L_{M_1} are maximal (57 and 37; 2.07 and 4.21 units, respectively) at ratio of the initial monomers 50:50, 75:25. It follows that by selection of determined compositions of the monomer mixtures one can realize the directed formation of microstructure of copolymers, which is one of the most perspective ways of modification of their properties.

An availability of the synthesized copolymer of the reactive groups of various chemical nature in links of macromolecule arouses interest for investigation of photochemical structuring of this copolymer, i.e. to cross-linking under action of UV-irradiation and such polymers showing as negative type photoresists. These polymers with properties of high light sensitivity, film-forming ability, good solubility before irradiation, resistance to solvents, plasma and etchants after cross-linking and good thermal stability, which are very important for photoresist.

Due to availability of strongly absorbing light energy of groups (cyclopropane, glycidyl, cinnamate >C=O etc.) the synthesized copolymers are photosensitive and under the influence of UV-irradiation are subjected to the photochemical conversions leading to formation of crosslinked structures. The influence of irradiation on photosensitive polymers has been investigated by measurement in UV-spectrum.[10] The photoreactive fragments have been considered with various concentrations 15-150 mg in thin films. The absorption bands in the UV-spectrum of polymers at 296 and 300 nm, respectively, are referred to π→π transitions. The intensities of absorption through various intervals of irradiation were changed in the UV-spectrum of the copolymer with ratio 59.19:40.81 (Fig.2).

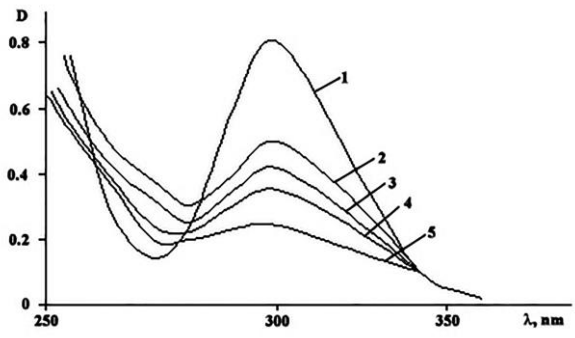

Figure 2. Change of UV-spectrum of absorption of made film from poli (PhCPC-co-GDMA) at ratio [59.19:40.81]. 1-5 light-striking time, respectively, t=5, 10, 15, 20 second.

During irradiation decrease or disappearance of photoactive fragments could be observed. The irradiation led to fast decrease of the absorption intensity at 296 and 300 nm and to disappearance of the bands almost completely after 6 min irradiation. This behaviour evidently indicates the formation of cyclobutane ring.[22] All this process is explained in reference 22.

It is also possible that due to irradiation a cyclohexane fragment is formed via cycloaddition of cinnomoil unit of the polymer which destroys the conjugation in the electron system of cyclopropane ring. It has been revealed that an increase of concentration of polymers raises a photocross-linking rate due to large quantity of photosentive units.

Table 1. Parameters of copolymerization of PhCPC (M_1) with GDMA (M_2).

Composition of initial mixture, mol.%		**B. N.**	**Composition of copolymers, mol.%**		r_1	r_2	Q_1	e_1	$r_1 \cdot r_2$	**Microstructure of copolymer**		
PhCPC M_1	**GDMA** M_2		**PhCPC** m_1	**GDMA** m_2						L_{M_1}	L_{M_2}	R
10	90	7.7	18.7	81.3	1.07	0.42	1.82	-0.79	0.44	1.11	4.78	34
25	75	15.0	37.11	62.89	±0.03	±0.02	±0.01	±0.02		1.35	2.26	55
50	50	23.5	59.19	40.81						2.07	1.42	57
75	25	31.1	78.7	21.3						4.21	1.13	37
90	10	36.0	91.04	8.96						10.63	1.04	17

L_{M1} and L_{M2} – average length link blocks of monomers; R – Harwood blocking factor

In films of copolymer, a conversion rate of the photosensitive fragments depends on composition of the light-sensitive links in the copolymer chain. The crosslinking rate grows with increase of composition of cinnomoil units (Fig.3). It could be concluded that after 40-80 sec. irradiation (transformation is 50-70 %), the polymer films become insoluble in organic solvents in which they were dissolved at room temperature to do irradiation experiments. Such behaviour is caused by formation of hard three-dimensional network due to intermolecular photoinduced cycloaddition of hanging units.

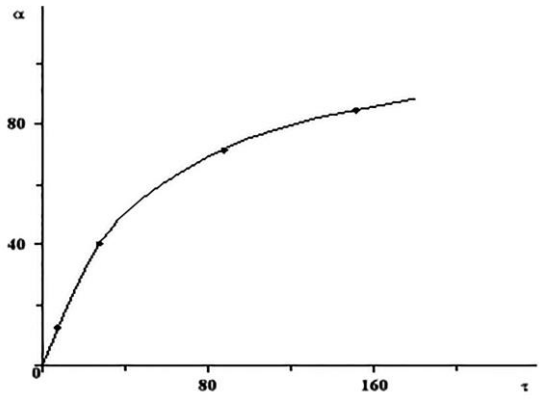

Figure 3. Influence of irradiation time τ(s) on solubility of copolymer (α- content of insoluble fraction).

The three-dimensional structure during irradiation has a form of a loose net with large cells, which swells strongly during development and is compressed during drying of the polymer layer, causing folds and wrinkles.

The good results have been prepared in work with films of thickness 0.2-0.3 μm.

The process of 3D-structure evolution during irradtiation of the prepared cyclopropane-ring containing copolymers has been followed by IR spectroscopy as well (Fig.1.). The intensity of the absorption bands characteristic for cyclopropane ring (1030-1035 cm^{-1}), double bonds (1635 cm^{-1}), carbonyl group (1720-1725 cm^{-1}), and epoxide ring (830, 920, 1260 cm^{-1}) were decreased with increasing of irradiation time and were completely disappeared ~ 8 min irradiation due to 3D-structure evolution with opening of double bonds and cyclopropane rings. The absorption band at 1720 cm^{-1}, characteristic for carbonyl group in ester fragments being in conjugation with double bond is shifted to 1740 cm^{-1} during irradiation which can be attributed to the opening reaction of double bond and as a consequence the disappearence of conjugation. It is confirmed with following change of the content of double bonds in cinnamate fragment controlled by measurement of bromine number.[23]

Conclusions

A new copolymer has been synthesized and its composition, structure and properties have been established. The availability of cyclopropane ring, cinnamate and glycidyl carbonyl groups in macromolecules of the prepared copolymer allowed to create a material with high photosensitivity. These copolymers have high photochemical crosslinking ability to create solid elastic layers with good adhesion to substrates and to prepare polymer films with low microdeficiency.

References

[1]Mizoguchi, K, Hasegaawa, E., *Polym Adv Technol.*, **1996**, *7*, 471.

[2]Reichmanis, E, Nalamasu, O., Houhihan, F. M., Novembre, A. E., *Polymer Int.*, **1999**, *48*, 1053.

[3]Ohe, Y., Ito, H., Watanabe, N., Ichimura, K., *J. Appl. Polym. Sci.*, **2000**, *77*, 2189.

[4]Filichkina, V. N., *Khim. Prom. Rubezh*,, **1985**, *11*, 11.

[5]Galaktionov, D., *Plastics*, **2007**, *7-8*, 53.

[6]Vainer, A. Ya., Dyumayev, K. M., *Khim. Prom.*,. **1989**, *7*, 3.

[7]Vainer, A. Ya., Dyumaev, K. M., Likhachev, I. A., Shalatonova, A. D., and Yartsev, Yu. A., *Dokl, Phys, Chem.*, **2004**. *396*. 115.

[8]Hou, H., Jiang, J., Ding, M., *Eur. Polym. J.*, **1999**, *35*. 1993.

[9]Guliyev, K. G., Ponomaryova, G. Z., Guliyev, A.M., *Russ. J. Appl. Chem.*, **2006**, *79*, 488.

[10]Guliyev, K. G., Ponomaryova, G. Z., Guliyev, A. M. *Polym. Sci.*, **2007 B**, *8*, 196.

[11]Guliyev, K. G., Ponomaryova, G. Z., Mamedli, S. B., *Process. Neftekhim. Neftepererab.*, **2009**, *2*. 183.

[12]Subramanian, K., Ramai Reddy, A. V., Krishnasamy, V., *Macromol. Chem. Rapid Commun.*, **1991**, *12*, 211.

[13]Rehab, A., Salahuddin, N., *Polymer*, **1999**,*40*, 2197.

[14]Guliyev, K. G., Mamedli, S. B., Guliyev, A. M., *Sb. Mater. XIX Mendeleev. Syezda Obsh. Pkikl. Khim.*, **2011**., 276, Volgograd (Russia)

[15]Guliyev, K. G., *Plast. Massy*, **2009**, *9*, 25.

[16]Guliyev, K. G., Garayeva, A. A., Ponomaryova, G. Z., Aliyev, A. M., Guliyev, A. M., *Russ. J. Appl. Chem.*. **2015**, *88*. 1047.

[17]Guliyev, K. G., Aliyeva, A. M., Ponomaryova, G. Z., Nurullayeva, D. R, Guliyev, A. M., *American Journal of Applied Chemistry*, **2015**, *3*, 21.

[18]Guliyev, K. G., Aliyeva, A. M., Guliyev, A. M., *Russ. J. Appl. Chem.*. **2013**. *86*, 92.

[19]Topoptseva, A. M., Belogorodskaya, K. B., Bondarenko, V. M. *Laboratorniy praktikum po khimii i tekhnologii vysokomolekulyarnikh soedineniy*, *Khimiya*, 1972, 415, L.:Khimiya

[20]Zilberman, E. N., *Vysokomoled. Soed.*, **1979 B**, *21*, 33.

[21]Guliyev, K. G., Ponomaryova, G. Z., Mamedli, S. B., Guliyev, A. M., *J. Struct. Chem.*, **2009**, *50*. 693.

[22]Fang, S. W.,, Time, H. J.,, Gandini, A., *Polymer*, **2002**, *43*, 3505.

[23]Kuznetsov E.V., Divgun S.M. Budarina, L. A., Abbakumova, N. I., Kurenkov, V. F., *Praktikum po khimii i phizike polimerov*, Khimiya, **1977**., M.: Khimiya

Received: 24.02.2016
Accepted: 20.05.2016

REMOVAL OF TITAN YELLOW DYE FROM AQUEOUS SOLUTION BY POLYANILINE/Fe_3O_4 NANOCOMPOSITE

Mohamed A. Salem,[a]* Ibrahim A. Salem,[a] Mahmoud G. Hanfy,[b] and Ahmed B. Zaki[a]

Keywords: Adsorption, Magnetite, Polyaniline nancomposites, Titan yellow, wastewater treatment, dye removal

The efficiency of polyaniline/Fe_3O_4 (PANI/Fe_3O_4) nanocomposite (NC) as an adsorbent was investigated in the removal of Titan yellow (TY) dye from aqueous solution. The PANI/Fe_3O_4 was synthesized by polymerization of aniline in H_2SO_4 medium in the presence of Fe_3O_4 nanoparticles with ammonium persulfate as an oxidant. The NC formed was characterized by SEM and FT-IR methods. The dye removal process was studied under various conditions and was found that the adsorption activity of the PANI/Fe_3O_4 NC was greater than that of the bare PANI and Fe_3O_4 nanoparticles. Adsorption kinetics fitted with pseudo-first-order kinetic model.

Corresponding Authors
Fax: +20403350804
E-Mail: masalem@science.tanta.edu.eg
[a] Chemistry Department, Faculty of Science, Tanta University, Tanta 31527, Egypt
[b] West Delta Electricity Production Company, Alex, Egypt

Introduction

The pollutants in wastewater effluents from industrial sources must be removed or destroyed before water can be discharged into the environment.[1] Textile industry is known to be one of the major sources for the pollution of the environment.[2]

Adsorption is a widely used method for the removal of organic and inorganic pollutants from wastewater effluents,[3] including the removal of dyes from aqueous solutions. The most promising adsorbents of the textile dyes are polyaniline(PANI),[4,5] polyaniline/silica,[6] polyaniline/ sawdust,[7] Fe_3O_4/C/polyaniline composites,[8] humic acid/Fe_3O_4,[9] Fe_3O_4/C composites,[10] Fe_3O_4/sodium dodecyl sulphate (SDS)[11] and activated carbon.[12,13]

Among the mentioned adsorbents, conducting polymers like PANI and their composites have been the subject of intensive research and development due to theirs unique properties including theirs high environmental stability.[14] Aniline polymerization in an aqueous acidic medium yields the most conductive form of PANI, the emeraldine salt (ES), and this can be converted to the corresponding emeraldine base (EB) with an alkaline treatment. The ES and EB are used as excellent adsorbents for both anionic[4] and cationic[6] textile dyes.

The NC of polyaniline with Fe_3O_4 has received great attention because of its magnetic and electrical properties. It can be prepared via two steps. The first is the preparation of magnetic iron oxide (Fe_3O_4) nanoparticles then the second step is polymerization of aniline in the presence of Fe_3O_4 formed using an oxidant in acidic medium.[15-17]

In the present article, we report the results of the removal of Titan yellow (TY) dye from aqueous solution by PANI/Fe_3O_4 NC as an adsorbent. The adsorption processes was carried out under controlled reaction conditions to reach the highest removal efficiency.

Experimental

Materials

Aniline (Adwic) was distilled twice until it turned colorless. Titan yellow (Figure 1) from Winlab was used without further purification.

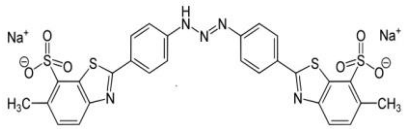

Figure 1. Structure of Titan Yellow.

Ammonium peroxydisulfate (APS) (Sigma-Aldrich) was high grade quality and used as received. The measurements were performed in distilled water all over the experimental work.

Synthesis of oleic acid-coated Fe_3O_4 nanoparticles

The oleic acid-coated Fe_3O_4 was prepared by co-precipitation of aqueous Fe^{3+}/Fe^{2+} ions in the presence of oleic acid (OA). $FeCl_3$ (14.62 g, 0.09 mol) and $FeSO_4.7H_2O$ (12.52 g, 0.045 mol) were dissolved in little amount of water (60 mL), followed by 140 mL water and stirred vigorously at 85 °C. Ammonium hydroxide (50 ml) was added slowly to reach the pH 9. At this stage, oleic acid (4 g) was then added and the reaction was left to continue for 2 h at 50 °C. The black precipitate formed was centrifuged and washed thoroughly with ethanol then water and dried at 60 °C overnight.

Synthesis of polyaniline (PANI)

Polyaniline in the form of ES was prepared by oxidative polymerization of aniline in aqueous H_2SO_4 solution in the presence of APS as oxidizing agent. APS (7.5 g, 0.033 mol) and SDS (0.06 g) were transferred into a beaker (500 mL) containing 200 mL of H_2SO_4 (0.5 M). The mixture was stirred magnetically in an ice bath at 5 ºC. Aniline (3 mL, 0.033 mol) was then added dropwise with continuous stirring for 1 h at temperature below 10 ºC. The APS/aniline mole ratio was kept at 1:1 in all experiments unless otherwise stated. The deep green precipitate of polyaniline salt was filtered and washed with H_2SO_4 acid (0.5 M) until the acid filtrate turned colorless. It was further washed with water and dried overnight at 60 ºC.

Synthesis of PANI/Fe_3O_4 nanocomposite

The nanocomposite was prepared by in situ oxidative polymerization of aniline in the presence of Fe_3O_4 nanoparticles in an aqueous suspension. Fe_3O_4 NPs (0.3 g) were dispersed in 200 mL of H_2SO_4 (0.5 M) and sonicated for 1 h in the presence of SDS (0.06 g). APS (7.5 g, 0.033 mol) was then added and the mixture was stirred continuously at 5 ºC followed by the slow addition of aniline (3 mL, 0.033 mol). The polymerization reaction was allowed to proceed under these conditions for 1 h until a dark precipitate of PANI/Fe_3O_4 NC was obtained. The NC was collected by filtration and washed with the acid solution (0.5 M) until the acid filtrate turned colorless. The product was further washed with large amount of distilled water until the filtrate became colorless. It was dried in oven at 60 ºC overnight and the yield was weighed.

Characterization techniques

Characterization of above samples was performed by conventional techniques. The morphology of samples was studied by the scanning electron microscope (SEM) (JSM, JEOL, 5300). FT-IR measurements were recorded on Jasco FT-IR 4100 (Japan) in the range 4000 – 400 cm^{-1}.

X- ray diffraction (XRD) patterns beam was nickel - filtered CuKα (λ = 1.5405 Å) radiation operated at 40 kV and 30 mA. The scanning range was from 2θ = 0 to 90 º with rate of 2.4º/min.

The UV/Vis spectra were recorded on the UV/Vis spectrophotometer (T80PG instruments ltd) linked with a temperature control unit to adjust the cell holder temperature to the desired value ± 0.1 ºC.

The thermogravimetric analysis (TGA) technique was used primarily to determine the thermal properties of the prepared NC (SDT Q600 V20.5 Build 15). The technique can analyze materials that exhibit either mass loss due to decomposition, oxidation or loss of volatiles (such as moisture).

The PANI/Fe_3O_4 composite (0.02 g) was transferred into a conical flask (100 ml) containing 20 ml of the dye solution at 30 ºC. The mixture was stirred at 120 rpm. The initial concentration of the dye was varied from 17 to 44 mg L^{-1}.

Results and Discussion

Transmission electron microscopy (TEM)

The TEM image of the OA-Fe_3O_4 nanoparticles is shown in (Figure 2c). Spherical nanoparticles of OA-Fe_3O_4 with average diameter about 12 nm are observed. Figure 2d indicated that the encapsulated OA-Fe_3O_4 nanoparticles in PANI have average diameter 14 nm.

Scanning electron microscopy (SEM)

(Figure 2a) shows the SEM micrograph of the free Fe_3O_4 nanoparticles. The nanoparticles seen to be aggregated in an irregular shape due to their high surface energy. Different appearance was observed in (Figure 2b) for the PANI/ Fe_3O_4. The nanoparticles of composite bind with PANI-chains to form multiparticles aggregates, which keep the free Fe_3O_4 nanoparticles tightly bound.

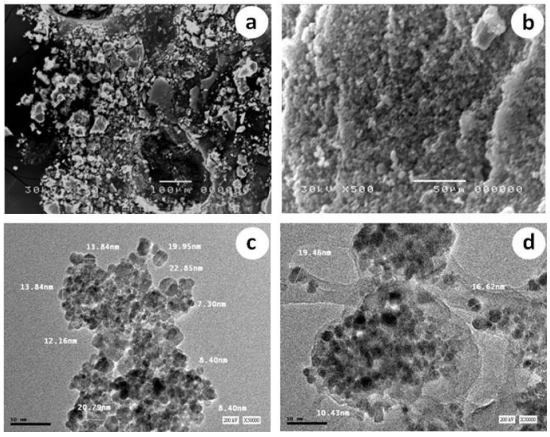

Figure 2. SEM images: (a) Oleic acid/Fe_3O_4, (b) PANI/OA-Fe_3O_4; TEM images: (c) Oleic acid/Fe_3O_4, (d) PANI/OA-Fe_3O_4.

FT-IR

The FT-IR spectrum of Fe_3O_4 nanoparticles (Supplementary material, S1) shows a band at 3429 cm^{-1}, which is a characteristic of the free OH groups on the nanoparticle surface. The peaks at 2924 cm^{-1} and 2854 cm^{-1} correspond to the stretching vibration of saturated –C-H groups due to the oleic ester. The stretching vibration of C=O of oleic acid is at 1703 cm^{-1}. The peaks at 587 cm^{-1} and 451 cm^{-1} are assigned to the vibration of Fe^{2+}-O and Fe^{3+}-O bonds, respectively. The band at 1102 cm^{-1} is assigned to the C-N bonds, while the peak at 3231 cm^{-1} corresponds to the N-H stretching vibration.

The PANI/OA-Fe_3O_4 nanoparticles formation is attributed to the strong interaction between PANI and OA-Fe_3O_4. Iron has the capability to form coordination bonds with the –NH group of PANI chain.[16,18] and hydrogen bond can also be formed between the O atom of the carbonyl group of OA-Fe_3O_4 and the –NH of PANI. Hydrogen bonds may also formed between the hydroxyl group at the surface of OA-Fe_3O_4 and N atom of the quinonoid structure (peaks at 1565 cm^{-1} and 1444 cm^{-1} are assigned to quinonoid and benzenoid structures, respectively).

X- ray diffraction

Figure 3 shows the XRD pattern of OA-Fe_3O_4 nanoparticles and PANI/Fe_3O_4 NC. A comparison between both the patterns revealed that a single peak at θ = 25° appears in the PANI/Fe_3O_4, which is characteristics of the PANI. The rest of peaks are assigned to the OA-Fe_3O_4 which has a cubic crystal system. These results agree with the reported results.[19] Crystallite size of magnetic nanoparticles is calculated from Scherrer equation.[20,21] The average size of the Fe_3O_4 particles is found to be 8 - 10 nm which is consistent with the results of TEM.

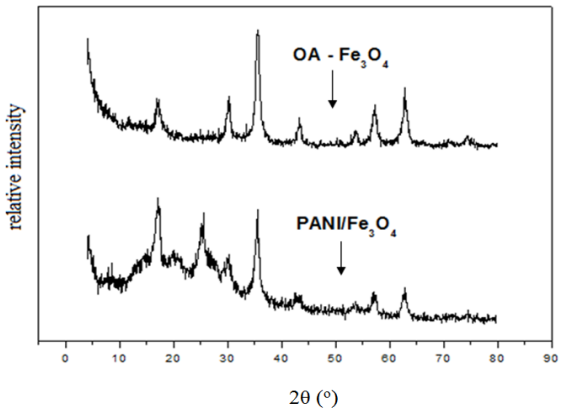

Figure 3. XRD patterns of OA-Fe_3O_4 and PANI/ OA-Fe_3O_4.

Adsorption of TY on PANI/Fe_3O_4

On the addition of the dye solution to the NC sample, a relative fast decolourization took place (Figure 4). The absorbance of the dye solution decreased by ca. 80 % over 90 min, depending on the operating reaction conditions. Adsorption of TY onto the bare Fe_3O_4, PANI and the NC was also investigated. The rate constant of dye adsorption from solution follows the order PANI/Fe_3O_4 > Fe_3O_4 > PANI under similar conditions. Adsorption of the dye by PANI occurred due to the electrostatic interactions between the -NH^{+}- centers of PANI (ES form) and dye anions. The difference between the amount of the dye adsorbed on Fe_3O_4 nanoparticles and PANI/Fe_3O_4 NC illustrates the presence of active sites for TY adsorption. The increase in the functional O and N atom containing groups content in the NC comparing that in bare Fe_3O_4 makes the NC to be desirable for dye adsorption.[22] The results obtained may be explained in terms of the increasing the amount of this groups and the surface area of the PANI/Fe_3O_4 NC.

Effect of PANI/Fe_3O_4 NC and dye concentrations

The rate of adsorption increased with increasing the NC amount. This can be explained in terms of the availability of active sites on the PANI/Fe_3O_4 surface that is eligible to interact with the TY molecules. The effect of dye concentration on the rate of reaction was investigated by keeping the amount of PANI/Fe_3O_4 constant and the dye concentration varies in the range (0.5 - 1.5)x10^{-4} M. The rate of adsorption decreases with an increase in the dye concentration.

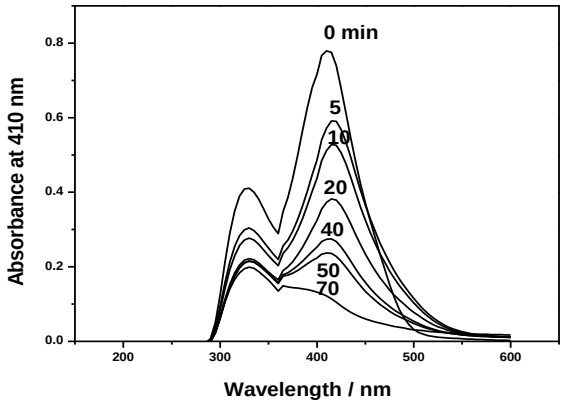

Figure 4. Absorbance traces of TY with time in the presence of PANI/OA-Fe_3O_4[TY] = 2.6 ×10^{-4} mol L^{-1}, PANI/OA-Fe_3O_4 = 0.02 g.

The more dye concentration the greater loading of NC surface with dye molecules are occurred. A slower adsorption would then be expected with the continuous blocking of the available active sites on the NC surface with the previously adsorbed molecules of the dye.

Effect of pH

The rate of dye removal by adsorption on the NC depends greatly on the pH of the medium. The measurement of the rate was carried out in the pH range 2-8 using phosphate buffer. The rate constant decreased with increasing the pH of from 2 to 8 (Figure 5). In strong acidic medium, the PANI always exists in the form of ES. This form is rich with the positively charged sites that undergo interaction with anionic moiety of the dye molecule. The ES form transforms into the EB form at higher pH. As the pH increases, the transition continues leading to the depletion of active sites in the polymer skeleton and consequently the interaction of PANI with TY is inhibited.

Adsorption kinetics

The effect of the initial dye concentration on the adsorption parameters was studied. The amount of dye adsorbed, q_t (mg g^{-1}), at time t for each concentration was estimated by the mass balance equation.

$$q_t = V\frac{C_0 - C_t}{m} \qquad (1)$$

where

C_0 is the initial concentration (mg L^{-1}) of TY,

C_t is the concentration of the remaining dye in solution at time t (mg L^{-1}),

V is the total volume (L) of reaction mixture and

m is the mass in gram of PANI/Fe_3O_4 sample.

The q_t increased with the contact time of the dye with the adsorbent and also with the initial concentration of the dye. The dye adsorption on PANI/Fe_3O_4 was initially fast and then slowed down thereafter.

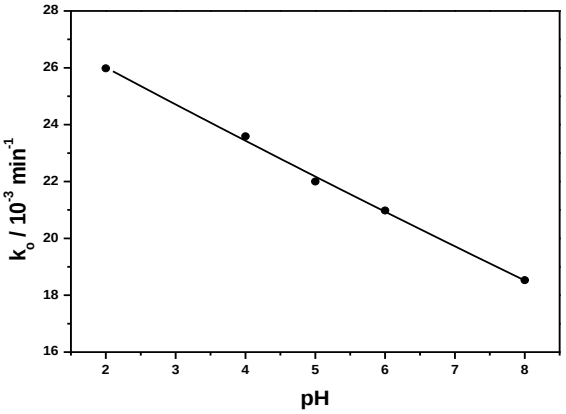

Figure 5. The dependence of the rate constant upon the pH. PANI/OA-Fe_3O_4 = 0.02 g,[TY] = 2.6 ×10^{-4} mol L^{-1}, T = 30ºC.

The adsorption kinetic data were analyzed in terms of different types of mathematical models. The first is pseudo-first-order kinetic model proposed by Lagergren's [23] in eqn. (2).

$$\log(q_e - q_t) = \log q_e - t \qquad (2)$$

where

q_t and q_e (mg g^{-1}) are the amounts of dye adsorbed per unit mass of the NC at time *t* and at equilibrium, respectively.

k_1 (min^{-1}) is the pseudo-first-order rate constant of adsorption.

Figure 6 shows the linear relationship between log(q_e-q_t) and *t*. The slope of the plot is k_1 and the intercept is log (q_e).

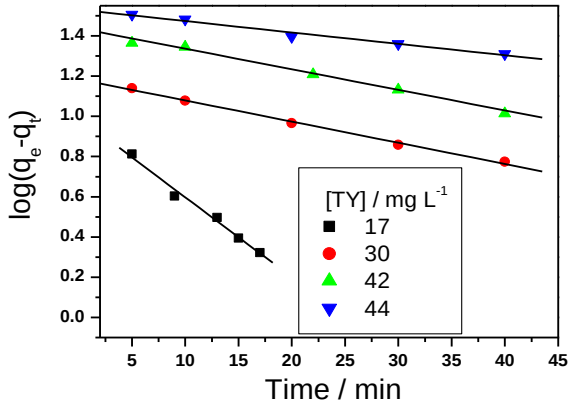

Figure 6. Pseudo-first-order kinetics for adsorption of TY onto PANI/OA-Fe_3O_4.PANI/OA-Fe_3O_4 = 0.02 g, T = 30ºC.

The second model is pseudo-second-order kinetic, proposed by Ho and McKay[24] which is represented by the equation,

$$\frac{t}{q_t} = \frac{1}{k_2 q_e^2} + \frac{t}{q_e} \qquad (3)$$

where

q_e is the amount of dye adsorbed at equilibrium (mg g^{-1}), and

k_2 is pseudo-second-order rate constant for adsorption (g $mg^{-1}min^{-1}$).

$k_2 q_e^2$ is the initial rate of adsorption at $t \rightarrow 0$.

Values of q_e, $k_2 q_{e2}$ and k_2 are calculated from the slope and intercept of the straight line obtained from the plot t/q_t *vs* *t* at various dye concentrations. Values of *k* and q_e, and correlation coefficient for this kinetic model are given in Table 1. Because of the correlation coefficients obtained for pseudo-first-order kinetic model are higher than for pseudo-second-order models, then the adsorption process follows better the former one.

Table 1. Kinetic parameters for adsorption of TY onto PANI/Fe_3O_4 NC

Kinetic models and parameters	**C_o of TY (mg L^{-1})**			
	17	**30**	**42**	**44**
q_e (exp) , mg g^{-1})	12	20	30	34
Pseudo-first-order				
q_e (calcd.), mg g^{-1}	10	18	28	34
k_1, min^{-1}	0.0915	0.0243	0.0236	0.013
R^2	0.993	0.998	0.992	0.992
Pseudo-second-order				
q_e (calcd.), mg g^{-1}	15	21	26	56
k_2 x 10^{-3}, g mg^{-1} min^{-1}	9.3	5.4	2.6	14
R^2	0.998	0.996	0.964	0.980

Adsorption isotherms

The Langmuir and Freundlich isotherm models were applied to estimate the adsorption capacity of the PANI/Fe_3O_4 NC towards the TY in view of the adsorption results obtained.

Langmuir adsorption isotherm

The following equation describes the monolayer surface coverage of the NC with the adsorbed dye molecules.[25]

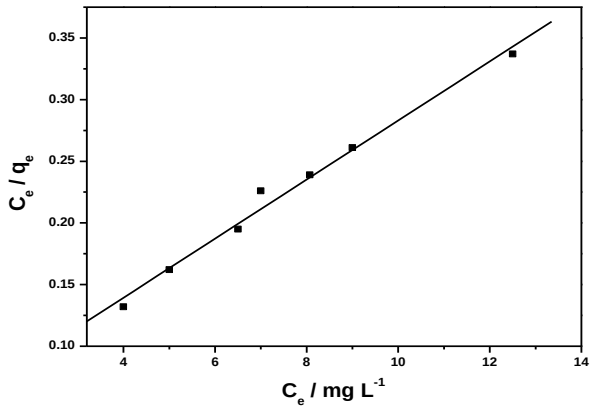

Figure 7. Langmuir isotherm for adsorption of TY on PANI/OA-Fe_3O_4. PANI/OA-Fe_3O_4 = 0.02 g, T = 30º C

 DOI: 10.17628/ecb.2016.5.113-118

Table 2. Isotherms constants for the adsorption of TY onto PANI/ Fe_3O_4 PANI/Fe_3O_4 = 0.02 g, Temp = 30 °C.

Langmuir isotherm parameters				**Freundlich isotherm parameters**			
q_m	K_L	R_L range	R^2	K_f	$1/n$	n	R^2
50	0.415	0.12–0.05	0.998	3.8	0.86	1.16	0.997

$$\frac{C_e}{q_e} = \frac{C_e}{q_m} + \frac{1}{q_m K_L} \quad (4)$$

where,

q_e is the amount of dye adsorbed at equilibrium (mg g^{-1})

C_e is the equilibrium concentration of the dye (mg L^{-1}) in bulk solution.

K_L is the equilibrium constant (L g^{-1}) while

q_m represents the maximum adsorption capacity when one layer of dye molecules is completed on the surface of the NC.

K_L and q_m are derived from the intercept and slope of C_e/q_e versus C_e plot which is shown in (Figure 7). It is known that the Langmuir isotherm is related to a dimensionless separation factor R_L that is defined as

$$R_L = \frac{1}{1 + K_L C_s} \quad (5)$$

The R_L denotes to the state of the adsorption process. If ($0 < R_L < 1$) the adsorption is favorable, ($R_L > 1$) it is unfavorable, ($R_L = 1$) is linear, and ($R_L = 0$) is irreversible.

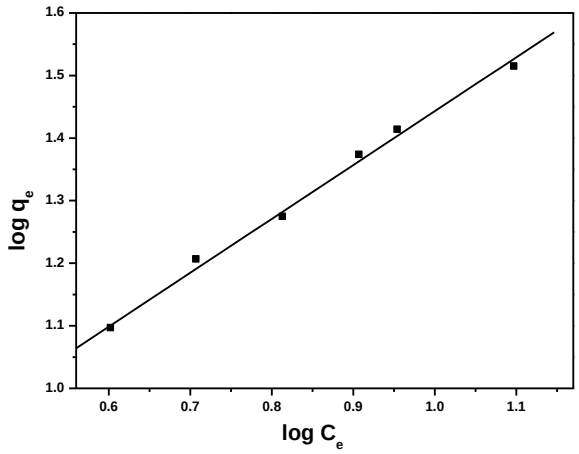

Figure 8. Freundlich isotherm for adsorption of TY on PANI/OA-Fe_3O_4.PANI/OA-Fe_3O_4 = 0.02 g, T = 30°C.

In the present study the value of R_L is ranging from 0.12 to 0.05 for the different initial concentrations of TY used. Table 2 indicates a favorable adsorption of the dye by PANI/Fe_3O_4 NC.

Freundlich adsorption isotherm

Freundlich model is given by the eqn. (7).[26]

$$\log q_e = \log K_F + (1/n) \log C_e \quad (6)$$

Values of K_F and n denote to the adsorption capacity and adsorption intensity, respectively. They were calculated from the intercept and the slope of the log q_e vs log C_e plot (Figure 8). $1/n$ describes the heterogeneity in adsorbent surface. Its small value indicates a favorable. A value close to or equals 1 indicates a material with relatively homogenous binding sites. A high value of K_F confirms a high adsorption capacity of the adsorbent. Adsorption isotherms of both Langmuir and Freundlich are depicted in (Figures 7, 8). The adsorption parameters derived from these isotherms are summarized in Table 2. The correlation coefficients (R^2) confirm that both isotherms are satisfactory.

Adsorption mechanism

The possible proposed adsorption mechanism of the dye on the surface of PANI/Fe_3O_4 involves two routes. The first is the electrostatic interaction between the dye molecules and the polyaniline salt. The second is the formation of a coordination bond between Fe_3O_4 and the dye as shown in Figure 9.

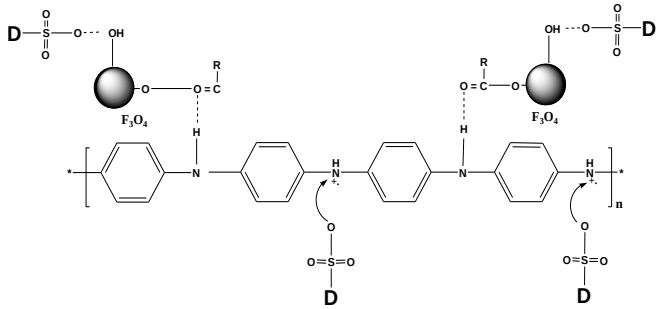

Figure 9. Adsorption mechanism between PANI/Fe_3O_4 NC and TY.

On dissolution of the dye in water it dissociates into dye anions(D-SO_3^-) and Na^+ ions, where D denotes to the organic moiety of the dye molecule. This anion interacts with the positive centres (–$NH^{+\cdot}$–) on the PANI surface. The effect of pH given (Fig. 5) is a good evidence for this phenomena. In acidic medium the adsorption is great due to the existence of more –$NH^{+\cdot}$– species on the PANI skeleton. In the basic medium the concentration of these species decreases and therefore the interaction between the adsorbent and the adsorbate is declined.

Regarding the participation of Fe_3O_4 in the adsorption process, it may be attributed to the development of a bond between the Fe_3O_4 and the dye molecule.

Conclusion

Adsorption of TY dye is more efficient onto the PANI/Fe_3O_4 NC compared with the bare PANI and Fe_3O_4. It obeyed both the Langmuir and Freundlich adsorption isotherms. The adsorption process was spontaneous and followed pseudo-first-order kinetic model. This method is promising towards the treatment of wastewater containing dyes.

References

[1]Ghasemzadeh, G., Momenpour, M., Omidi, F., Hosseini, M. R., Ahani, M., Barzegari A., *Front. Environ. Sci. Eng.*, **2014**, *8*, 471.

[2]Carge, V. K., Kumar, R., Gupta, R., *Dyes Pigment*, **2004,** *62*, 1.

[3]Juang, R., Tseng, R., *Colloids and Surf. A*, **2002**, *201*, 191.

[4]Salem, M. A., *Reactive & Functional Polymers*, **2010**, *70*, 707.

[5]Ayad, M. M., El-Hefnawy, G. , Zaghlol, S., *Chem. Eng.***,** **2013**, *217*, 460.

[6]Ayad, M. M., Abu El-Nasr, A., Stejskal, J., *Indus. Eng. Chem.* **2012**, *18*, 1964.

[7]Ansari, R., Dezhampanah, H., *Eur. Chem. Bull*., **2013**, *2(4)*, 220.

[8]Yao, W., Shen, C., Lu, Y., *Composite Sci. Technol*., **2013**, *87*, 8.

[9]Zhang, X., Wu, P., Zhang, L., Zeng G., Zhou C., *Colloids Surf. A*, **2013**, *435*, 85.

[10]Zhang, Z., Kong, J., *J. Hazard. Mat*., **2011**, *139*, 325.

[11]Shariati, S., Faraji, M., Yamini, Y., Rajabi, A., *Desalination*, **2011**, *270*, 160.

[12]Gupta, V. K., *Environ. Manag*., **2009**, *90*, 2313.

[13]Kumar, P. S., Ramalingam, S., Sathishkumar, K., *Korean J. Chem. Eng*., **2011**, *28*, 149.

[14]Quadrat, O., Stejskal, J., Kratochvil, P., Kubát, J., Sáha, P., Mcqueen, D., *Synth. Met*., **1998**, *97*, 37.

[15]Guo, H., Zhu, H., Lin, H., Zhang, J., *Mater. Lett*., **2008**, *62*, 2196.

[16]Wang, H., Wang, R., Wang, L., Tian, X.. *Colloids Surface A*, **2011**, *384*, 624.

[17]Tamilarasan, P., Ramaprabhu, S., Int. *J. Greenhouse Gas Control*, **2012**, *10*, 486.

[18]Deng, J., Ding, X., Zhang, W., Peng, Y., Wang, J., Long, X., *Polymer*, **2002**, *43*, 2179.

[19]Iton, H., Sugimoto, T., *J. Colloid. Interf. Sci*., **2003**, *265*, 283.

[20]Gass, J., Poddar, P., Almand, J., Srinath, S., Srikanth, H., *Adv. Funct. Mater*., **2006**, *16*, 71.

[21]Wang X., Chen, X., Ma, X., Zhang, Z., Zhang, Z., *Chem. Phys. Lett*., **2004**, *384*, 391.

[22]Illés, E., Tombácz, E., *Colloid Surf. A*, **2003**, *230*, 99.

[23]Lagergren, S., *Kung. Sven. Vetenskapsak. Handl*., **1898**, 24, 1.

[24]Ho, Y.S., Mckey, G., *process biochem.*,**2009**, *34*, 451.

[25]Langmuir, I., *J. Am. Chem. Soc*., **1918**, *40*, 1361.

[26]Freundlich, H. M. F., *J. Phys. Chem*., **1906**, *57A*, 385.

Received: 04.04.2016.
Accepted: 21.05.2016.